2-D blood vector velocity estimation using a phase shift estimator

Udesen, Jesper; Jensen, Jørgen Arendt

Publication date:
2006

Document Version
Publisher's PDF, also known as Version of record

2-D blood vector velocity estimation using a phase shift estimator.

Jesper Udesen

December 2, 2005

Center for Fast Ultrasound Imaging
Ørsted·DTU
Technical University of Denmark
2800 Kgs. Lyngby
Denmark

SUBMITTED IN PARTIAL FULFILLMENT OF THE
REQUIREMENTS FOR THE DEGREE OF
DOCTOR OF PHILOSOPHY
AT
THE TECHNICAL UNIVERSITY OF DENMARK
APRIL 2006

Signature of Author

Contents

Preface

It seems to be a law of nature that when you are really having fun, then time is up. This always happened to me in kindergarten when my mother picked me up at the time of the best play, and it still happens today when I have to finish my PhD thesis and end this project.

It has been three years of joy and frustration, excitement and anger working with ultrasound. There have been times when all my scripts crashed, and the scanner seemed to have its own will and just ignored me. But ultrasound has also been an exciting topic to work with and it has always been a great pleasure to work in a field where new diagnostic tools were invented. Tools which potentially could make a big difference to other people.

Jesper Udesen
Kgs. Lyngby.
December 2005

Notes on how this PhD project was financed

This project was made as an industrial PhD project in collaboration between B-K Medical and DTU. The financing was made by B-K Medical and by *the Danish Ministry of Science Technology and Innovation*.

Notes on the supervisors for the project

Michael Jørgensen the industrial PhD supervisor is from B-K Medical and professor Jørgen Arendt Jensen the university supervisor is from Ørsted·DTU.

Acknowledgments

First of all I would like to thank my girlfriend Lisbeth Rose for her support during the last three years. Our little daughter Astrid has not received the care she deserves from her father during the last couple of months, but hopefully that will change now.

A big thank you also goes to my two supervisors Jørgen A. Jensen and Michael Ø. Jørgensen for guiding me through this project and for having made this PhD project possible. Thank you for that!

I have shared office (and hotel rooms) with PhD Fredrik Gran. Many good cups of coffee have been digested, and both ultrasound topics and life in general discussed with him. Thank you Fredrik.

Niels Oddershede is my new office mate, and he has managed to offer me some resistance in our regular chess playing. Thank you Niels.

My other colleges at CFU, Svetoslav Nikolov, Borislav Tomov, Louise Taylor, Jakob Kortbek deserve a big thank you. Also my colleges at B-K Medical and the technical staff at CFU Elna Sørensen, Dorthe Lundsgaard and Henrik Laursen have all been very helpful. Thank you for that!

Abstract

In this PhD thesis a method for 2-D blood velocity estimation called *the transverse oscillation method* (TO) is investigated.

The thesis is divided into two parts. In the first part the basic principles in conventional 1-D flow estimation are described, and the state of the art for 2-D velocity estimation is discussed. The TO method is introduced, and the basic theory behind the method is explained. This includes the creation of the acoustic fields, beamforming, echo-canceling and the velocity estimator.

In the second part of the thesis the eight papers produced during this PhD project are presented. Here the TO method is tested both in simulations using the Field II program and in flow phantom experiments using the RASMUS scanner. Both simulations and flow phantom experiments indicate that the TO method can estimate the 2-D vector velocity with an acceptable low bias and standard deviation when the angle between the blood and the ultrasound beam is above 50°. Furthermore, the TO method is tested in-vivo where the scannings are performed by skilled sonographers. The in-vivo scannings resulted in a sequence of 2-D vector CFM images which showed 2-D flow patterns in the bifurcation of the carotid artery.

Dansk resumé

Denne afhandling er en undersøgelse af en metode kaldet *the transverse oscillation method* (TO) til bestemmelse af blodets 2-D hastighed ved hjælp af ultralyd. Afhandlingen er inddelt i to dele. I den første del introduceres de grundlæggende principper i konventionel 1-D blodhastighedsestimering ved hjælp af ultralyd. Dernæst introduceres nye teknikker til 2-D estimering af blodets hastighed, og TO metoden præsenteres. I den anden del af afhandlingen præsenteres de otte artikler, som er skrevet under dette PhD projekt. I fem af artiklerne undersøges TO metoden ved hjælp af simuleringer med Field II og ved hjælp af den eksperimentelle ultralydsskanner RASMUS. Både simuleringer og eksperimenter indikerer, at TO metoden kan estimere hastigheden med en lav bias og standardafvigelse, når vinklen mellem blodflowet og ultralydsstrålen er større end ca. 50°. Endeligt er TO metoden testet *in-vivo*, hvor skanningerne er foretaget af erfarne sonografer. In vivo skanningerne resulterede i en sekvens af 2-D vektor CFM billeder, som viste flowmønstre i bifurkationen af carotis.

CHAPTER

ONE

Introduction

Diagnostic ultrasound imaging has become one of the most successful methods to display the interior of the human body. Without any risk for the patient, images of tissue structures and blood flow within the body can be shown real-time on a (relatively) small portable scanner, which furthermore is significantly less expensive than other image modalities like MRI and CT. Due to this combination of low-cost, portability, and real-time performance, the ultrasound scanner has become one of the leading diagnostic tools for cardiovascular diseases.

Even though diagnostic ultrasound used for blood flow estimation has proven to be a highly successful tool, there are still challenges to face. One of the basic problems is the fact that the estimated blood velocity is not the full 3-D vector velocity of the blood, but only the vector velocity projected onto the ultrasound beam. This is illustrated in Fig. 1.1 which shows the blood flow in the jugular vein that leads the blood from the brain back to the heart. Even though the volume flow in the vein is constant throughout the image, different colors appear along the vessel, and at the center of the image the scanner fails to detect any blood flow at all. One might argue that this problem only has relevance for the engineer looking for esoteric challenges and not for the medical doctor who is skilled in working with ultrasound scanners. This might also be the case for many applications where it is possible to angle the transducer or the ultrasound beam. However, if a blood vessel, where different flow directions are present, is to be scanned, even a skilled medical doctor will not be able to gain the full information of the blood flow - information which potentially could be important for a correct diagnosis of the patient.

As an example of such a blood vessel the bifurcation of the carotid artery at the time of the peak systole is shown in Fig. 1.2. To the left the conventional CFM image is depicted. It is easy too see that different flow directions are present within the bifurcation, and the result is a confusing image, where the true flow is hidden. To the right in Fig. 1.3 a 2-D vector velocity image obtained with the method to be discussed in this thesis is shown. A big vortex is now seen in the internal carotid artery and information concerning the direction of the flow can now be acquired.

One might ask why 2-D estimation methods are not implemented in all commercial scanners when the improvement compared to 1-D techniques are so significant as illustrated in Fig. 1.2 and 1.3. The answer is mainly that the 2-D methods introduce complicated signal processing compared to 1-D techniques. They are therefore more expensive in terms of computational power, electronics and thus money. However, this problem is not significant for all the 2-D methods and especially one of the 2-D methods is nearly as fast and

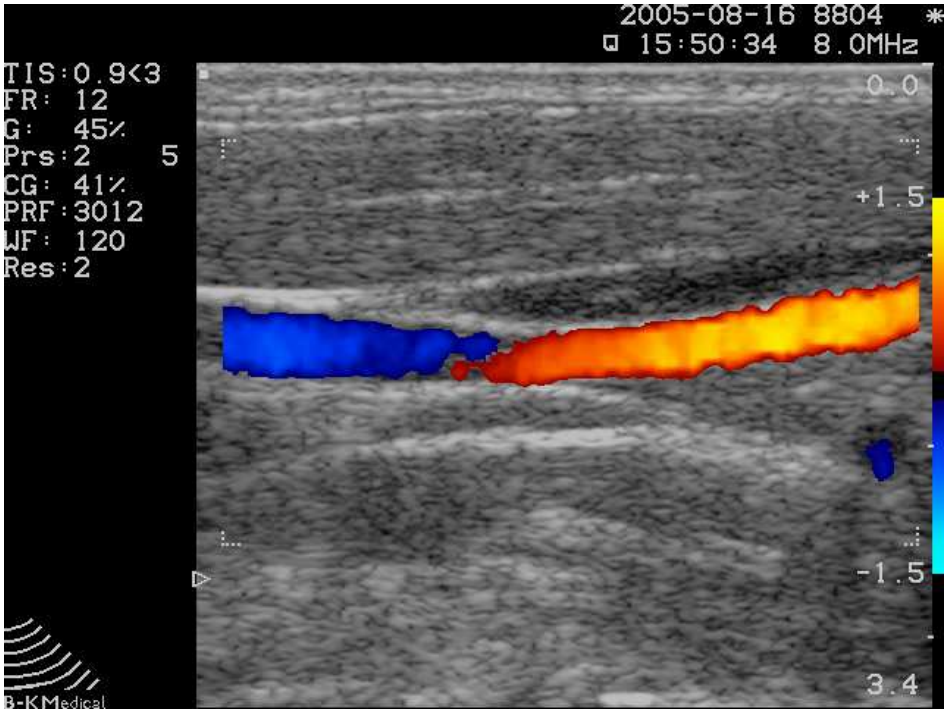

Figure 1.1: *Conventional CFM image of the flow in the jugular vein of the author. The image was acquired with a B-K medical 2102 scanner and a linear array BK-8804 transducer. The change in color and intensities in the blood vessel illustrates one of the fundamental problems with conventional flow estimation techniques.*

simple as a conventional 1-D method.

During the last 9 years a 2-D blood estimation technique titled the *transverse oscillation* (TO) method has been developed at the Center for fast Ultrasound (CFU) at the Technical University of Denmark. Two journal papers [1, 2] have been published and one master project [3] and one PhD project [4] have successfully been completed, all with the purpose of investigating the TO method. The conclusion of the previous investigations was that the TO method has the potential to be implemented in an ultrasound scanner, since the method is both fast and reliable. The problem, so far, has been the lack of a suitable scanner at CFU for the implementation of the TO method. This has changed due to the development of the experimental RASMUS scanner [5] which was completed in 2001.

1.1 The purpose of the PhD project

The main objective of the project behind this thesis has been to investigate, optimize and implement the TO method into the RASMUS scanner for both flow-phantom measurements and clinical scannings. This has been done in three steps:

- The ultrasound simulation tool Field II [6, 7] has been used to investigate and optimize the TO method in a simulated environment, where different simple blood

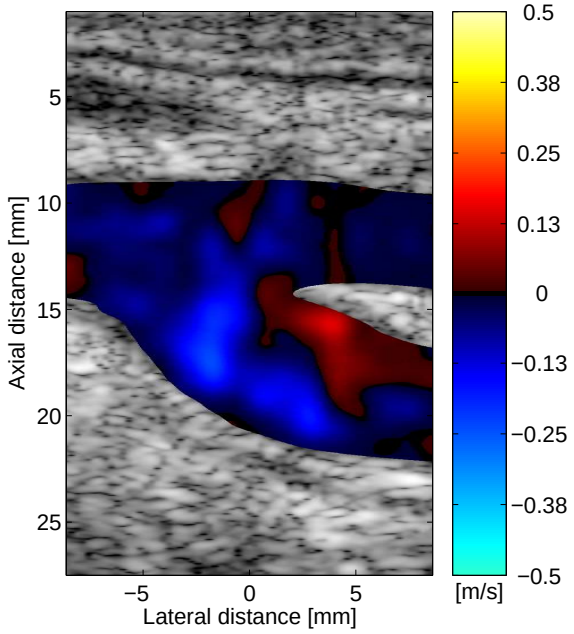

Figure 1.2: *The bifurcation in the carotid artery obtained with a conventional CFM technique*

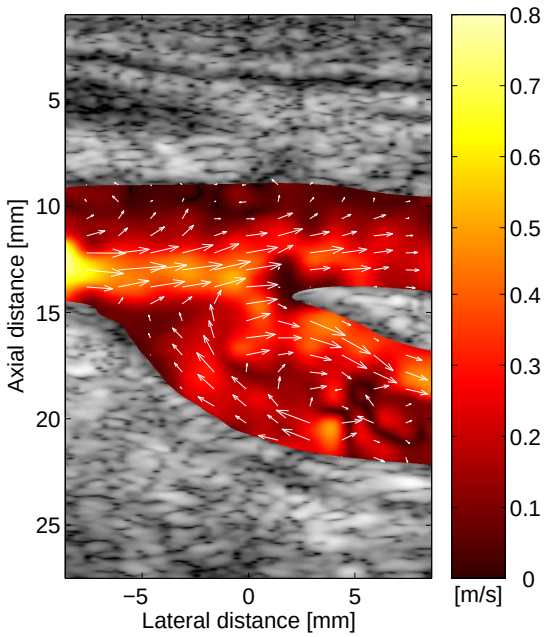

Figure 1.3: *Same as Fig. 1.2 but obtained with the 2-D vector estimation method to be discussed in this thesis.*

vessel geometries were simulated.

- The TO method has been tested and optimized in flow phantom experiments using the experimental RASMUS scanner.
- A clinical investigation has been performed using the RASMUS scanner, whith all scannings performed by experienced medical doctors.

It has been the intention that if these three goals could be successfully met, the TO method should be implemented into a commercial ultrasound scanner from the company B-K Medical - a work which has turned into a master project.

1.2 Structure of the thesis

During this PhD project a number of journal and conference papers have been written to document the research done throughout the project, and the core of this thesis consists of these papers. The thesis should therefore not be seen as a comprehensive book introducing all that is relevant to know about ultrasound used for blood velocity estimation. It is merely a document written to introduce the papers.

To achieve a readable form of the thesis, it is divided in two major parts. The first part (chapter 2,3,4) contains an introduction to the papers and the last part (chapter 5) contains the papers themselves. The structure of the thesis is thus:

Chapter 2 gives a short introduction to conventional ultrasound imaging used for blood velocity estimation. The state of the art of 2-D velocity methods is also presented in this

chapter.

Chapter 3 introduces the TO method. This is the introduction to the two journal papers and three conference papers. Furthermore the future perspectives for work with the TO method is discussed.

Chapter 4 introduces the additional two conference papers and one working paper which are not related to the TO method.

Chapter 5 contains the papers:

Udesen, J. , Jensen, J. A. , Investigation of Transverse Oscillation Method, *IEEE Transactions on Ultrasonics, Ferroelectrics and Frequency Control, 2005*. Accepted for publication.

Udesen, J. Nielsen, M. B. , Nielsen, K. R. , Jensen, J. A. , Examples of in-vivo blood vector velocity estimation, submitted to *Ultrasound in medicine and biology* in December 2005.

Udesen, J. , Jensen, J. A. , Experimental investigation of transverse flow estimation using transverse oscillation, *In Proceedings IEEE Ultrason. Symp., pp 1586-1589, 2003*

Udesen, J. , Jensen, J. A. , An In-vivo investigation of transverse flow estimation, *Proceedings of SPIE Medical Imaging meeting, Ultrasonic Imaging and Signal Processing, pp 307-314, 2004*

Udesen, J. , Nielsen, M. B. , Nielsen, K. R. , Jensen, J. A. , Blood vector velocity estimation using an autocorrelation approach: In vivo Investigation., *IEEE International Ultrasonics Symposium 2005.*

Udesen, J. , Nikolov, S. , Jensen, J. A. , A simple method to reduce aliasing artifacts in color flow mode imaging., *IEEE International Ultrasonics Symposium 2005.*

Udesen, J. , Gran, F. , Jensen, J. A. , Fast color flow mode imaging using plane wave excitation and temporal encoding, *Proceedings of SPIE Medical Imaging meeting, Ultrasonic Imaging and Signal Processing, pp 427-436, 2005.*

Udesen, J. , Gran, F. , Jensen, J. A. , A frequency splitting method for blood flow estimation., *Working paper. To be submitted in 2006.*

CHAPTER

TWO

Ultrasound used for blood flow estimation

Ultrasound used for blood flow estimation is now common practice in all modern hospitals. This development in ultrasound technology has occurred during less than 50 years, and (as this thesis hopefully may prove) important research is still carried out to extend the current methods even further.

In this chapter an introduction to the amazing history of ultrasound as a diagnostic tool for blood velocity estimation will be given as well as a discussion of the different techniques for axial 1-D blood velocity estimation. One of these techniques, the phase shift estimator, will be the subject for further investigation when a simple model of the physics behind the technique is developed. Also a description of the signal processing involved in the implementation of the estimator is given. Finally, the discussion of 1-D estimation techniques will be extended to the 2-D case, when a review of the state-of-the-art for 2-D velocity estimation techniques is given.

2.1 A brief review of ultrasound used for blood velocity estimation

The first ultrasound system for blood velocity estimation was developed in 1957 by Satomura, who used a simple continuous wave scanner working at 1 MHz [8, 9]. The method was based upon the well known Doppler effect, where a frequency change f_p between the center frequency f_0 of the emitted and received signal is observed, when the blood has a velocity component v_z along the ultrasound beam direction. The Doppler effect is governed by the relation

$$f_p = \frac{2v_z}{c} f_0 \tag{2.1}$$

where c is the speed of sound ($\sim$ 1540 m/s in human tissue). Using $v_z = 1$ m/s as a typical value for the blood velocity, this gives a frequency shift on the order of 1 kHz, i.e. frequencies detectable by the human ear. Playing the Doppler signal in a loudspeaker thus gave the medical doctor valuable information about the blood flow, and the method has proven to be so succesfull that it is still implemented in most modern scanners. However, one of the drawbacks of the continuous wave system is the lack of ability to determine the

axial position of the blood vessel under investigation. As a result of this, the pulsed wave systems emerged in the early 1970's [9].

The pulsed wave (PW) system uses a short ($\sim 1\ \mu$s) excitation pulse usually consisting of 4-8 oscillations of a sinusoid, instead of a continuous sinusoidal signal. The time difference between emission and reception at the transducer scales with the distance traveled by the pulse and the PW system therefore has the ability to determine the depth of the blood vessel under investigation. However, the method also has drawbacks compared to the continuous wave system, since the pulse repetition frequency (f_{prf}) introduces aliasing effects which limits the velocity range[10].

Different ways to estimate the blood velocity is possible within the family of PW systems. The sonogram (or Doppler mode) estimates the power spectrum as a function of time for consecutive pulses sampled at the depth of interest. This method is used when the medical doctor needs a quantitative measure of the blood velocity.

Another PW method which gives only a qualitative measure of the blood flow, is the Power Doppler (PD) method. The PD method does not estimate the velocity of the blood, but determines the power of the received signals after the contribution from tissue has been removed. When averaging of the power estimates is done over a certain time period, the presence of blood vessels can be determined. Furthermore the PD method usually superimposes a B-image of the tissue upon the blood image, thus allowing the medical doctor to see the positions of the blood vessels relative to the tissue. The result is an image easier to interpret than most other display modes.

The most sophisticated of the commonly used PW method is the color flow mapping (CFM) technique, which emerged in the early 1980's. This method, like the PD method, also superimposes a B-image of the tissue onto an image of the blood vessels, but the colors in the CFM images relate to the axial velocities in the blood vessels. The CFM method therefore combines both the quantitative measurements of the Sonogram with the 2-D performance of the PD method. However, the CFM method is only in principle quantitative in the sense that colors in the CFM image depict the axial velocity. In practice it is difficult to get a precise velocity estimate. This is illustrated in Fig. 2.1 which shows a CFM image of the carotid artery. The user has to relate the colors in the blood vessel to the colors in the color-bar from which the velocity can be read.

The CFM technique uses a so called phase shift estimator to derive the axial velocity. The basic physical concepts governing this phase shift estimator are in the literature often referred to as the "Doppler effect"[1] due to the presence of an equation in the estimator similar to (2.1). However, as it now will become apparent, the Doppler effect does not play a significant role in the physics governing a phase shift estimator.

2.2 A simple model of a phase shift system

The model is based on the assumption of linearity of the ultrasound transducer as well as linearity of the propagation of ultrasound in the medium. If the linearity criteria is satisfied, the received signal from a collection of red blood cells can be regarded as the

[1] See e.g. [11]

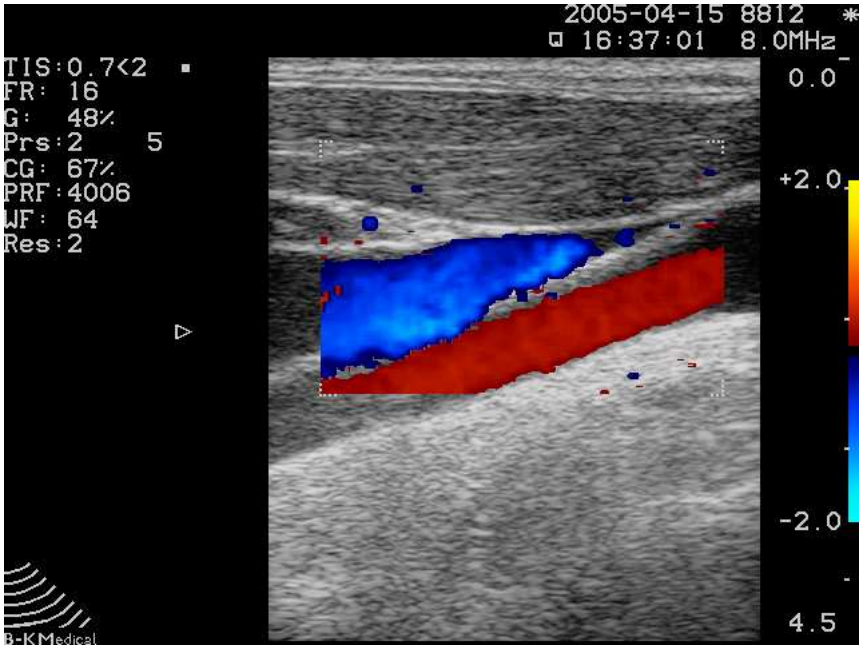

Figure 2.1: *A CFM image showing the blood flow in the carotid artery and the jugular vein. Blue color indicates flow towards the transducer and red color indicates flow away from the transducer.*

sum of the received signals from individual scatters. Instead of having a model with N scatters where $N \gg 1$ it is possible to formulate the model with only one moving scatter. Due to the principle of linearity the model will then also be valid for N scatters [9].

Assume that a red blood cell is positioned at a point $R = (0, 0, z_0)^T$ in space and moving with velocity $V = (v_x, v_y, v_z)^T$ as shown in Fig. 2.2. The task is now to formulate a model which determines v_z as a function of known variables.

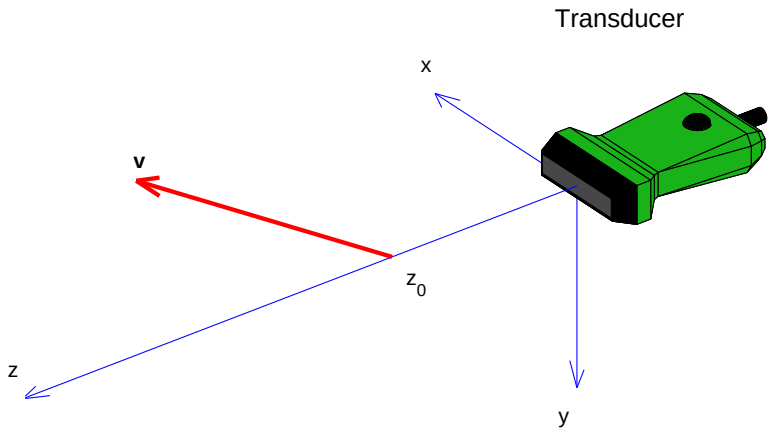

Figure 2.2: *The geometry of the model. A red blood cell is positioned at depth z_0 and moving with velocity* $\mathbf{v} = (v_x, v_y, v_z)^T$

An ultrasound transducer is situated at origo from where it emits consecutive focused

ultrasound pulses along the z-axis with a time interval $1/f_{prf}$ between pulses. The center frequency of each pulse is f_0 and the time duration T. The emitted signal $e(t)$ will then be given by,

$$e(t) = B(t;T)\sin(2\pi f_0 t), \tag{2.2}$$

where B is the *Boxcar* function which is one in the time interval $0 < t < T$ and zero elsewhere. For the purpose of simplicity $B(t;T)$ will be ignored in the following derivation.

A part of the energy of each emitted pulse is reflected from the red blood cell and received by the transducer at time t_0. After reception the signals are delay-and-sum beamformed, and one signal trace is constructed from each pulse emission. This is shown in Fig. 2.3, where each horizontal signal corresponds to one beamformed line.

One received beamformed signal from the red blood cell can be written as[2],

$$r(t) \quad = \quad a\sin(2\pi f_0'(t-t_0)), \tag{2.3}$$

where a is a scaling constant, which will be ignored in this model. Since the depth z of the beamformed signal is related to the time of arrival of the echo by the relation[3]

$$\frac{2z}{t} = c, \tag{2.4}$$

where c is speed of sound, (2.3) can be expressed in the spatial domain as

$$r(z) \quad = \quad \sin\left(2\pi f_0' \frac{2(z-z_0)}{c}\right). \tag{2.5}$$

Note that the emitted pulse had a center frequency f_0, which is changed to f_0' in equation 2.5. This is due to the Doppler effect, which relates the difference between the emitted frequency and the received frequency through 2.1.

When the blood cell is moving towards or away from the transducer, i.e. $|v_z| > 0$, the echo from the blood cell will be received at different times at the transducer. E.g. if the blood cell is moving away from the transducer the signals will be shifted in space with an amount given by[4] $\Delta z = v_z/f_{prf}$. The n'th received signal will therefore be given by

$$r_n(z) \quad = \quad \sin\left(2\pi f_0' \frac{2(z-z_0+n\Delta z)}{c}\right) \tag{2.6}$$

$$\quad = \quad \sin\left(2\pi f_0' \left(\frac{2(z-z_0)}{c} + n\frac{2v_z}{c\,f_{prf}}\right)\right). \tag{2.7}$$

[2]This signal is often called the *fast time signal* due to the sampling frequency f_s which usually is ~ 50 MHz in a typical scanner.

[3]The scaling with "2" is due to the sound which has to travel back and forth between the transducer and the blood cell.

[4]The effect of movement in the other two directions ($|v_x| > 0$, $|v_y| > 0$) will generally be much less significant due to lack of oscillations in the ultrasound pulse in these directions - an issue which will be discussed in the next chapter.

Sampling of this signal at depth z_0 results in a signal[5] $p_{z_0}(n)$

$$p_{z_0}(n) = \sin\left(2\pi f_0'\left(\frac{2(z_0 - z_0)}{c} + n\frac{2v_z}{c\, f_{prf}}\right)\right) \tag{2.8}$$

$$= \sin\left(2\pi \underbrace{\frac{2v_z}{c} f_0'}_{f_p} \frac{1}{f_{prf}} n\right), \tag{2.9}$$

where the oscillation frequency f_p of $p_{z_0}(n)$ will be

$$f_p = \frac{2v_z}{c} f_0'. \tag{2.10}$$

Equation 2.10 relates the axial velocity v_z to the frequency of the sampled signal $p_{z_0}(n)$. It is similar to the famous "Doppler relation" for waves (equation 2.1). However, the Doppler effect does not play any role in the derivation of equation 2.10 except for the scaling of f_0, which is changed to f_0'. It is important to understand that it is not this change in frequency due to the Doppler effect that is measured in a pulsed echo ultrasound system, but the change in phase of the received signal.

If the scaling of f_0 due to the Doppler effect were to be measured, it would indeed be a very difficult task. Typical values for the Doppler shift in blood velocity estimation are (as mentioned in the previous section) on the order of 1/1000 of f_0. Frequency dependent attenuation does also shift the frequencies by a comparable value [9], and it would therefore be nearly impossible to distinguish between these two effects.

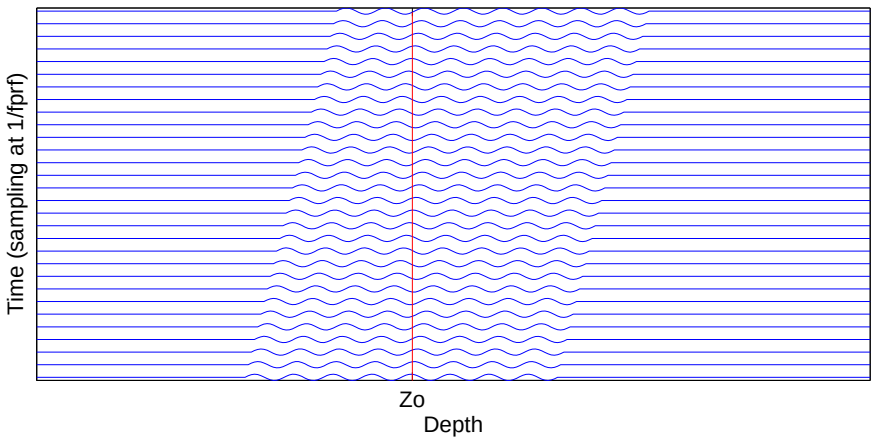

Figure 2.3: *The received and beamformed signals from a red blood cell starting at depth z_0 and moving away from the transducer. The sampling frequency of the ultrasound system is $f_s \sim$ MHz, and the time between each pulse firing is $1/f_{prf}$ where $f_{prf} \sim$ kHz*

[5] This signal is often called the *slow time signal* due to the sampling frequency f_{prf} which is approximately 10^{-3} of the scanners sampling frequency f_s.

2.3 Implementation and performance of a phase shift system

The simple model of the phase shift system illustrates the basic physics involved. However, in a real ultrasound scanner different kinds of signal processing algorithms have to be applied to improve the velocity estimates[6]:

- The signals from individual channels of the scanner are matched filtered with the transmitted pulse to improve signal-to-noise-ratio (SNR).
- To identify the direction of the flow (towards or away from the transducer) an analytical signal is constructed by Hilbert transforming the fast time signal. The imaginary part of the signal will then be 90° phase shifted in the axial direction compared to the real part.
- To seperate stationary tissue from moving blood the slow time signals are echo canceled using an appropriate high pass filter.
- An estimator algorithm is applied to the echo canceled slow time data to find the axial velocity. Depending on the type of scanning mode (i.e. power Doppler, CFM imaging or sonogram) different types of algorithms exists. For CFM imaging the autocorrelation method [12] is mostly used. The autocorrelation method finds the mean velocity from the slow-time signal by estimating the phase of the lag one autocorrelation value of the slow-time signal [9].

If these signal processing steps are carefully implemented in the ultrasound scanner, the autocorrelation algorithm will yield velocity estimates which can be used for diagnostic purposes. To get an impression of the performance of such a scanner the velocity was estimated in a circulating flow rig using the RASMUS scanner together with a linear array transducer from B-K medical and the autocorrelation algorithm. All relevant parameters concerning the setup can be found in Table 2.1.

The mean axial velocity profile and the corresponding standard deviation is shown in Fig. 2.4, where the thick black curve represents the theoretical parabolic profile. Two numbers which (to some extent) can be used to characterize the performance are the scaled mean standard deviation over the vessel $\tilde{\sigma}_{v_z}$ and the scaled mean absolute bias $\tilde{B}_{v_z}$. The two non-dimensional numbers are defined as

$$\tilde{\sigma}_{v_z} = \frac{1}{v_0(z_2 - z_1)} \int_{z_1}^{z_2} \sqrt{\frac{1}{M} \sum_{i=1}^{M} \left(\hat{v}_z^i(z) - \bar{v}_z(z)\right)^2} dz \tag{2.11}$$

$$\tilde{B}_{v_z} = \frac{1}{v_0(z_2 - z_1)} \int_{z_1}^{z_2} |\bar{v}_z(z) - v_z(z)| \, dz \tag{2.12}$$

where $\hat{v}_z^i(z)$ is the i'th velocity estimate at a certain depth z, $\bar{v}_z(z)$ is the mean of the velocity estimates, and $v_z(z)$ is the actual parabolic velocity. z_1 and z_2, respectively, are the depth to the beginning of the vessel and the end of the vessel, and M is the number

[6] It is out of the scope of this thesis to give a comprehensive description of these methods. The interested reader can find such in Jensen(1996)[9] or Evens(1989)[10]

Table 2.1: *Experimental setup for RASMUS scanning.*

Parameter	Value
Transducer	Linear array
Active number of elements	64
Pitch	0.208 mm
Kerf	0.035 mm
Center frequency	8 MHz
Number of cycles pr. pulse	8
f_{prf}	4 KHz
Sampling frequency	40 MHz
Transmit and receive apodization	Hanning
Focus in transmit	40 mm
Focus in receive	Dynamic
Artificial blood vessel	heat shrinking material
Radius of vessel	6.0 mm
Vessel axial center position	42 mm
Angle between beam and vessel	70°
Type of flow	parabolic
Center velocity	0.4 m/s
Reynolds number	< 2000
Shots per velocity estimate	16
Velocity estimates	12
Echo canceling	Mean value subtraction

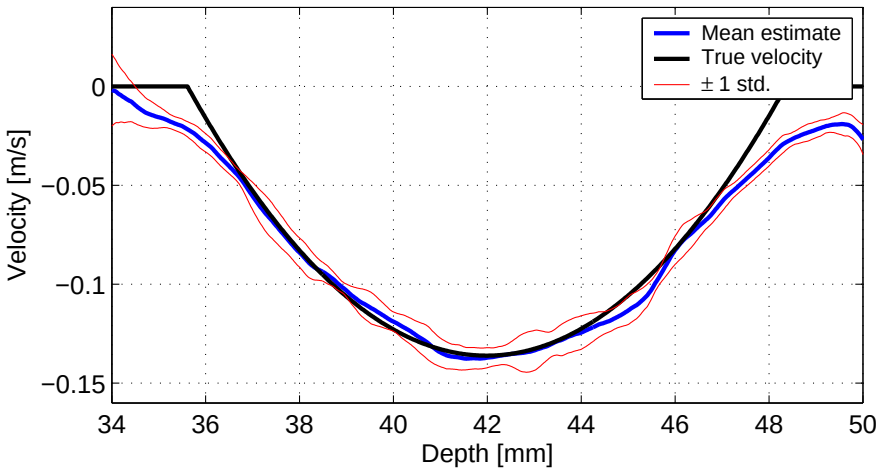

Figure 2.4: *An example of the performance of the autocorrelation estimator using the RASMUS scanner when 16 pulse emissions are used for each velocity estimate. The thick black curve is the theoretical parabolic profile. The thick blue curve is the mean of the 12 estimates, and the thin red curves indicate* ± 1 *standard deviation.*

of velocity estimates $\hat{v}_z^i(z)$ used to calculate $\tilde{\sigma}_{v_z}$ and $\tilde{B}_{v_z}$. For the measurement presented in Fig. 2.4 these numbers are $\tilde{\sigma}_{v_z} = 1.5\%$ and $\tilde{B}_{v_z} = 1.2\%$. When other measurements

are presented later in this thesis, it will be apparent that these values characterize a good performance at this angle of flow.

2.4 Previous work on estimating the 2-D vector velocity

So far the discussion has been limited to the case in which only the axial velocity along the beam direction has been estimated, i.e. the estimation is said to be 1-dimensional. But for the rest of this thesis the focus will be on estimating the 2-D vector velocity, i.e. the components (v_x, v_z) shown in Fig. 2.2. Such estimation techniques have been the subject of investigation for many authors during the years, and it is the purpose of this section to give a brief review of their work.

2.4.1 The crossing beam method

The 2-D vector method first proposed by Fox et al.[13] is perhaps the 2-D method that mostly resembles the 1-D case. The original idea was to use two crossing transmit beams and one receive beam to estimate the velocity at the point of the beam crossing. This approach is not very flexible, and only a relative small angle between the beams can be obtained. However, other variants of the crossing beam method are possible. If a larger angle between the two beams is desired, the transmitting apertures can also be used in receive, so that the transducer works in a phased array fashion, with crossing beams. Then the velocity is estimated at the position of the beam crossings. However, this approach is still cumbersome since a large number of pulse emissions has to be performed to cover the whole region of interest.

Alternatively one transmit aperture and two receive apertures can be used [14]. This method is more flexible, since the rotation of the pulse-echo field is done solely in the receive beamforming. The method can therefore (in principle) estimate the 2-D vector velocity in the region of interest from the same number of pulse emissions as the conventional 1-D method. Furthermore, the process of removing stationary echoes originating from tissue (echo-canceling) is significantly more simple for this method compared to most other 2-D methods, since the echo-canceling can be performed separately on each received beam.

One of the major drawbacks of the crossing beam method (whether the crossing beams are constructed in transmit or receive beamforming) is the fact that the performance depends on the angle between the two beams, and the angle is limited by the width of the transducer. If a blood vessel deep inside the body is to be scanned, the angle thus becomes small, and the 2-D velocity estimates will degrade significantly. However, even with this limitation, which in some way is present in all 2-D methods, it is the author's opinion that the basic principle in the crossing beam method is healthy. The physics behind the method is simple and echo-canceling can easily be applied - properties which are not present in all of the 2-D methods.

2.4.2 Spectral width estimation

Newhouse et al. [15] proposed a 2-D method in which the spectral width of the Doppler spectrum was used to determine the lateral component v_x of the velocity. The method uses the fact that the lateral component of the pulse-echo field at the focal point is approximately a scaled version of the Fourier transform of the convolution between the transmit and receive apodization; a property which will be extensively discussed in the next chapter. The method is very interesting from a signal processing point of view due to the beautiful mathematics involved. But unfortunately the core of the method relies on several weaknesses. First of all the method is absolute in the sense that the width of the spectrum has to be determined. If noise is present, this estimation might be difficult, since it has to be decided at which amplitude level the width of the spectrum should be estimated. Furthermore, if large velocity gradients are present within the resolution volume of the system, e.g. when a small vessel is scanned, the Doppler spectrum will be broad even in cases where no lateral velocity component is present.

2.4.3 Speckle tracking

A more fruitful approach is 2-D speckle tracking first proposed by Trahey et al. [16]. The idea is to obtain a number of consecutive B-mode images of the region of interest. After echo-canceling of the B-mode images the 2-D velocity vector can be found by 2-D cross correlating the B-mode images. The spatial displacement is then proportional to the position of the maximum lag of the correlation. Dividing this displacement with the time between images then gives the magnitude of the 2-D vector velocity.

This method is simple and has a higher axial resolution than other 2-D methods based on phase shift estimation due to the lower number of oscillations in the emitted pulse. However, as it is the case with most 2-D methods, severe drawbacks are also present. First of all it is not a straight forward task to do echo canceling on a broad band slow-time signal, since the tissue component and the blood component will overlap at small velocities. Furthermore, the echo-canceling is complicated by the asymmetry of the pulse echo field - a problem present in most 2-D methods [17, 18].

Another problem of the speckle tracking method is the acquisition speed of the B-mode images to be correlated. If e.g. the heart is to be scanned with this method, the blood speckle pattern in one of the B-mode images will be blurred in lines following the blood motion and the velocity estimates will consequently be poor. Finally, the problem of computation time also has to be considered. The 2-D cross-correlation involves significantly more computations than e.g. an 1-D autocorrelation estimator - an issue that might not concern the research minded engineer. But the company producing scanners will most likely find this issue a major limitation to the method.

It should be noted that a qualitative 2-D method called *B-flow* or *BMI* has been successfully implemented in commercial scanners [19]. The method is basicly the same as the speckle tracking methods only without the final velocity estimation step. The echo-canceled B-mode images are displayed, so an impression of the blood movement is obtained by the user.

2.4.4 Directional beamforming

An interesting 2-D method close to the speckle tracking approach just discussed is the method of *directional beamforming* proposed by Jensen [20]. The method is based on beamformed lines along the flow direction, and uses 1-D cross-correlation on consecutive lines to find the spatial displacement. Dividing this displacement with the time between each beamformed line then gives the velocity. The problem here is, of course, that the angle of flow must be known in advance before the velocity can be estimated. This obstacle has been solved by correlating lines at different angles. The angle along the flow direction will then be characterized by having the highest correlation coefficient.

This method has been successfully implemented for both focussed beams [21] and synthetic aperture flow [22]. The resulting velocity estimates has a standard deviation and bias significantly lower than the corresponding values from the TO method described in this thesis. However, also the *directional beamforming* method has limitations. The correlation length of each line is ~ 1 mm, which causes problems around vessel borders, where the lines will cross the tissue. Also the echo-canceling is difficult due to the asymmetry of the point spread function. Last but not least it imposes heavy computational demands on the beamformation.

CHAPTER

THREE

The TO method

This chapter presents the TO method for 2-D velocity estimation. The method is basicly an extension of the 1-D phase shift system using an autocorrelation estimator to the 2-D case, and the basic idea is therefore to create

1. a pulse echo field, which oscillates in both the lateral and the axial direction.
2. in-phase and quadrature signals each 90° phase shifted both in the axial and lateral direction.
3. an echo-canceling filter which is applied on the slow-time signals to remove signals originating from stationary tissue.
4. a velocity estimator based on the autocorrelation technique which calculates the axial velocity v_z and the lateral velocity v_x from the two complex slow-time signals.

The TO method is thus seen to consist of seperate parts, which together form the complete method. These parts are discussed separately in the following sections[1].

3.1 The pulse-echo field

One of the basic results from theoretical ultrasound states, that the pulse-echo field can be described as the product of two seperate fields: the transmit field and the receive field [8]. The main difference between these two fields is that the receive field is much more flexible, due to the fact that the focus and apodization can be adjusted dynamically. This flexibility is not present in the transmit field, where only a fixed focus and fixed apodization can be applied.

Due to the flexibility of the receive field the double oscillation in the pulse echo field of the TO method is solely constructed by manipulating the receive field. It should therefore be emphasized that **the transmitted field of the TO method is exactly the same as a conventional transmitted field for an ultrasound system using an 1-D autocorrelation estimator**.

[1] A method very similar to the TO method called *spatial quadrature* has been developed by Anderson. The spatial quadrature method will not be discussed in this thesis, but the interested reader can find a comprehensive description in the papers [23, 24]

3.1.1 A simple model of the transverse oscillation

The basic principle behind the double oscillating receive field can be observed if two stones are dropped simultaneously into a pond. Two spherical waves will propagate outwards and interfere with each other creating a pattern like the one shown in Fig. 3.1. At the region of inteference between the two waves, an oscillation is present both in the axial and lateral direction.

The curious experimentor will observe some interesting properties of the waves if the experiment is repeated. The lateral oscillation wavelength of the inteference pattern can be controlled by changing the distance between the two stones. If the lateral distance between the two stones is small the observed lateral wave length will be large and visa versa. Furthermore, if the two stones has small diameters the lateral oscilation will be well defined i.e. the lateral frequencies will be narrow band, and visa versa if the stones are large.

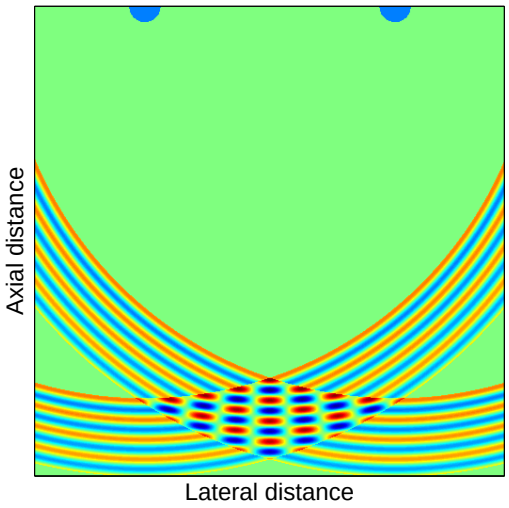

Figure 3.1: *Illustration of the interference field from two stones dropped in a pond. The two blue dots indicate the positions of the stones.*

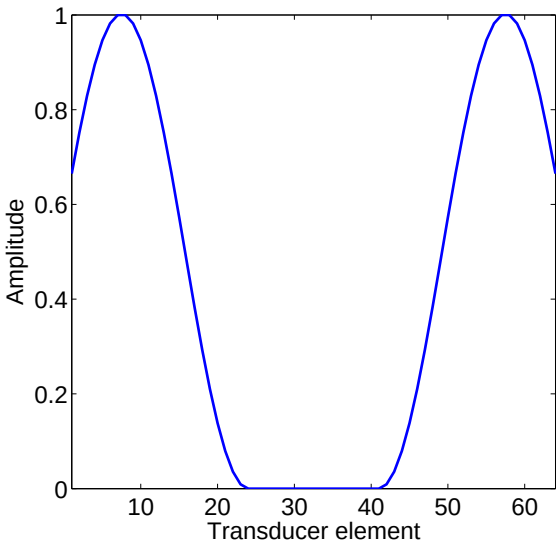

Figure 3.2: *The receive apodization used to create a double oscillating field.*

Even though this two-stones-in-a-pond model does not involve ultrasound waves, it can be directly used in an ultrasound context. If the receive apodization[2] function of the ultrasound transducer is divided into two disconnected parts as shown in Fig. 3.2, each part will resemble the stone in the pond, and the resulting pulse echo field will oscillate both in the axial and lateral direction.

So far these considerations have been solely qualitatively and only based upon Fig. 3.1. To give the two-stones-in-a-pond model a more solid ground it is therefore necessary to give a quantitative derivation of the model.

Assume that two point sources are separated a distance L in space, and that each point source emits a spherical wave with angular frequency ω and k-vector k. The task is now to derive a simple expression for the pressure P at a certain point in space and time (R, θ, t),

[2] The apodization is the sensitivity along the transducer surface.

where (R,θ) is the cylindrical coordinates of the point and t is time. The geometry of the problem is depicted in Fig. 3.3.[3] If both point sources are emitting spherical waves in

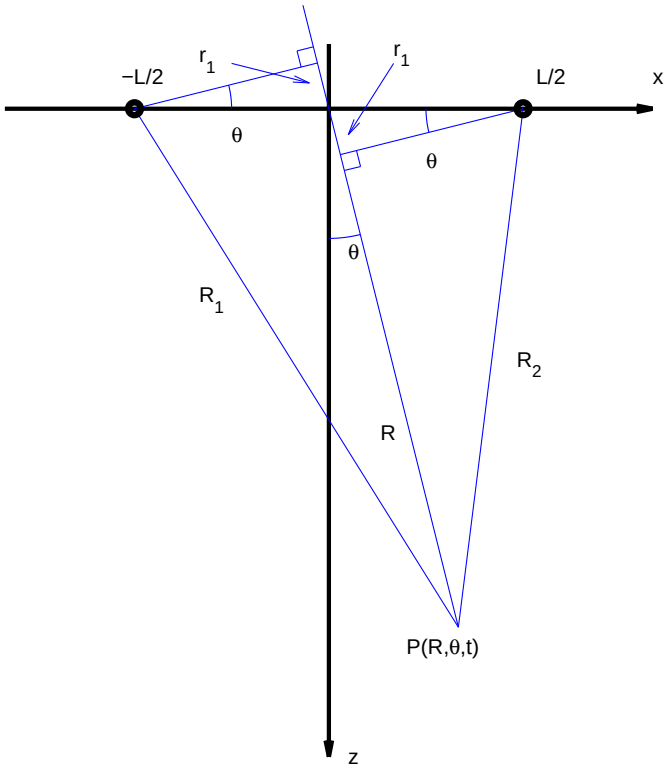

Figure 3.3: *The pressure P from two point sources is derived at the point* (R,θ).

phase with an amplitude A, the complex pressure at time t at the spatial position (R,θ) is given by

$$P(R,\theta,t) = \frac{A}{R_1}e^{j(\omega t-kR_1)} + \frac{A}{R_2}e^{j(\omega t-kR_2)}. \tag{3.1}$$

This expression is an exact description of the pressure but also far too complicated in terms of the number of variables involved. However, it can be simplified further by using some geometric approximations on R_1, R_2 and θ.

Assume that the point of interest is situated far from the two point sources, so that $R \gg L$ and furthermore $\theta \ll 1$. The error made by exchanging R_1 and R_2 with R in the denominators of (3.1) will then be small compared to the actual pressure at point (R,θ,t). However, this approximation cannot be used for R_1 and R_2 in the exponentials of (3.1), since the phase can chance rapidly over small distances and time intervals. In the exponentials of (3.1) the following approximations are made

$$\begin{aligned} R_1 &\approx R + r_1 \\ &= R + \frac{L}{2}\sin\theta \end{aligned} \tag{3.2}$$

[3]This section describes a special case of "the continuous line source" which is derived in [25]

$$
\begin{aligned}
R_2 &\approx R - r_1 \\
&= R - \frac{L}{2}\sin\theta. \qquad (3.3)
\end{aligned}
$$

Substituting these expressions into 3.1 yields

$$
\begin{aligned}
P(R,\theta,t) &= \frac{A}{R}e^{j(\omega t - kR - k\frac{L}{2}\sin\theta)} + \frac{A}{R}e^{j(\omega t - kR + k\frac{L}{2}\sin\theta)} \qquad (3.4)\\
&= \frac{A}{R}e^{j(\omega t - kR)}\left[e^{-j(k\frac{L}{2}\sin\theta)} + e^{j(k\frac{L}{2}\sin\theta)}\right] \qquad (3.5)\\
&= \frac{2A}{R}e^{j(\omega t - kR)}\cos\frac{kL\sin\theta}{2}, \qquad (3.6)
\end{aligned}
$$

where the complex definition of the cosine function has been used. Since it was assumed that $\theta \ll 1$, it follows that

$$
\sin\theta \approx \tan\theta = \frac{x}{z}, \qquad (3.7)
$$

where (x,z) are the Cartesian coordinates of the point (R,θ). Furthermore we have that $k = 2\pi/\lambda$, where λ is the wave length of the emitted pressure field. The pressure can then be written as

$$
P(x,z,t) \approx \frac{2A}{R}e^{j(\omega t - kR)}\cos 2\pi \underbrace{\frac{L}{2\lambda z}}_{1/\lambda_x} x. \qquad (3.8)
$$

The first term in this expression is simply the pressure field from one point source situated at $R = 0$ having a field strength equal to twice the strength of each point sources. The cosine term in (3.8) describes the lateral oscillation in the field resulting from the two point sources, and the spatial oscillation wave length λ_x will be given by

$$
\lambda_x = 2\lambda\frac{z}{L}. \qquad (3.9)
$$

This relation gives valuable informations about how to adjust the position of the two point sources to get a desired oscillation at the field point (x,z). To get a small oscillation length λ_x in the lateral field, the distance L between the two point sources has to be large. Hence, a wide ultrasound transducer has to be used if such a field is desired.

3.1.2 An advanced model

The simple model just derived is in fact only a part of a much more general principle from theoretical acoustics and optics. This principle states, that the Fourier transform[4] of the apodization function $a(x)$ gives the lateral component of the field in the focal point $(0,0,z_0)$ and in the far field. This relation is known as the Fraunhofer diffraction pattern

[4]It should be noted that the Fourier integral in (3.10) is preceded by a quadratic phase factor also involving the x_0^2. The relation can therefore only be interpreted as a Fourier transform for small values of x_0^2/z_0.

and is given by [26]

$$P(x_0,z_0) = \frac{e^{\frac{j\pi x_0^2}{z_0}}}{j\lambda z_0}\int_{-\infty}^{\infty} a(x)e^{-\frac{j2\pi x x_0}{\lambda z_0}}\,dx \tag{3.10}$$

$$= \frac{e^{\frac{j\pi x_0^2}{z_0}}}{j\lambda z_0}\mathcal{F}\left\{a_t\left(\frac{x}{\lambda z_0}\right)\right\} \tag{3.11}$$

The result from (3.8) could therefore also have been derived using (3.10), and the two point sources would have corresponded to an apodization function $a(x)$ consistent of two delta functions. Taking the Fourier transform of two delta functions yields a cosine - a result which is seen to be equivalent with (3.8).

3.1.3 The resulting pulse-echo field

So far the discussion has been limited to the receive field, but (3.10) applies equally well for both the transmit P_t and the receive P_r ultrasound field at the focal point. Denoting the transmit apodization function by a_t, the receive apodization function by a_r and the lateral component of the pulse-echo field at the focal point by P_{tr} yields [27, 8]

$$\begin{aligned} P_{tr} &= P_t P_r \\ &= \mathcal{F}\{a_t\}\,\mathcal{F}\{a_r\} \\ &= \mathcal{F}\{a_t * a_r\} \\ &= \mathcal{F}\{a_{tr}\}, \end{aligned} \tag{3.12}$$

where $\mathcal{F}$ denotes the Fourier transform, and $a_{tr} = a_t * a_r$ is called the effective aperture. It follows directly from (3.12), that if

$$a_t(x) = \delta(x), \quad a_r(x) = \delta(x-x_c) + \delta(x+x_c), \tag{3.13}$$

where x_c denotes the position on the transducer of the delta function, the lateral component of the pulse-echo field will be a cosine, and the oscillation length will be given by (3.9).

In practice delta functions are not realizable as apodization functions on an ultrasound transducer due to the low SNR, which would result from using only two elements, and also because the focusing would be poor. Instead *Hanning* functions are used as depicted in Fig. 3.2. This results in a less well defined lateral oscillation frequency, but SNR increases, and receive focusing is possible. The resulting pulse-echo field can easily be investigated with the simulation program Field II. Using the setup from Table 3.1, where the transmit apodization is a *Hanning* function covering 18 elements, and the receive apodization is two half *Hanning* function each 32 elements wide as shown in Fig. 3.2, gives the double oscillating pulse-echo field shown to the left in Fig. 3.4. Note that this setup of transducer and scanner is the same as used for the in-vivo investigation of the TO method.

Taking the 2-D FFT (fast Fourier transform) of the pulse-echo field yields the amplitude spectrum shown to the right in Fig. 3.4. Here four peaks are positioned at ± 5 MHz and $\sim \pm 1$ mm^{-1}. The peaks at 5 MHz are a result of the center frequency of the emitted pulse, and the peak at ± 1 mm^{-1} is a result of the receive apodization function.

Table 3.1: *Setup for the TO method. These parameters are also used for the in-vivo investigation of the TO method.*

Parameter	Value
Transducer	Linear array
Active number of elements	64
Pitch	0.300 mm
Kerf	0.035 mm
Center frequency	5 MHz
Number of cycles per pulse	8
f_{prf}	6 KHz
Sampling frequency	40 MHz/100 MHz
Transmit apodization	Hanning
F-number in transmit	3.3
Focus in transmit	18 mm
Receive apodization	two Hanning windows
Width of each Hanning in receive	32 el.
Lateral wave length at focus	0.96 mm
Focus in receive	Dynamic

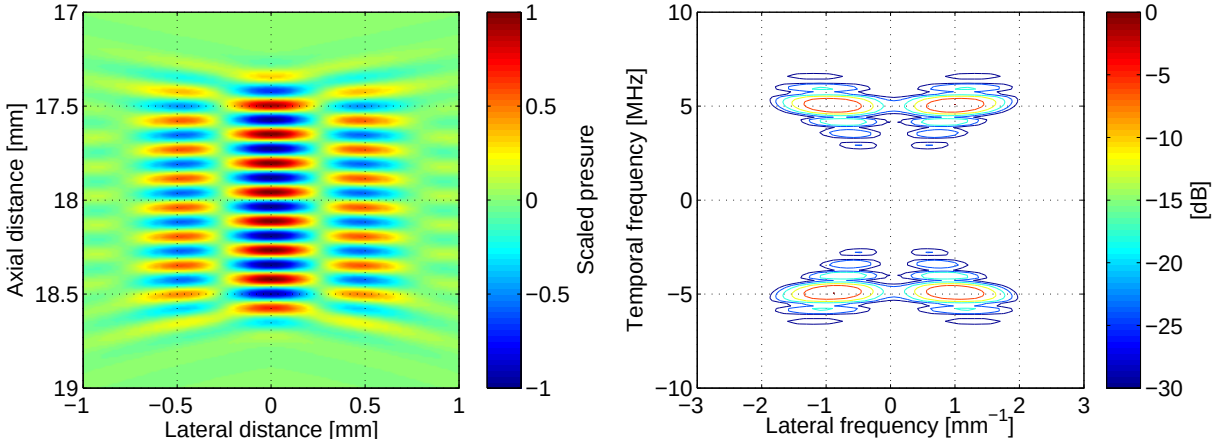

Figure 3.4: *Left: The pulse echo field (PSF) for the TO method. Right: the 2D-Fourier transform of the pulse-echo field. Note that the shape of the lateral component of the spectrum is the same as the effective aperture - a result which is of great importance for the TO method and subject for further discussions in the following sections.*

3.2 The in-phase and the quadrature signals

The double oscillating pulse-echo field shown in Fig. 3.4 will result in a slow-time signal where an oscillation is present if the blood is moving. This will be the case even if the angle between the beam and the flow is 90°. However, it will not be possible to determine, whether an oscillation in the slow time signal is a result of axial or lateral movement of the blood.

This can be illustrated by assuming that one blood scatterer travels with velocity $v = (v_x, v_z)$ through the pulse-echo field. Assuming monocromatic spatial frequencies the resulting slow time signal $r(n)$ can then be modeled as

$$r(n) = \cos\left(2\pi \frac{v_x}{\lambda_x f_{prf}} n\right) \cos\left(2\pi \frac{v_z}{\lambda_z f_{prf}} n\right), \tag{3.14}$$

where $\lambda_z = \lambda/2$ is the axial wave length. This equation has two unknowns (v_x and v_z), and it is therefore insolvable unless some further information is gathered.

One way to gather further information to the model is to use the method of in-phase and quadrature signals, which is also applied in a conventional phase shift system, where the two signals are 90° phase shifted with respect to each other usually by applying a *Hilbert* transform. If the two velocity components in the TO method are to be uniquely estimated (within the aliasing limit), four in phase and quadrature signals have to be constructed so that,

$$\begin{aligned}
r_a(n) &= \cos\left(2\pi \frac{v_x}{\lambda_x f_{prf}} n\right) \cos\left(2\pi \frac{v_z}{\lambda_z f_{prf}} n\right) \\
r_b(n) &= \sin\left(2\pi \frac{v_x}{\lambda_x f_{prf}} n\right) \cos\left(2\pi \frac{v_z}{\lambda_z f_{prf}} n\right) \\
r_c(n) &= \cos\left(2\pi \frac{v_x}{\lambda_x f_{prf}} n\right) \sin\left(2\pi \frac{v_z}{\lambda_z f_{prf}} n\right) \\
r_d(n) &= \sin\left(2\pi \frac{v_x}{\lambda_x f_{prf}} n\right) \sin\left(2\pi \frac{v_z}{\lambda_z f_{prf}} n\right).
\end{aligned} \tag{3.15}$$

In practice the four slow-time signals r_a, r_b, r_c, r_d are constructed by focusing two beams in receive, where the lateral displacement between the beams corresponds to $\lambda_x/4$ i.e a 90° phase shift. The resulting two fast-time signals are thereafter *Hilbert* transformed to yield the phase shift in the axial direction, and finally the signals are sampled at the depth of interest. The procedure is illustrated in Fig. 3.5.

3.3 Echo canceling

Before the four slow-time signals r_a, r_b, r_c and r_d can be used to estimate the vector velocity, the contribution from slowly moving tissue has to be removed from the signals, i.e. echo-canceling has to be performed. This is necessary since the amplitude of signals originating from tissue can be up to 40 dB higher than the amplitude of the blood signals [9]. In a conventional phase shift system echo-canceling is usually done by applying a highpass filter on the slow-time signal [9], but other more advanced approaches have also been suggested [28, 29].

Echo-canceling for 2-D velocity estimation is significantly more complex than in the conventional 1-D case [17, 18]. This can be illustrated with an example. Assume that a blood scatterer travels through the pulse-echo field shown in Fig. 3.4 with velocity $v_0 = 0.225$ m/s, $f_{prf} = 6$ kHz, and the angle between flow and beam is varied between 0° and 90°. The corresponding slow-time signals can be found by sampling the pulse-echo field, and

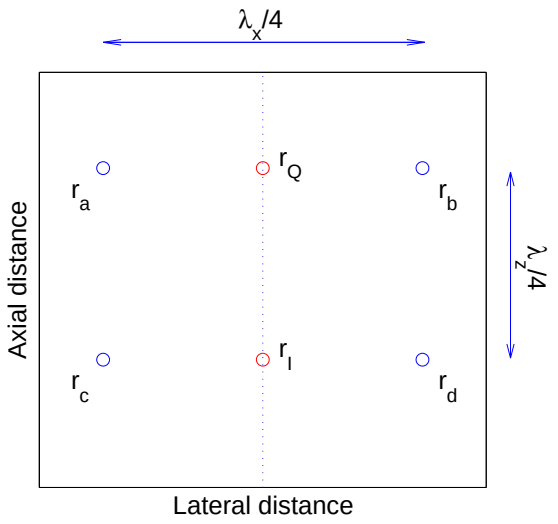

Figure 3.5: *The receive focusing of the TO method. The dotted line indicates the center line of the transmit beam, and the conventional in-phase and quadrature signals are sampled at r_I and r_Q.*

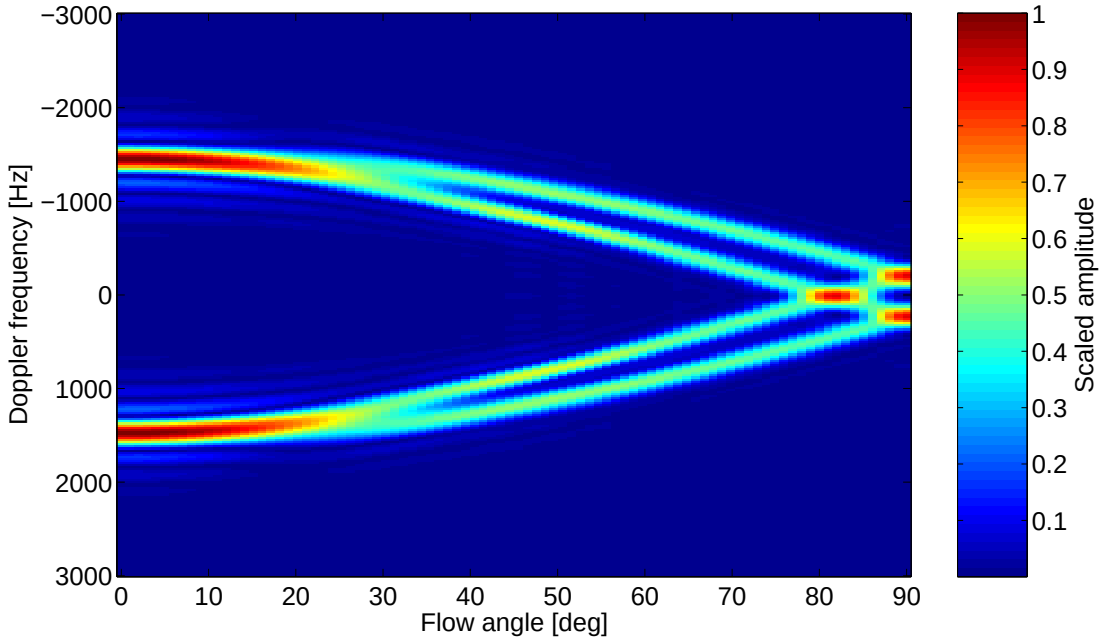

Figure 3.6: *The amplitude spectrum of the slow-time (Doppler) signal as a function of flow angle.*

the amplitude spectrum of the slow-time signals is shown in Fig. 3.6.

A number of interesting conclusions can be drawn from Fig. 3.6. At 90° flow the amplitude spectrum is seen to consist of two peaks which have the same shape as the effective aperture. This observation can be confirmed by taking the Fourier transform with respect

to spatial distance of (3.12). This yields [26]

$$\mathcal{F}\{P_{tr}(x_0)\} = \mathcal{F}\left\{\frac{e^{\frac{j\pi x_0^2}{z_0}}}{j\lambda z_0}\int_{-\infty}^{\infty} a_{tr}(x)e^{-\frac{j2\pi x x_0}{\lambda z_0}}dx\right\} \tag{3.16}$$

$$= (A\lambda z)a_{tr}(-\lambda z f_x). \tag{3.17}$$

where A is a scaling constant. This result is illustrated in Fig. 3.7 where the curves for the apodization functions a_t, a_r and the effective aperture a_{tr} are shown. For comparison also the Fourier transform of the PSF with respect to lateral distance is shown when the spatial frequency variable f_x has been multiplied with λz. The shapes of $a_{tr}(x)$ and $\mathcal{F}\{P_{tr}(x_0)\}|_{\lambda z f_x}$ are nearly identical although there is a bias of $\sim 15\%$ between the position of the peaks for $a_{tr}(x)$ and $\mathcal{F}\{P_{tr}(x_0)\}|_{\lambda z f_x}$. It should be expected that this bias will show up as an under estimation of the lateral velocity. From Fig. 3.6 it can be seen

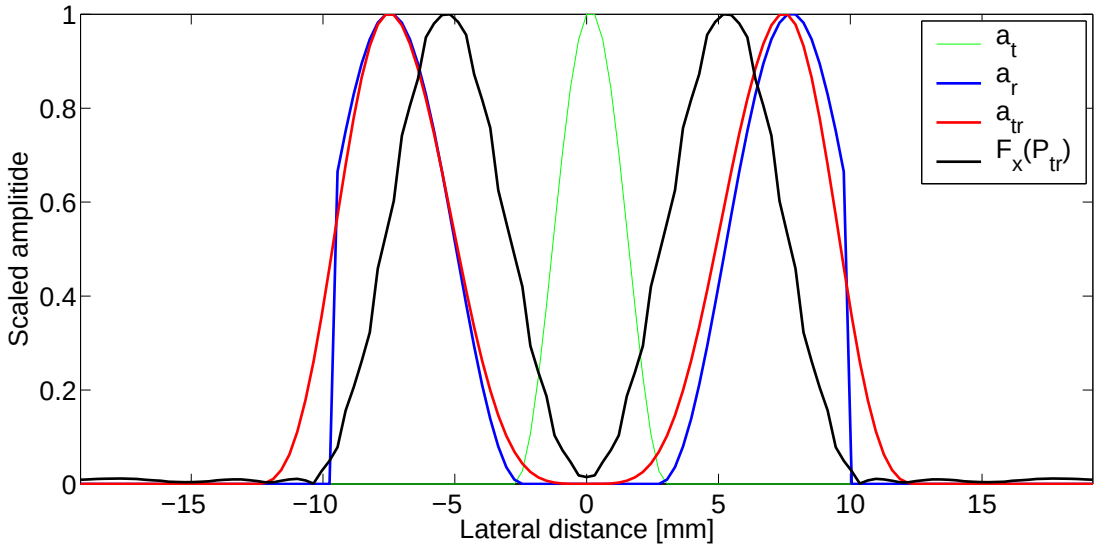

Figure 3.7: *The apodization functions on the transducer shown together with $\mathcal{F}\{P_{tr}(x)\}$ where the frequency variable f_x has been multiplied with λz.*

that the center frequency of the slow-time signal at 90° is approximately 200 Hz. This implies that a conventional highpass filter would remove both the tissue content and the blood. At flow angles of $\sim 82°$ the center frequency of the slow-time signal is seen to be ~ 0 Hz with two peaks at ~ 500 Hz, i.e. a significant amount of the blood signal would be removed by using conventional echo-canceling. At flow angles less than 80° the axial oscillation is seen to dominate and the spectrum attains the shape of a cosine function with a value of ~ 1500 Hz at an angle of 0°.

The 0 Hz center frequency at 82° is a result of the scatter traveling through the pulse echo field at an angle where the contribution from the axial oscillation of the field is the same as the lateral oscillation of the field. The amplitude spectrum will then attain the shape of the Fourier spectrum of a squared cosine. I.e. a high center peak at 0° surrounded by two smaller peaks of half the amplitude. This phenomenon is a general feature of the TO method and will always be present in the amplitude spectrum of the slow-time signal. The

angle where it takes place can be shifted by changing the lateral oscillation frequency, but this would not remove the problem of echo-canceling.

Another problem which makes echo-canceling at angles close to 90° even more challenging, is the fact that artery vessel walls also oscillate in a direction perpendicular to the blood flow [30]. At blood flow angles close to 90° the vessel wall movement will therefore mainly be along the ultrasound beam axis, and the vessel will give rise to a slow-time signal with a frequency component which can be higher than the frequency of the blood signal. However, this phenomenon is also present in a conventional 1-D system.

To reduce the problems of echo-canceling the TO method generally uses a simple mean subtraction algorithm. I.e. the mean value of the slow-time signal is subtracted from each sample in the signal. This corresponds to removing the center frequency of the slow-time signal, which is illustrated in Fig. 3.8 where the amplitude spectrum from Fig. 3.6 has been echo-canceled with the mean-subtraction filter. This filter also corresponds to subtracting a zero order polynomial from the slow time data. In cases where high blood velocities are present, it can be useful to use a filter with a larger stop band. In these cases first or second order regression filters have been used.

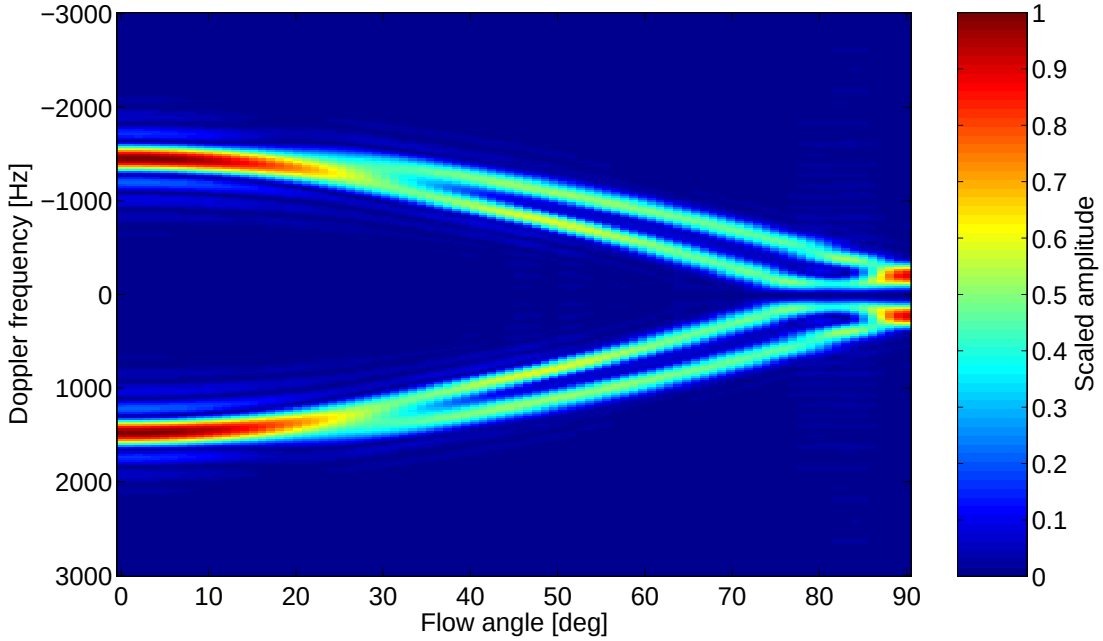

Figure 3.8: *The amplitude spectrum of the slow-time (Doppler) signal as a function of angle after mean-subtraction echo-canceling.*

It should be noted that the general problem of echo-canceling at angles near 90° has not been solved by using the mean-subtraction filter. The problem has been reduced since the filter only removes a relative small part of the spectrum, but in many cases it is expected that a significant amount of the tissue signal will remain after echo-canceling and reduce the performance of the velocity estimator.

3.4 Velocity estimation

After the slow time signals have been echo-canceled, the TO method uses an extended autocorrelation estimator to find the two velocity components v_x and v_z. The estimator[5] is based on a model where the four slow-time signals can be expressed as in equation (3.15), i.e. it is assumed that the two spatial frequencies are monocromatic.

The starting point for deriving the estimator is the four real slow-time signals $r_a(n), r_b(n), r_c(n)$ and $r_d(n)$, which have been sampled at the depth of interest. The task is now to express the vector velocity v_x and v_z as a function of known variables.

To ease the notation, the four slow-time signals are first expressed as two complex signals

$$\begin{aligned} \hat{r}_{even}(n) &= r_a(n) + jr_c(n) \\ &= \cos(\theta_x(n))e^{j\theta_z(n)} \qquad (3.18) \\ \hat{r}_{odd}(n) &= r_b(n) + jr_d(n) \\ &= \sin(\theta_x(n))e^{j\theta_z(n)}, \qquad (3.19) \end{aligned}$$

where the signals for simplicity are assumed to have unit amplitude, and the phase factors $\theta_x(n)$ and $\theta_z(n)$ are given by

$$\begin{aligned} \theta_z(n) &= 2\pi f_z \frac{n}{f_{prf}} \qquad (3.20) \\ &= 2\pi \frac{2v_z}{c} f_0 \frac{n}{f_{prf}} \qquad (3.21) \\ \theta_x(n) &= 2\pi f_x \frac{n}{f_{prf}} \qquad (3.22) \\ &= 2\pi v_x \frac{1}{\lambda_x} \frac{n}{f_{prf}}. \qquad (3.23) \end{aligned}$$

From (3.18) and (3.19) two new signals are now formed

$$\begin{aligned} r_1(n) &= \hat{r}_{even}(n) + j\hat{r}_{odd}(n) \\ &= e^{j(\theta_z(n)+\theta_x(n))} = e^{j\theta_1(n)} \qquad (3.24) \\ r_2(n) &= \hat{r}_{even}(n) - j\hat{r}_{odd}(n) \\ &= e^{j(\theta_z(n)-\theta_x(n))} = e^{j\theta_2(n)}. \qquad (3.25) \end{aligned}$$

The phase difference $\Delta\theta_1(n) = \theta_1(n+1) - \theta_1(n)$ and $\Delta\theta_2(n) = \theta_2(n+1) - \theta_2(n)$ between each pulse emission for the signals in (3.24) and (3.25) can be estimated using a conventional phase shift estimator [12]. This yields

$$\begin{aligned} \Delta\theta_z(n) + \Delta\theta_x(n) &= \Delta\theta_1(n) \\ &= \arctan \frac{\Im\{R_1(1)\}}{\Re\{R_1(1)\}} \qquad (3.26) \\ \Delta\theta_z(n) - \Delta\theta_x(n) &= \Delta\theta_2(n) \\ &= \arctan \frac{\Im\{R_2(1)\}}{\Re\{R_2(1)\}}, \qquad (3.27) \end{aligned}$$

[5] The estimator is derived in [2]

where $R(1)$ is the complex autocorrelation for lag 1

$$R_1(1) = \frac{1}{N-1}\sum_{i=0}^{N-1} r_1^*(n)r_1(n+1)$$
$$R_2(1) = \frac{1}{N-1}\sum_{i=0}^{N-1} r_2^*(n)r_2(n+1), \tag{3.28}$$

with N being the number of samples used for each velocity estimate. Rewriting equation (3.20) and (3.23) into the form

$$\begin{aligned}\Delta\theta_z(n) &= \theta_z(n+1)-\theta_z(n) \\ &= \frac{4\pi f_0 v_z}{c f_{prf}} \end{aligned} \tag{3.29}$$
$$\begin{aligned}\Delta\theta_x(n) &= \theta_x(n+1)-\theta_x(n) \\ &= \frac{2\pi v_x}{\lambda_x f_{prf}} \end{aligned} \tag{3.30}$$

and substituting them into equation (3.29) and (3.30) yields two equations with two unknowns. This finally gives[6]

$$\begin{aligned} v_x &= \frac{\lambda_x f_{prf}}{4\pi}\left[\text{atan}\left(\frac{\Im\{R_1(1)\}}{\Re\{R_1(1)\}}\right) - \text{atan}\left(\frac{\Im\{R_2(1)\}}{\Re\{R_2(1)\}}\right)\right] \\ &= \frac{\lambda_x f_{prf}}{4\pi}\times \\ &\quad \text{atan}\left(\frac{\Im\{R_1(1)\}\Re\{R_2(1)\}-\Im\{R_2(1)\}\Re\{R_1(1)\}}{\Re\{R_1(1)\}\Re\{R_2(1)\}+\Im\{R_1(1)\}\Im\{R_2(1)\}}\right) \end{aligned} \tag{3.31}$$
$$\begin{aligned} v_z &= \frac{c f_{prf}}{8\pi f_0}\left[\text{atan}\left(\frac{\Im\{R_1(1)\}}{\Re\{R_1(1)\}}\right) + \text{atan}\left(\frac{\Im\{R_2(1)\}}{\Re\{R_2(1)\}}\right)\right] \\ &= \frac{c f_{prf}}{8\pi f_0}\times \\ &\quad \text{atan}\left(\frac{\Im\{R_1(1)\}\Re\{R_2(1)\}+\Im\{R_2(1)\}\Re\{R_1(1)\}}{\Re\{R_1(1)\}\Re\{R_2(1)\}-\Im\{R_1(1)\}\Im\{R_2(1)\}}\right). \end{aligned} \tag{3.32}$$

The model described by equation (3.18) and (3.19) is valid for a single scatter. However, assuming that the acoustics of the medium is linear, the received signal trace from a collection of scatterers passing through the region of interest will be a sum of the signals from each individual blood scatterer. The model will therefore also be valid for a collection of scatterers. A schematic illustration of the velocity estimator is shown in Fig. 3.9, where the boxes represent the operations performed by the estimator.

3.5 Display methods

When a full 2-D velocity map has been estimated over the region of interest, there are still decisions to make concerning the way the velocity is displayed on the monitor for

[6] Here the relation $\tan(a+b) = \frac{\tan(a)+\tan(b)}{1-\tan(a)\tan(b)}$ has been used.

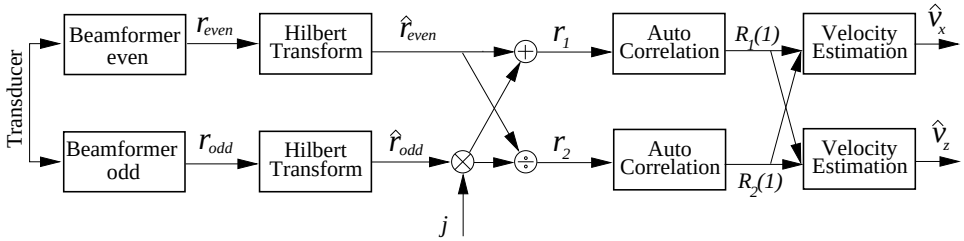

Figure 3.9: *The block diagram shows data flow from transducer (left) to estimated velocities (right). For simplicity the echo canceling and matched filtration is not shown. The box "Hilbert transform" represents (3.19), the box "Auto Correlation" represents (3.28) and the box "Velocity Estimator" represents (3.31) and (3.32)*

the medical doctor. The TO method is well suited for CFM imaging, so in most cases this would be the choice of display mode. However, it is not a simple matter to display a 2-D vector field on top of a B-mode image on a 2-D screen without introducing confusing information. In this project basicly three methods have been tried:

1. Displaying the magnitude of the 2-D vector velocity using a simple color bar (Fig. 3.10, left).
2. Displaying the magnitude of teh 2-D vector velocity using a simple color bar with an overlay of vector arrows indicating the direction and speed of the flow (Fig. 3.10, center).
3. Using a circular color map where the direction of flow is indicated by the specific color, and the speed of the flow is given by the intensity of the color (Fig. 3.10, right).

In general the optimal display method depends on the scanning situation. When no turbulence is present in the flow and the geometry of the vessel is simple, all three methods give velocity images which can be easily interpreted.

3.6 Perspectives of the TO method

The TO method is one of the few vector velocity methods in ultrasound which has successfully resulted in in-vivo CFM imaging. There is therefore a huge potential for using the TO method in a comprehensive in-vivo study on the vascular system. So far only the carotid artery of a few healthy volunteers has been studied, but a comprehensive study could involve

- Scanning and identification of stenosed carotid arteries. The TO method could potentially be an important diagnostic tool for stenosis identification.
- Scanning of bifurcations in the vascular system. In these areas the flow has a turbulent structure, and the conventional CFM method yields a confusing impression of the flow (see e.g. page 9). So far simulations and MRI are the only tools to visualize the vector flow in these regions, and ultrasound could be an important supplement.

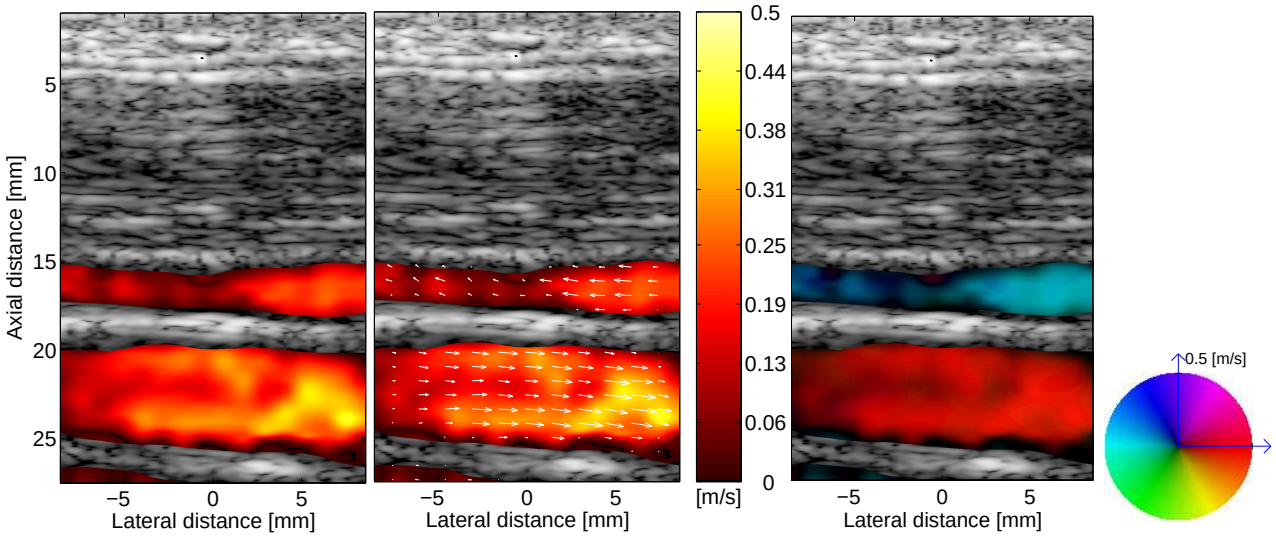

Figure 3.10: *The carotid artery and the jugular vein. Left: Only the 2-D blood speed is shown. Center: Same as the leftmost figure, but with additional arrows indicating speed and direction. Right: A 2-D color map is used to indicate speed and direction.*

- Comparison with other 2-D methods. These could e.g. be: Synthetic aperture flow, 2-D speckle tracking or dual beam methods.
- Other display methods (e.g. vectors, 2-D color maps). A number of medical doctors should determine the optimal display method for a given application.
- Estimating tissue motion using the TO method.

There is also the possibility of combining the TO method with the frequency splitting method discussed in the working paper [31]. This method uses a chirp which is divided into narrow frequency bands in receive from which the velocity is found and averaged for each frequency band. This could potentially improve performance of the TO method for scannings deeper than the 30 mm, which currently is the maximum scanning depth. The ultimate goal must be to image the vector flow in the heart which is located at a depth of 10-15 cm. This would require a large transducer if a high lateral frequency is to be attained.

A comprehensive discussion of the TO method can be found in the papers:

Udesen, J. Nielsen, M. B. , Nielsen, K. R. , Jensen, J. A. , Clinical investigation of a blood vector velocity estimation method, submitted to *Ultrasound in medicine and biology* in December 2005.

Udesen, J. , Jensen, J. A. , Investigation of Transverse Oscillation Method, *IEEE Transactions on Ultrasonics, Ferroelectrics and Frequency Control, 2005*. Accepted for publication.

Udesen, J. , Jensen, J. A. , An In-vivo investigation of transverse flow estimation, *Proceedings of SPIE Medical Imaging meeting, Ultrasonic Imaging and Signal Processing, pp 307-314, 2004*

Udesen, J. , Jensen, J. A. , Experimental investigation of transverse flow estimation using transverse oscillation, *In Proceedings IEEE Ultrason. Symp., pp 1586-1589, 2003*

Udesen, J. , Nielsen, M. B. , Nielsen, K. R. , Jensen, J. A. , Blood vector velocity estimation using an autocorrelation approach: In vivo Investigation., *IEEE International Ultrasonics Symposium 2005.*

CHAPTER

FOUR

Additional projects

During this PhD study a number of minor projects not related to the TO method have been completed. Two of these projects have resulted in conference papers and a third paper is nearly completed for submission in 2006. This chapter introduces the three papers.

4.1 Plane wave imaging

One of the major limitations in conventional CFM- and B-Mode imaging is the relatively slow frame-rate. A typical CFM frame is made by emitting ~ 500 pulses with a f_{prf} which depends on the depth of interest. If e.g. the heart (situated at z ~ 0.1 m) is to be scanned, the maximum f_{prf} is

$$\begin{aligned} f_{prf} &= \frac{c}{2z} \\ &= \frac{1540 \text{ m/s}}{2 \cdot 0.1 \text{ m}} = 7.7 \text{ kHz} \end{aligned} \tag{4.1}$$

which results in a frame-rate of 7700/500 Hz=15.5 Hz. The blood flow produced by the heart has temporal variations much faster than 15.5 Hz at e.g. the heart valves. If these fast temporal details are to be imaged, it is therefore necessary to consider other methods to increase the frame rate.

Another application which demands an even higher number of pulses to generate one CFM- or B-mode frame is 3-D ultrasound imaging. Instead of having a typical number of 65 scanlines per B-mode image, the 3-D B-mode image needs $65^2 = 4225$ pulse emissions. If 3-D flow is to be estimated the necessary number of pulses is even higher.

One way to overcome the frame rate limitation is to use each emitted pulse to illuminate the whole region of interest by e.g. a plane wave. Focusing is then solely done in the receive beamforming which degrades contrast compared to conventional CFM imaging. However, the resolution of the plane wave method is comparable to conventional CFM imaging due to the larger active aperture which can be used for a given transducer. If e.g. a 128 element transducer is used, the plane wave method uses all 128 elements to illuminate the region of interest in each pulse emission. The conventional CFM method will typically use a sliding aperture of 64 elements in both transmit and receive. The result is that the plane wave method has worse transmit focusing but better receive focusing than conventional CFM imaging.

Plane wave illumination with a conventional pulse results in poor SNR, and therefore a chirp is used as excitation pulse. Due to the duration of the chirp which typically is $\sim 20\,\mu s$, data from the first ~ 15 mm cannot be acquired. However, in most cases this is not a problem since the chirp is intended for scanning of deeper laying structures. As described in the included paper the chirp results in a SNR comparable with conventional CFM imaging.

To estimate the velocity of the blood, different approaches can be used. If the emitted chirp is narrow band, a conventional auto correlation estimator can be used. Another approach is to use a broad band chirp and apply a time shift estimator. This estimator uses cross correlation to find the spatial shift in position of the blood scatters between consecutive images. Dividing this spatial shift with the time between the pulses ($1/f_{prf}$) then gives the blood velocity.

In the included paper a 1-D cross correlation technique has been used where data are cross correlated along flow lines. This means that the angle of flow has to be known in advance from e.g. the B-mode images if the 2-D vector velocity is to be estimated. Another approach to find the angle of flow could be to use the *directional beamforming* method [21, 22]. However, due to the poor contrast of the plane wave method, this might not be possible especially at angles close 90° flow. This, however, has to be confirmed by future investigations.

A comprehensive discussion of the plane wave method can be found in the paper:

Udesen, J. , Gran, F. , Jensen, J. A. , Fast color flow mode imaging using plane wave excitation and temporal encoding, *Proceedings of SPIE Medical Imaging meeting, Ultrasonic Imaging and Signal Processing, pp 427-436, 2005.*

4.2 Anti aliasing estimator

It is a well known problem in conventional CFM imaging that aliasing phenomena occur when the axial blood velocity v_z exceeds a value of

$$v_z^{max} = \frac{c f_{prf}}{4 f_0} \tag{4.2}$$

If the velocity exceeds the aliasing limit the resulting CFM image will contain false velocity estimates as shown in Fig. 4.1. One way to overcome the aliasing limit is to use a variable sampling frequency. I.e. the f_{prf} becomes a function of time. In the most simple form this can be done by having a sequence of N_1 pulses emitted with pulse repetition frequency f_{prf}. After a time interval of $3/(2f_{prf})$ another sequence of N_2 pulses are emitted with pulse repetition frequency $3/(2f_{prf})$. This transmit sequence is illustrated in Fig. 4.2. It can shown that this sequence shifts the aliasing limit to a value of $2v_z^{max}$

A comprehensive discussion of the anti aliasing method can be found in the paper:

Udesen, J. , Nikolov, S. , Jensen, J. A. , A simple method to reduce aliasing artifacts in color flow mode imaging., *IEEE International Ultrasonics Symposium 2005.*

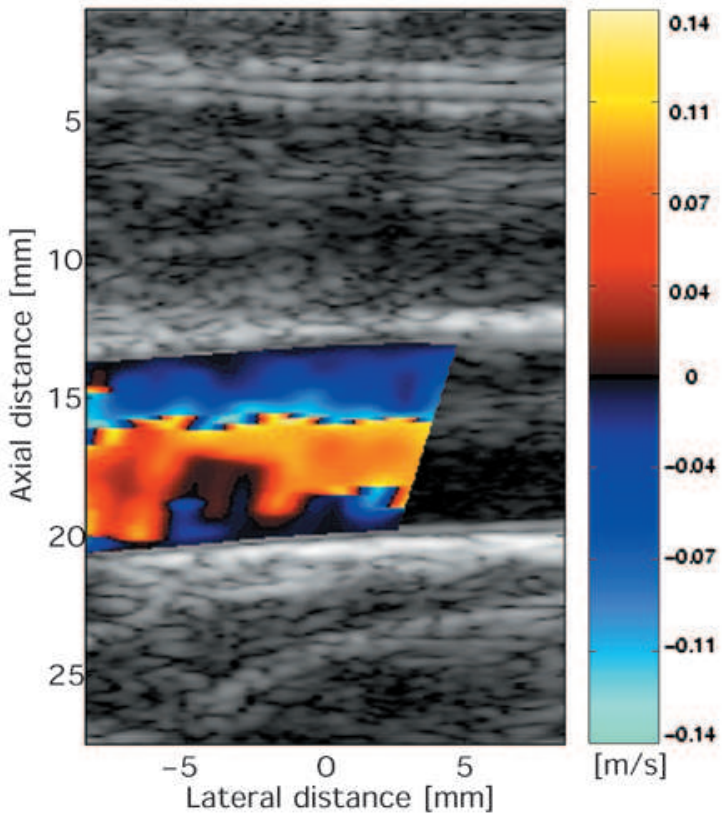

Figure 4.1: *Aliasing in the carotid artery. The image is obtained with the RASMUS scanner using tilted beams for the velocity estimation.*

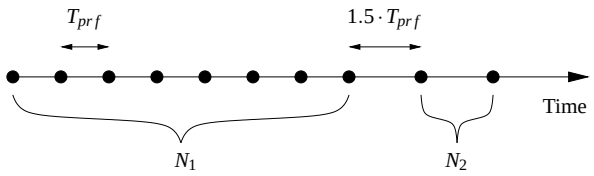

Figure 4.2: *The shot sequence for the method. First N_1 pulses are emitted from the transducer at a pulse repetition time T_{prf} followed by N_2 pulses at $1.5 \cdot T_{prf}$*

4.3 Frequency splitting flow estimation

When blood flow is estimated deep inside the body the quality of the estimates will often be poor. This is due to the relatively small number ($\sim 4-10$) of pulses which can be used for each estimate if an acceptable frame-rate is to be obtained. It is therefore desirable to improve performance when using only few pulses.

Performance can be improved by using a broad band chirp as excitation pulse. The chirp has superior SNR compared to a conventional narrow band pulse, but the broad band chirp is not suited for an autocorrelation estimator.

The basic idea in the *Frequency splitting method* (FSM) is to use broad band chirps as pulses instead of narrow band pulses as in conventional CFM imaging. By appropriate

filtration, the returned signals can be divided into a number of narrow band signals which are approximately disjoint. After echo canceling the velocity is found from each frequency band using a conventional autocorrelation estimator, and finally the velocities are averaged to obtain an improved velocity estimate.

Another approach which has not been investigated, is to shift each frequency band to the same center frequency and estimating the lag 1 value of the complex autocorrelation function. The phase of this value is then proportional to the axial velocity[1].

A discussion of the frequency splitting method can be found in the working paper:

Udesen, J. , Gran, F. , Jensen, J. A. , A frequency splitting method for blood flow estimation., *Working paper. To be submitted in 2006.*

[1] This is the basic principle of an autocorrelation estimator [12]

CHAPTER

FIVE

Papers

In this chapter the reader will find the papers which have been produced during this PhD project. The presentation order of the papers are:

Journal papers related to the TO method:

Udesen, J. , Jensen, J. A. , Investigation of Transverse Oscillation Method, *IEEE Transactions on Ultrasonics, Ferroelectrics and Frequency Control, 2005*. Accepted for publication.

Udesen, J. Nielsen, M. B. , Nielsen, K. R. , Jensen, J. A. , Examples of in-vivo blood vector velocity estimation, submitted to *Ultrasound in medicine and biology* in December 2005.

Conference preceedings related to the TO method:

Udesen, J. , Jensen, J. A. , Experimental investigation of transverse flow estimation using transverse oscillation, *In Proceedings IEEE Ultrason. Symp., pp 1586-1589, 2003*

Udesen, J. , Jensen, J. A. , An In-vivo investigation of transverse flow estimation, *Proceedings of SPIE Medical Imaging meeting, Ultrasonic Imaging and Signal Processing, pp 307-314, 2004*

Udesen, J. , Nielsen, M. B. , Nielsen, K. R. , Jensen, J. A. , Blood vector velocity estimation using an autocorrelation approach: In vivo Investigation., *IEEE International Ultrasonics Symposium 2005.*

Additional papers not related to the TO method:

Udesen, J. , Gran, F. , Jensen, J. A. , Fast color flow mode imaging using plane wave excitation and temporal encoding, *Proceedings of SPIE Medical Imaging meeting, Ultrasonic Imaging and Signal Processing, pp 427-436, 2005.*

Udesen, J. , Nikolov, S. , Jensen, J. A. , A simple method to reduce aliasing artifacts in color flow mode imaging., *IEEE International Ultrasonics Symposium 2005.*

Udesen, J. , Gran, F. , Jensen, J. A. , A frequency splitting method for blood flow estimation., *Working paper. To be submitted in 2006.*

Investigation of Transverse Oscillation Method

Jesper Udesen and Jørgen Arendt Jensen *Senior Member, IEEE,*

***Abstract*— Conventional ultrasound scanners can only display the axial component of the blood velocity vector, which is a significant limitation when vessels nearly parallel to the skin surface are scanned. The transverse oscillation method (TO) overcomes this limitation by introducing a transverse oscillation and an axial oscillation in the pulse echo field. The theory behind the creation of the double oscillation pulse echo field is explained as well as the theory behind the estimation of the vector velocity. A parameter study of the method is performed, using the ultrasound simulation program Field II. A virtual linear array transducer with center frequency 7 MHz and 128 active elements is created, and a virtual blood vessel of radius 6.4 mm is simulated.**

The performance of the TO method is found around an initial point in the parameter space. The parameters varied are: flow angle, transmit focus depth, receive apodization, pulse length, transverse wave length, number of emissions, signal to noise ratio, and type of echo canceling filter used.

Using the experimental scanner RASMUS, the performance of the TO method is evaluated. An experimental flowrig is used to create laminar parabolic flow in a blood mimicking fluid and the fluid is scanned under different flow-to-beam angles. The relative standard deviation on the transverse velocity estimate is found to be less than 10% for all angles between 50° and 90°. Furthermore the TO method is evaluated in the flowrig using pulsatile flow which resembles the flow in the femoral artery. The estimated volume flow as a function of time is compared to the volume flow derived from a conventional axial method at an flow-to-beam angle of 60°. It is found that the method is highly sensitive to the angle between the flow and the beam direction. Also the choice of echo canceling filter affects the performance significantly.

I. Introduction

Today ultrasound scanners can display an image of the interior of the human body with a blood velocity image superimposed. However, the scanner do not yield the magnitude of the vector velocity, but only the vector velocity projected onto the axis of the ultrasound beam direction. This causes a severe problem when the angle between the ultrasound beam and the flow is close to 90° since in this case the blood velocity is not detected. Many authors have addressed this issue, and different methods for calculating the two dimensional vector velocity have been suggested[1], [2], [3], [4], [5].

One promising method for calculating the two dimensional vector velocity has been suggested by Jensen and Munk [6], [7], [8] (Transverse Oscillation(TO)) and Anderson [9], [10] (Spatial Quadrature). The method introduces two double oscillating point spread functions (PSFs) each 90° transverse phase shifted in space, and it uses an autocorrelation estimator to find the velocity. In terms of computation time, the method is superior to existing cross correlation approaches, e.g. speckle tracking, since only two beamformers in receive are needed.

We have previously shown that the TO method is capable of estimating the velocities in simulations, experiments and under in-vivo conditions, when the angle between the ultrasound beam and the blood velocity vector is approximately 90° [11], [12]. In order to estimate the vector velocity of the blood, the TO method should be able to give velocity estimates with low bias and standard deviation for any angle. However, a full evaluation of the method has not yet been performed, and a systematic parameter analysis in simulations and experiments still needs to be caried out.

This paper evaluates the TO method. A systematic parameter analysis is performed using the ultrasound simulation program Field II [13], [14] and the the experimental scanner RASMUS [15].

A brief introduction to the method is presented in Section II where the theory for the field generation is explained and the autocorrelation velocity estimator is introduced. In Section III the parameter analysis of the TO method is presented. This is done using the Field II program which is used to simulate signals from a virtual blood vessel. Nine independent parameters are then varied around a fixed point in the parameter space, and the relative standard deviation and relative bias on the estimated transverse velocity v_x are calculated. The RASMUS scanner and the flowrig are presented in Section IV along with the other used experimental equipment and the parameters used to perform the experiments. The TO method is then evaluated under different angles of flow where the flow is laminar, has a parabolic velocity profile, and does not accelerate. The results for this experiment will be discussed in Section V. Finally, in Section VI, the TO method will be evaluated under more realistic conditions where the flow resembles the blood velocity in the femoral artery.

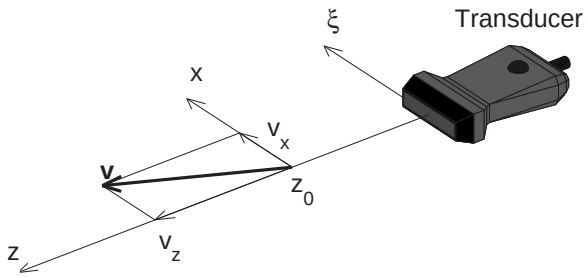

Fig. 1. A conventional ultrasound system will only estimate the axial velocity component v_z of a single blood scatterer situated at a depth z_0 and moving with velocity vector $\mathbf{v}$. The TO method estimates both v_x and v_z. The ξ-axis is parallel to the x-axis.

Jesper Udesen and Jørgen Arendt Jensen are with department Ørsted•DTU, Bldg. 348, Technical University of Denmark, DK-2800 Kgs. Lyngby, Denmark (e-mail: ju@oersted.dtu.dk).

II. THEORY

In a conventional ultrasound system for blood velocity estimation, the pulse echo field only oscillates in the axial direction, i.e. along the axis of the ultrasound beam. Blood scatterers passing through the field of interest will produce a signal with a frequency component f_z proportional to the axial velocity v_z and no knowledge is gained about the transverse velocity component v_x. This is illustrated in Fig. 1 where the ultrasound beam propagates along the z-axis and only the velocity component v_z along the z-axis can be estimated. To overcome this limitation, a new pulse echo field has to be created.

A. Field generation

The basic idea in the TO method is to create a pulse echo field with an oscillation present both in the axial and transverse direction. Blood scatterers traveling through the region of interest will, thus, produce a signal where two frequency components f_x and f_z are present. The frequencies f_x and f_z are related to the velocity components v_x and v_z by the equations [6], [7].

$$f_z = \frac{2v_z}{c} f_0 \quad (1)$$

$$f_x = \frac{v_x}{\lambda_x}, \quad (2)$$

where c is speed of sound, f_0 is the center frequency of the emitted pulse and λ_x is the wave length in the transverse direction of the pulse echo field. The fundamental acoustic property of grating lobes is used to create the transverse oscillation in the pulse echo field. This is done by adjusting the apodization of the receive aperture in such a way that the whole aperture resembles two point sources. Two point sources separated in space will give rise to a field where grating lobes are present, and thereby the grating lobes creates the transverse oscillation. Note that this can be done in the receive beamforming, so that the emitted beam in the TO method is similar to the emitted beam in a conventional velocity estimation system.

If the transverse field is assumed to be known, a formal expression for the apodization function can be derived. This is due to the fact that a Fourier relation exists between the apodization function $r(\xi)$ and the transverse field $R(x)$ at the focal point z_0. Here, x is transverse distance at the focal point and ξ is the distance from the center of the transducer as shown in Fig. 1. The Fourier relation is then [16]

$$\begin{aligned} R(x) &= k_1 \int_{-\infty}^{\infty} r(\xi) \exp\left(-j\frac{2\pi}{\lambda_z z} x\xi\right) d\xi \\ &= k_1 \mathcal{F}'\{r(\xi)\}. \end{aligned} \quad (3)$$

where $\mathcal{F}'$ is the Fourier transform in which the kernel function uses a spatial frequency variable $1/(\lambda_z z)$. Here λ_z is the spatial axial wave length, and z is depth.

In the following the constant of proportionality k_1 in (3) is omitted. A transversely oscillating field $R(x)$ with a spatial wave length λ_x and a lateral width L

$$R(x) = \text{rect}(L)\cos(2\pi\frac{x}{\lambda_x}), \quad (4)$$

thus yields an apodization function $r(\xi)$ given by

$$\begin{aligned} r(\xi) &= \mathcal{F}'^{-1}\{R(x)\} \\ &= \mathcal{F}'^{-1}\{\text{rect}(L)\} * \mathcal{F}'^{-1}\{\cos(2\pi\frac{x}{\lambda_x})\} \\ &= \frac{L}{2z\lambda_z}\left\{\text{sinc}\left(\pi\left(\frac{\xi}{z\lambda_z}+\frac{1}{\lambda_x}\right)L\right) + \right. \\ &\quad \left. \text{sinc}\left(\pi\left(\frac{\xi}{z\lambda_z}-\frac{1}{\lambda_x}\right)L\right)\right\}. \end{aligned} \quad (5)$$

Here the operator $*$ denotes spatial convolution. The two Sinc functions in (5) have maxima located at

$$\frac{\xi}{z\lambda_z} = \pm\frac{1}{\lambda_x}, \quad (6)$$

so the peak position is at

$$\xi_p = \pm\frac{z\lambda_z}{\lambda_x}. \quad (7)$$

The distance $D = |2\xi_p|$ between the main-lobes of the two Sinc functions is then related to the transverse wave length λ_x by the relation

$$\lambda_x = \frac{2\lambda_z z}{D} \quad (8)$$

The implementation of (5) into the transducers apodization function will yield a pulse echo field where an oscillation is present in both the axial and transverse direction. The transverse wave length of the pulse echo field can then be adjusted by changing the distance between the mainlobes of two Sinc functions as stated by (8). To ensure that the transverse wave length λ_x is constant at any depth, the apodization function should be dynamic.

Other apodization functions can be used to create the transverse oscillation. Two delta functions, seperated by a distance D, will give the most narrow banded transverse field, but the signal to noise ratio (SNR) will be poor due to the extensive loss of acoustic energy from only using a small part of the aperture. On the other hand, two wide Gaussian functions seperated a distance D would yield a good SNR, but the transverse wave length λ_x would be poorly defined. Different apodization functions will be investigated further in the next Section.

In a conventional flow system the beamformed in-phase RF signals are phase shifted 90° in the axial direction to yield the quadrature signals. Thereby it is possible to determine the sign of the axial velocity which could not be derived from the in-phase signals alone. The TO method makes use of two 90° phase shifts in space; one for each spatial direction. This is needed because two frequency components are present in the signals, and hence the phase shift has to be performed in both the axial direction and in the transverse direction. The axial phase shift is created using a Hilbert transformation, and the 90° phase shift in the transverse direction can be accomplished by having two parallel beamformers in receive. The two receive beams are steered so that the transverse distance between each beam is $\lambda_x/4$ which corresponds to a 90° phase shift in space. This is illustrated in Fig. 2 where the PSF from each beamformer is shown together with the corresponding spectrum.

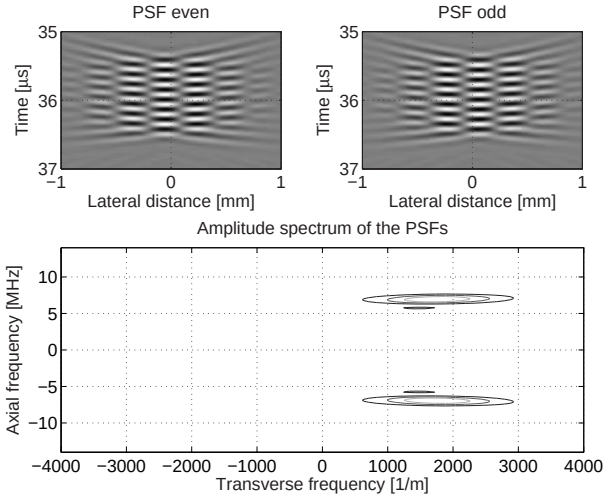

Fig. 2. The two double oscillating PSFs (top) and their corresponding spectrum (bottom) created with the Field II program for a point at 27 mm using a linear array transducer with a center frequency of 7 MHz. The amplitude spectrum is calculated by taking the 2D Fourier transform of $\text{PSF}_{\text{even}} + j\text{PSF}_{\text{odd}}$. Note that the PSFs are 90° phase shifted with respect to each other and that the amplitude spectrum is therefore one-sided.

B. Velocity estimation

When a single blood scatterer travels through the acoustic field with velocity $\mathbf{v} = (v_x, v_z)$, the two beamformers in the TO method acquire two signals[1]. Assuming that the signals are sampled at a certain depth with pulse repetition frequency f_{prf}, the signals $r_{even}(n)$ and $r_{odd}(n)$ from each beamformer can ideally be modeled as

$$\begin{aligned} r_{even}(n) &= \cos(\theta_x(n))\cos(\theta_z(n)) && (9)\\ r_{odd}(n) &= \sin(\theta_x(n))\cos(\theta_z(n)), && (10)\end{aligned}$$

where the signals for simplicity are assumed to have unit amplitude. The phase factors $\theta_x(n)$ and $\theta_z(n)$ are given by

$$\begin{aligned} \theta_z(n) &= 2\pi f_z \frac{n}{f_{prf}} && (11)\\ &= 2\pi \frac{2v_z}{c} f_0 \frac{n}{f_{prf}} && (12)\\ \theta_x(n) &= 2\pi f_x \frac{n}{f_{prf}} && (13)\\ &= 2\pi v_x \frac{1}{\lambda_x}\frac{n}{f_{prf}} && (14)\end{aligned}$$

with f_0 being the center frequency, c the speed of sound and the index n the pulse emission number. The factor $\theta_z(n)$ is the phase experienced due to a shift in position between the received signals. The phase factor $\theta_x(n)$ is the phase of the received signal from a point scatterer sampled with temporal frequency f_{prf} and traveling with transverse velocity v_x through an oscillating field with spatial wavelength λ_x.

Taking the Hilbert transform over the axial distance of (9) and (10) yields

$$\begin{aligned} \hat{r}_{even}(n) &= \cos(\theta_x(n))e^{j\theta_z(n)} && (15)\\ \hat{r}_{odd}(n) &= \sin(\theta_x(n))e^{j\theta_z(n)}. && (16)\end{aligned}$$

From (15) and (16) two new signals are now formed

$$\begin{aligned} r_1(n) &= \hat{r}_{even}(n) + j\hat{r}_{odd}(n)\\ &= e^{j(\theta_z(n)+\theta_x(n))} = e^{j\theta_1(n)} && (17)\\ r_2(n) &= \hat{r}_{even}(n) - j\hat{r}_{odd}(n)\\ &= e^{j(\theta_z(n)-\theta_x(n))} = e^{j\theta_2(n)} && (18)\end{aligned}$$

The phase difference $\Delta\theta_1(n) = \theta_1(n+1) - \theta_1(n)$ and $\Delta\theta_2(n) = \theta_2(n+1) - \theta_2(n)$ between each pulse emmisions for the signals in (17) and (18) can be estimated using a conventional phase shift estimator[17]. This yields

$$\begin{aligned} \Delta\theta_z(n) + \Delta\theta_x(n) &= \Delta\theta_1(n)\\ &= \arctan\frac{\Im\{R_1(1)\}}{\Re\{R_1(1)\}} && (19)\\ \Delta\theta_z(n) - \Delta\theta_x(n) &= \Delta\theta_2(n)\\ &= \arctan\frac{\Im\{R_2(1)\}}{\Re\{R_2(1)\}}, && (20)\end{aligned}$$

where $R(1)$ is the complex autocorrelation for lag 1

$$\begin{aligned} R_1(1) &= \frac{1}{N-1}\sum_{i=0}^{N-1} r_1^*(n)r_1(n+1)\\ R_2(1) &= \frac{1}{N-1}\sum_{i=0}^{N-1} r_2^*(n)r_2(n+1), && (21)\end{aligned}$$

with N being the number of samples used for each velocity estimate. Rewriting equations (11) and (14) into the form

$$\begin{aligned} \Delta\theta_z(n) &= \theta_z(n+1) - \theta_z(n)\\ &= \frac{4\pi f_0 v_z}{c f_{prf}} && (22)\\ \Delta\theta_x(n) &= \theta_x(n+1) - \theta_x(n)\\ &= \frac{2\pi v_x}{\lambda_x f_{prf}} && (23)\end{aligned}$$

and substituting them into equations (22) and (23), yields two equations with two unknowns. This finally gives[2]

$$\begin{aligned} v_x &= \frac{\lambda_x f_{prf}}{4\pi} \times\\ &\operatorname{atan}\left(\frac{\Im\{R_1(1)\}\Re\{R_2(1)\} + \Im\{R_2(1)\}\Re\{R_1(1)\}}{\Re\{R_1(1)\}\Re\{R_2(1)\} - \Im\{R_1(1)\}\Im\{R_2(1)\}}\right) && (24)\\ v_z &= \frac{c f_{prf}}{8\pi f_0} \times\\ &\operatorname{atan}\left(\frac{\Im\{R_1(1)\}\Re\{R_2(1)\} - \Im\{R_2(1)\}\Re\{R_1(1)\}}{\Re\{R_1(1)\}\Re\{R_2(1)\} + \Im\{R_1(1)\}\Im\{R_2(1)\}}\right) && (25)\end{aligned}$$

The model described by equation (9) and (10) is valid for a single scatter. However, assuming that the acoustics of the medium is linear, the received signal trace from a collection of scatterers passing through the region of interest will be a sum of the signals from each individual blood scatterer. The

[1]This discussion of the velocity estimator follows the one given in Jensen (2001)[8]

[2]Here the relation $\tan(a+b) = \frac{\tan(a)+\tan(b)}{1-\tan(a)\tan(b)}$ has been used.

model will therefore also be valid for a collection of scatterers. A schematic illustration of the velocity estimator is shown in Fig. 3 where the boxes represents the operations performed by the estimator.

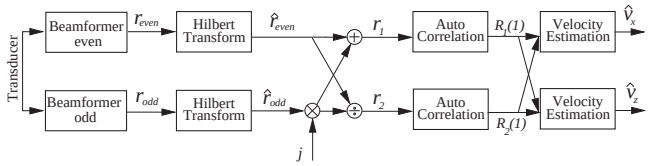

Fig. 3. The block diagram shows data flow from transducer (left) to estimated velocities (right). For simplicity the echo canceling and matched filtration is not shown. The box "Hilbert transform" represents (16), the box "Auto Correlation" represents (21) and the box "Velocity Estimator" represents (24) and (25)

III. Parameter variation

To optimize the TO method to give the best possible estimate of the velocity vector, a parameter analysis will be presented in this Section. The TO method is evaluated by examining the standard deviation and the bias of the estimated velocity. Since the axial velocity can be estimated using a conventional auto correlation algorithm the focus is on the estimated transverse velocity.

A. The set-up

The ultrasound simulation program Field II was used to emulate a virtual transducer and blood vessel as seen in Fig. 4. The vessel was placed at a fixed depth of 40 mm and had a radius of 6.4 mm. It was modeled using 36,255 point scatterers, which were moved with a parabolic velocity profile $v(r)$ given by

$$v(r) = v_0 \left(1 - \left(\frac{r}{R}\right)^2\right). \tag{26}$$

Here v_0 is the velocity at the center of the vessel, r is the distance from the center of the vessel to the scatterer moving with velocity $v(r)$ and R is the radius of the vessel. The geometry of the vessel and the peak velocity of the blood are within normal physiological range, e.g. the common carotid artery. However, the parabolic velocity profile is chosen to limit the complexity of the model and can not be found in the human body. The transducer used in the simulations was a linear array transducer with 128 active elements in transmit and receive and the set-up parameters can be seen in Table I. The vessel was scanned using 1000 repetitions of the same beam originating from the center of the transducer (the z-axis in Fig. 4). After reception of the data, beamforming was performed off-line on a 32 CPU Linux cluster yielding a computation time of approximately one week. The different parameters used in the simulations were grouped into two sets: those with fixed values (Table I and II) and those with values which were varied during the parameter analysis (Table III). All received data were matched filtered before beamforming and RF averaging was performed [8]. Echo canceling was applied using a simple mean subtraction filter which removes

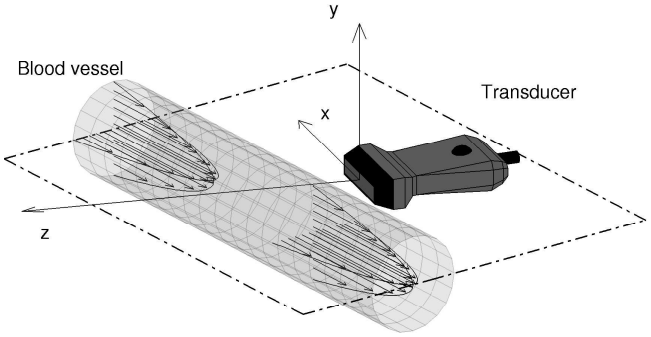

Fig. 4. The set-up for the simulations using Field II. The velocity profile in the blood vessel was parabolic, i.e. described by (26).

TABLE I
Transducer set-up

Parameter	Value
Transducer	Linear array
Number of elements	128
Pitch	0.208 mm
Kerf	0.035 mm
Center frequency	7 MHz
Sampling frequency	100 MHz
Apodization in transmit	Hamming

the zero frequency component in the signal. The filtered signal $y(n)$ is thus

$$y(n) = x(n) - \frac{1}{N}\sum_{i=1}^{N} x(i), \tag{27}$$

where $x(n)$ is the input signal of length N.

The TO method is evaluated using the relative standard deviation $\tilde{\sigma}_{v_x}$ and relative bias $\tilde{B}_{v_x}$ of the estimated transverse velocity. The non dimensional parameters $\tilde{\sigma}_{v_x}$ and $\tilde{B}_{v_x}$ are defined as

$$\tilde{\sigma}_{v_x} = \frac{1}{v_0(z_2 - z_1)} \int_{z_1}^{z_2} \sqrt{\frac{1}{M}\sum_{i=1}^{M} \left(\hat{v}_x^i(z) - \bar{v}_x(z)\right)^2} dz \tag{28}$$

$$\tilde{B}_{v_x} = \frac{1}{v_0(z_2 - z_1)} \int_{z_1}^{z_2} \left|\bar{v}_x(z) - v_x(z)\right| dz \tag{29}$$

where $\hat{v}_x^i(z)$ is one velocity estimate at a certain depth z, $\bar{v}_x(z)$ is the mean of the velocity estimates and $v_x(z)$ is the actual velocity described by (26). z_1 and z_2, respectively, are the depth to the beginning of the vessel and the end of the

TABLE II
Parameters which had fixed values in the simulations

Parameter	Value
Pulse repetition frequency	8 kHz
Speed of sound	1540 m/s
Max. velocity of blood v_0	1 m/s

TABLE III

PARAMETERS WHICH WERE VARIED IN THE SIMULATIONS. VALUES MARKED WITH BOLD FACE FORMS THE INITIAL POINT IN THE PARAMETER SPACE. FOR THE SNR THE INITIAL POINT IS ∞.

Parameter	Value
Transmit focus	$[30, \mathbf{40}, 50, 60]$ mm
Angle of the blood vessel	$[40, 50, 60, \mathbf{70}, 80, 90]^\circ$
No. transmit cycles in pulse	$[4, \mathbf{8}, 12, 16]$
Transmit focus	$[30, \mathbf{40}, 50, 60]$ mm
Transverse wavelength λ_x	$[\mathbf{0.8}, 1.1, 1.4, 1.7]$ mm
Width of each mainlobe	$[24, \mathbf{32}, 48, 64]$ Transducer el.
Signal to noise ratio (SNR)	$[-30, -24, -18, -12, -6, \infty]$ dB
Pulses per velocity estimate	$[4, 8, 16, 24, \mathbf{32}, 40]$

vessel, and M is the number of velocity estimates $\hat{v}_x^i(z)$ used to calculate $\tilde{\sigma}_{v_x}$ and $\tilde{B}_{v_x}$.

B. The initial point

A number of initial conditions were used to form an initial point, which is indicated with bold face in Table III. During the entire parameter analysis the initial conditions were kept constant except for the parameters which were investigated. Hereby it is ensured that only information concerning the variation of a single parameter at a time was determined.

The receive apodization used at the initial point is not the two sinc functions described by (5) but instead two Hanning functions are used. The Hanning function $h(\xi)$ is defined as

$$h(\xi) = \cos^2\left(\frac{\pi\xi}{2a}\right) \quad , -a \leq \xi \leq a \tag{30}$$

where a is the width of the Hanning function. The peaks of the two Hanning functions are placed at the positions of the peaks of the sinc functions and the width of each Hanning function is 32 transducer elements which corresponds to 6.7 mm. In the discussion of the receive parameters it will be shown that the shape of the two peaks is not crucial for the performance.

For the initial point the relative standard deviation is $\tilde{\sigma}_{v_x} = 0.061$, the relative bias is $\tilde{B}_{v_x} = 0.037$ and the corresponding velocity profile can be seen to the left in Fig. 5. The estimated transverse velocities for the initial point should be compared with the estimated axial velocity using a conventional axial autocorrelation estimator and the parameters for the initial point. Here the relative standard deviation is $\tilde{\sigma}_{v_z} = 0.0134$ and $\tilde{B}_{v_z} = 0.0068$ and the corresponding velocity plot can be seen to the right in Fig. 5. Thus, at an flow angle of 70° the conventional axial estimator estimates v_z approximately six times better than the TO method estimates v_x.

C. Variation of transmit parameters

The transmit parameters are related to the transmit of the ultrasound pulse from the transducer. Three transmit parameters have been investigated:

- Angle between the flow and the ultrasound beam.
- Focus depth of the transmitted ultrasound beam.
- Number of cycles in the transmitted pulse.

The angle between the ultrasound beam and the flow direction was varied between 90° and 40° in intervals of 10°, and the

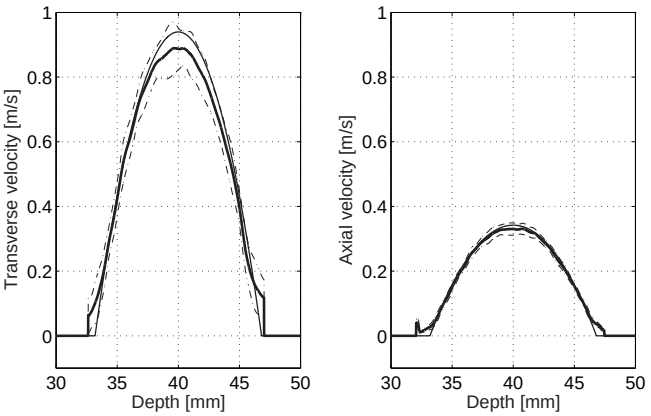

Fig. 5. Left: Estimated transverse velocity for the initial point in the parameter space. Right: estimated axial velocity for the initial point in the parameter space using a conventional axial estimator. The thick line is the mean of the velocity estimates. The thin line is the actual parabolic profile and the thin dotted lines are ± 1 standard deviation.

corresponding relative standard deviation and relative bias of the transverse velocity were estimated and can be seen in Fig. 6. For purely transverse flow (90°) both the standard deviation and the bias have a minimum, which is expected, since only one frequency component is present in the beamformed signals $r_{even}(n)$ and $r_{odd}(n)$ at this angle. For angles less than 60° the bias rises to above 0.08 and at 40° the estimated velocity profile differs significantly from the true profile.

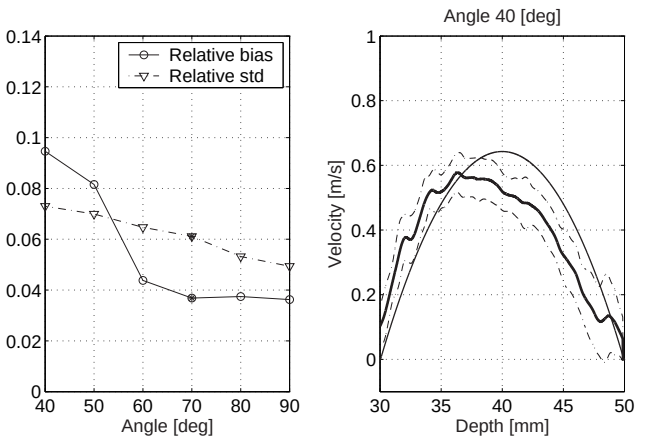

Fig. 6. Left: The relative standard deviation and relative bias as a function of flow angle. The points marked with $*$ is the initial position in the parameter space. Right: The estimated transverse velocity and standard deviation at a flow angle of 40°. The thin line indicates the true velocity as a function of depth. The thick line is the estimated mean transverse velocity, and the two dashed lines are the mean transverse velocity ± 1 standard deviation.

The focus depth of the transmitted beam was varied between 30 mm and 60 mm in intervals of 10 mm, which can be seen in Fig. 7. Relative standard deviation and relative bias have a minimum when the beam is focused at 60 mm and 50 mm respectively, i.e. behind the vessel. This suggests that the TO method performs best when the beam has a relative broad transverse extend and hence the transverse spatial frequency $1/\lambda_x$ is well defined and forms a narrow peak in the spectrum.

However, focusing the emitted energy in a large area also decreases the returned signal and hence decreases the signal to noise ratio, which will increase the bias and the standard deviation. Positioning the focus near the center of the vessel or slightly behind will therefore yield the best performance.

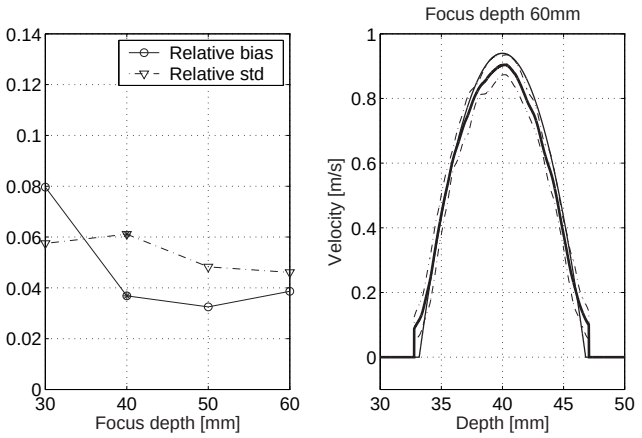

Fig. 7. Left: The relative standard deviation and relative bias as a function of transmit focus depth. The initial position in the parameter space is marked with $*$. Right: The estimated transverse velocity and standard deviation at a transmit focus depth of 60 mm. The thin line indicates the true velocity as a function of depth. The thick line is the estimated mean transverse velocity, and the two dashed lines are the mean transverse velocity ± 1 standard deviation.

The number of cycles in the transmitted pulse has been investigated with the number of cycles ranging from 4 to 16 in intervals of 4 cycles. The corresponding relative standard deviation and relative bias can be seen in Fig. 8. The performance of the TO method is not very sensitive to the number of transmitted cycles. However, the received signal amplitude will scale with the number of transmitted cycles and hence the SNR in a real scanning situation will increase for a high number of transmitted cycles. The drawback of having a high number of transmitted cycles is on the other hand that the axial resolution decreases. A compromise could be to use 12 cycles in the transmitted pulse. This corresponds to an axial extend of 2.6 mm which is approximately the same size as the transverse extent of the PSF.

D. Variation of receive parameters

The receive parameters characterize the process from the recording of the ultrasound pulse at the transducer to the estimation of the velocity. Six receive parameters have been investigated

- Number of transducer elements used to generate each of the two Hanning functions in the receive apodization.
- Transverse wavelength generated in the pulse echo field.
- Type of echo canceling filter used.
- Number of pulse firings used to make one velocity estimation.
- Type of receive apodization used.
- Signal-to-noise ratio of received signal.

The width of the two Hanning functions used in receive apodization was varied with the values $(24, 32, 48, 64)$ transducer elements (Fig 9). Changing the width of each Hanning

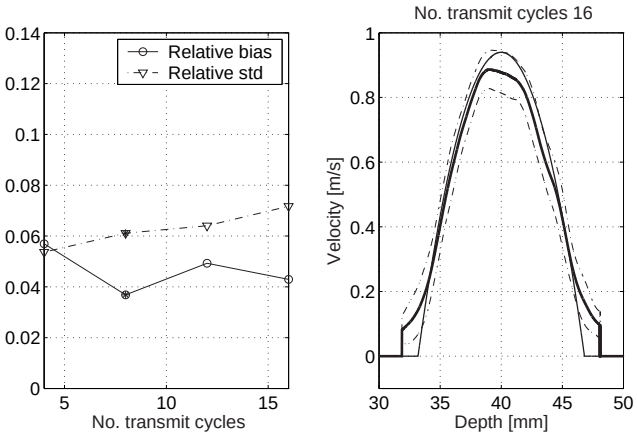

Fig. 8. Left: The relative standard deviation and relative bias as a function of number of transmit cycles. The points marked with $*$ is the initial position in the parameter space. Right: The estimated transverse velocity and standard deviation for a 16 cycle transmitted pulse. The thin line indicates the true velocity as a function of depth. The thick line is the estimated mean transverse velocity, and the two dashed lines are the mean transverse velocity ± 1 standard deviation.

function seems to have insignificant influence on the relative standard deviation, but increases the relative bias nearly linearly. This might be due to the fact that a broad Hanning will yield a PSF where the transverse component is broad banded due to the Fourier relation (3), and hence the velocity estimate will degrade. This effect seems, however, only to be present in the relative bias and not in the relative standard deviation. When the two Hanning functions are broad the transmitted energy will be large and hence the SNR in a real scanning situation will increase. A further study of the optimal width of each Hanning should therefore be conducted in a noisy environment, e.g. using a real scanner.

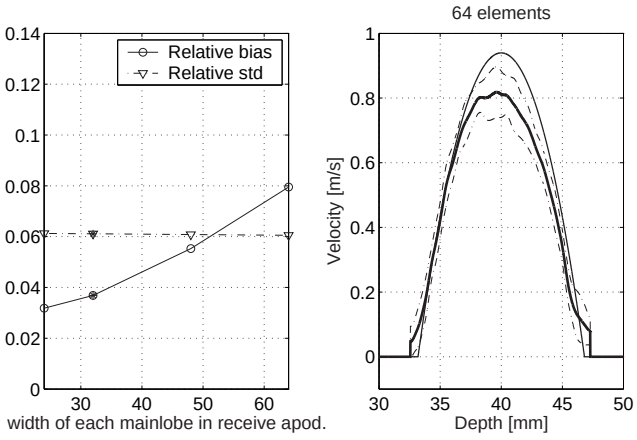

Fig. 9. Left: The relative standard deviation and relative bias as a function of the width of each Hanning functions used in the receive apodization. The points marked with $*$ is the initial position in the parameter space. Right: The estimated transverse velocity and standard deviation when each Hanning is 64 transducer elements in width. The thin line indicates the true velocity as a function of depth. The thick line is the estimated mean transverse velocity, and the two dashed lines are the mean transverse velocity ± 1 standard deviation.

The transverse wavelength λ_x was varied from 0.8 mm to 1.7 mm in intervals of 0.3 mm and the effect of the relative standard deviation and relative bias can be seen to the left in Fig. 10. Only the relative standard deviation is significantly effected by the variation in the wavelength, which is a result of the general properties of the autocorrelation estimator. The autocorrelation estimator is unbiased and the standard deviation is inversely proportional to the wavelength [18]. In principle the relative standard deviation could be decreased below 0.06 if a transverse wavelength shorter that 0.8 mm was used. However, a short wavelength for a fixed depth z and fixed center frequency f_0 can only be created by increasing the distance D between the two peaks in the receive apodization function (8). Since the transducer has a fixed width of 26.6 mm, this sets a lower limit to the transverse wavelength.

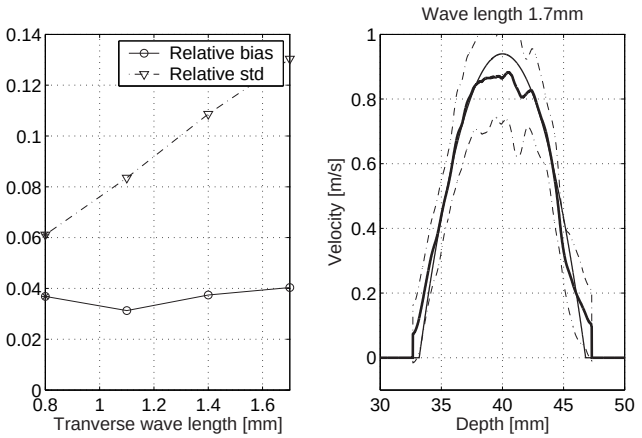

Fig. 10. Left: The relative standard deviation and relative bias as a function of the transverse wave length. The initial position in the parameter space is marked with $*$. Right: The estimated transverse velocity and standard deviation for a transverse wavelength of 1.7 mm. The thin line indicates the true velocity as a function of depth. The thick line is the estimated mean transverse velocity, and the two dashed lines are the mean transverse velocity ± 1 standard deviation.

Different types of echo canceling filters were tested on the received signal and the result can be seen to the left in Fig. 12. Stationary tissue with a scattering strength 100 times stronger than the blood signal, has been added in these simulations, in order to make the data more realistic. No echo canceling has been performed in filter a) and filter b) is the mean subtraction filter described by (27). Filter c) has the transfer function $H(z) = 1 - z^{-1}$ which implies that the filtered signal is simply the result of subtracting consecutive lines. Filter d) has the transfer function $H(z) = (1 - 1.5z^{-1} + 0.5z^{-3})/3$. This filter has a more well-defined cut-off frequency than filter c) which can be seen in Fig. 11.

Since tissue has been modeled in the Field II simulation, the result of having no echo canceling yield a velocity estimate with significant bias. Applying the mean subtraction filter (filter b) described by (27), removes the stationary component and no distortion on the signals originating from the blood is performed. This filter therefore has the lowest relative bias. The relative bias increases for filter c) and filter d) which is a result of the distortion of the frequency spectrum performed by these filters.

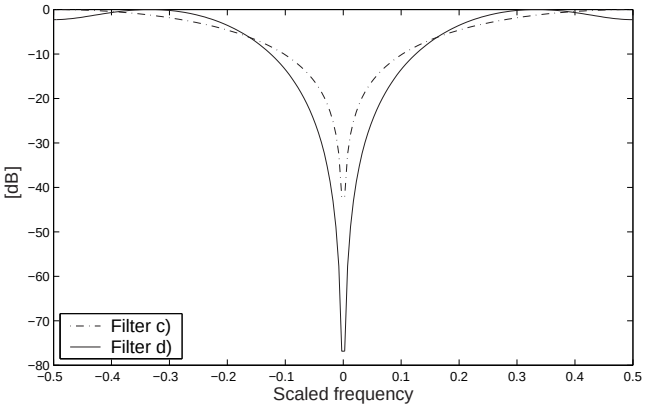

Fig. 11. The frequency characteristics of the echo canceling filters c) and d). Filter c) is defined by the transfer function $H(z) = 1 - z^{-1}$ and filter d) is defined by $H(z) = 1/3(1 - 1.5z^{-1} + 0.5z^{-3})$

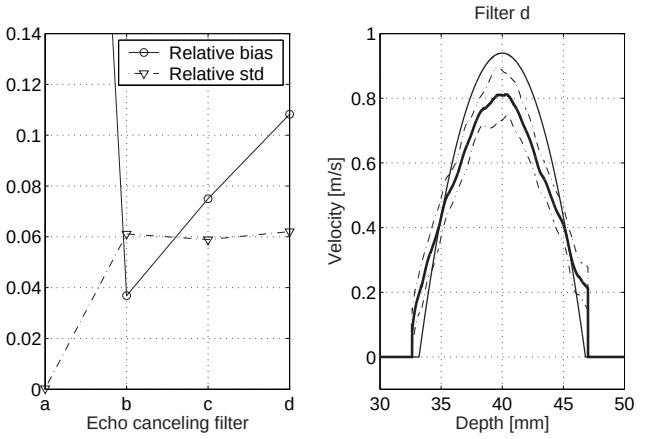

Fig. 12. Left: The relative standard deviation and relative bias as a function of different echo canceling filters. Filter a) corresponds to no echo canceling. Here the corresponding bias is 0.63. Filter b) is the mean subtraction echo canceling described by (27). c) is the filter with the transfer function $H(z) = 1-z^{-1}$ and d) has the transfer function $H(z) = 1/3(1-1.5z^{-1}+0.5z^{-3})$. Right: The estimated transverse velocity and standard deviation for the filter d) with the transfer function $H(z) = 1/3(1 - 1.5z^{-1} + 0.5z^{-3})$. The thin line indicates the true velocity as a function of depth. The thick line is the estimated mean transverse velocity, and the two dashed lines are the mean transverse velocity ± 1 standard deviation.

The number of pulse firings used for each velocity estimate has been varied between 8 and 40 in intervals of 8 firings. Also 4 firings for each estimate have been investigated. The result can be seen to the left in Fig. 13. The performance of the TO method degrades rapidly as the number of firings per estimate decreases. To obtain a reasonable low bias on the velocity estimate the number of firings should be at least 8. This is comparable to the number of firings used in most commercial scanners.

The type of receive apodization has been varied, and the relative standard deviation and relative bias have been measured and are shown to the left in Fig. 14. Apodization type a) is two Hanning functions $h(\xi - \xi_p) + h(\xi + \xi_p)$ each

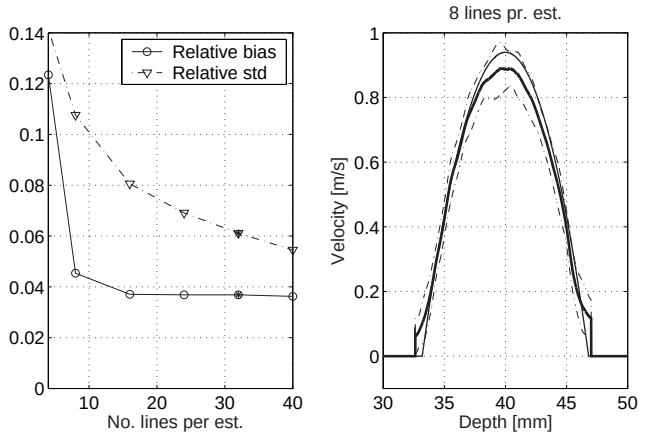

Fig. 13. Left: The relative standard deviation and relative bias as a function of number of samples pr. velocity estimate. The initial position in the parameter space is marked with $*$. Right: The estimated transverse velocity and standard deviation for 8 samples pr. estimate. The thin line indicates the true velocity as a function of depth. The thick line is the estimated mean transverse velocity, and the two dashed lines are the mean transverse velocity ± 1 standard deviation.

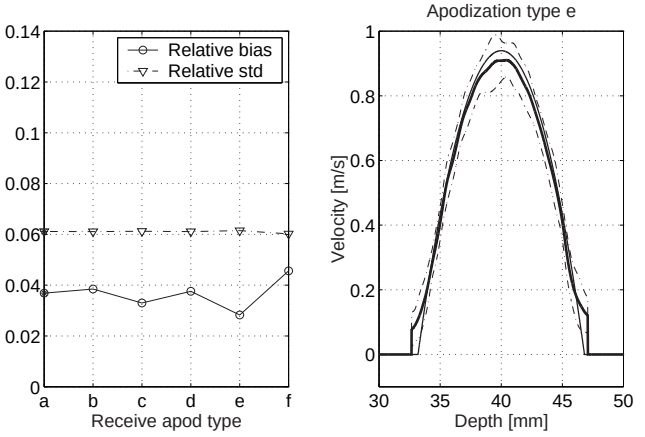

Fig. 14. Left: The relative standard deviation and relative bias as a function of the receive apodization type. a) is two Hanning functions. b) is two Hamming functions. c) is two Blackman functions. d) is two Gaussian functions and e) is two Sinc functions as described by equation 5. Type f) is the apodization functions suggested by Anderson. The points marked with $*$ is the initial position in the parameter space. Right: The estimated transverse velocity and standard deviation for the two Sinc apodization in receive. The thin line indicates the true velocity as a function of depth. The thick line is the estimated mean transverse velocity, and the two dashed lines are the mean transverse velocity ± 1 standard deviation.

having the width of 32 transducer elements and center position in ξ_p. Apodization type b) uses two Hamming functions. Apodization type c) is two Blackman functions. Apodization type d) is two Gaussian functions, and apodization type e) is two Sinc functions as described by (5). Type f) focus the beam from each of the two receive beamformer along the same line, and uses two different apodization functions on each beamformer. On the even beamformer two Hanning functions $h(\xi - \xi_p) + h(\xi + \xi_p)$ are used and on the odd beamformer the apodization given by $h(\xi - \xi_p) - h(\xi + \xi_p)$ is used. This is the apodization functions suggested by Anderson [9]. The two apodization functions shifts the pulse echo field 90° with respect to each other in the transverse direction.

The performance of the TO method does not seem to be effected significantly by the type of apodization. However, since the the energy in the received signal will scale with the area under the apodization function, it is advisable to use the functions which have the largest area.

The influence of noise on the performance has been tested. Zero mean white Gaussian noise $n(t)$ was added to the received signals $s(t)$ before beamforming, i.e. the noise was added to the signal from each transducer element. The SNR on each element was determined by

$$\text{SNR}_{dB}^{el} = 10 \log_{10} \frac{E\{s^2(t)\}}{E\{n^2(t)\}}. \tag{31}$$

After beamforming and matched filtration the SNR is [19]

$$\text{SNR}_{dB}^{beam} = 10 \log_{10} \left(\frac{\left| \sum_{k=1}^{N} a(k) \right|^2}{\sum_{k=1}^{N} |a(k)|^2} \right) + \text{SNR}_{dB}^{mat} + \text{SNR}_{dB}^{el}, \tag{32}$$

where $a(k)$ is the receive apodization on element k, N is the number of tranducer elements which is 128 and SNR_{dB}^{mat} is the improvement in SNR due to matched filtration. Using two Hanning functions as receive apodization, each with a width of 32 tranducer elements, yields

$$\text{SNR}_{dB}^{beam} = 29.2 + \text{SNR}_{dB}^{el} \tag{33}$$

where the contribution from the beamforming on the SNR is 16.4 dB and 12.8 dB from the matched filtration. The influence of SNR_{dB}^{el} between -30 dB and 0 dB was investigated in intervals of 6 dB and is shown in Fig. 15. The performance of the TO method only degrades significantly when the SNR_{dB}^{el} is below -18 dB which is due to averaging of the noise in the beamforming and the matched filtration. Also the influence of noise on the velocity estimator presented by Anderson [10] has been investigated. The estimator uses the multiplication of the two signals $\hat{r}_{even}(n)$ and $\hat{r}_{odd}(n)$ from (15) and (16) to obtain two signals, which only depends on the axial velocity and the transverse velocity respectively. It is tempting to split the received signal into a signal which depends on the axial velocity, and a signal which depends on the transverse velocity. Echo canceling can be applied on each signal and the frequencies originating from the axial movement of the tissue can be removed without destroying the frequencies originating from the transverse movement of the blood. However, multiplying two stochastic signals is not in general advisable, and the relative standard deviation and relative bias rise significantly, when noise is present, which can be seen in Fig. 15.

IV. The experimental set-up

The TO method was evaluated on a circulating flowrig, which pumps blood mimicking fluid around a closed circuit. To avoid entrance effects in the flow, the fluid was first led through a 1.2 m long inflow pipe with radius $R = 6.4$ mm.

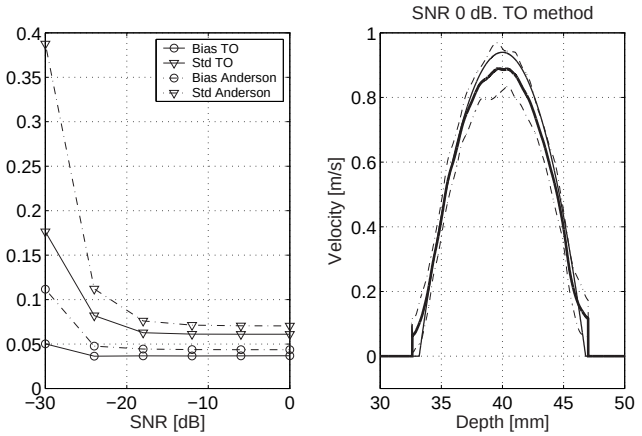

Fig. 15. Left: The relative standard deviation and relative bias as a function of SNR for white Gaussian noise added to the channel data before beamforming. The dotted line marked with "o" is the relative standard deviation on the velocity estimates using the TO velocity estimator and the thick line marked with "o" is the corresponding relative bias. The dotted line marked with "∇" is the relative standard deviation on the velocity estimates using the velocity estimator described by Anderson [10] and the thick line marked with "∇" is the corresponding relative bias. The initial position in the parameter space is marked with $*$. Right: The estimated transverse velocity and standard deviation for the TO estimator with a SNR of 0 dB. The thin line indicates the true velocity as a function of depth. The thick line is the estimated mean transverse velocity, and the two dashed lines are the mean transverse velocity ± 1 standard deviation.

At the end of the inflow pipe the fluid was led through a heat shrink tube submerged in a water container and scanned. The tube had a internal radius of 6.4 mm and the walls were 0.5 mm thick. The fluid volume flow Q was measured using a Danfoss MAG 1100 flow meter, which was situated after the heat shrink tube.

For the experiments, where the fluid velocity was constant over time, a Cole Parmer (Vernon Hills, IL) 75211-60 centrifugal pump was used. In this case the blood mimicking fluid consisted of water, glycerol, orgasol, Triton x-100, NaBenzoat and K_2EDTA diluted 10 to 1 with demineralized water. The blood mimicking fluid had viscosity $\mu = 2.6 \cdot 10^{-3}$ kg/(m s), density $\rho = 10^3$ kg/m^3, and the temperature during scanning was $T_0 = 24°C$.

For the experiments where the flow resembled the human femoral artery, a programable Compuflow1000 flow pump from Shelley (Toronto, Ontario) was used. In this case the blood mimicking fluid is described in [20], and the temperature during scanning was $T_0 = 24°C$.

To avoid turbulence in the fluid, the Reynolds number should be kept below approximately 2000 [21]. For flow in a pipe the Reynolds number R_e is defined as

$$R_e = \frac{2R\rho}{\mu}\overline{v} \tag{34}$$

where $\overline{v}$ is the mean velocity in the tube. Since $\overline{v}$ was kept below 0.4 m/s in all measurements, it was ensured that no turbulence was present in the flow.

A 7 MHz linear array transducer characterized by the parameters in Table IV was used to scan the blood mimicking fluid. The emitted pulse had a center frequency of 7 MHz. The pulse was focused at 40 mm at the center of the vessel, and Hamming apodization was applied on the transmit aperture in order to decrease sidelobe levels. The scanner used was the experimental scanner RASMUS which has 128 transmit channels and 64 receive channels with 2:1 multiplexing in receive. The sampling frequency is 40 MHz, and the dynamic range is 12 bits for each channel. Channel data were beamformed offline using a 32 CPU cluster system running Matlab (Mathworks, Inc., Natick, MA) under Linux. To acquire data from 128 elements in receive, two consecutive

TABLE IV
TRANSDUCER SET-UP

Parameter	Value
Transducer	Linear array
Elevation focus	25 mm
Number of elements	128
Pitch	0.208 mm
Kerf	0.035 mm
Center frequency	7 MHz
Sampling frequency	40 MHz
Apodization in transmit	Hamming
Number of cycles	8

shots were used. Each sampled on the left and right halfs of the transducer, respectively, and thereafter the data were combined to form a complete data set of 128 elements. The success of this interleaving procedure relies on the fact that the blood scatters moves a distance smaller than the width of the point spread function during two firings. Consecutive signals from the scatters can therefore be added, but the effective f_{prf} will be decreased by a factor 2.

The transverse oscillation in the pulse echo field was introduced by manipulating the receive apodization function as described in section II . Two Hanning functions, each with a width of 32 transducer elements, were used to create the receive apodization. The distance between the peaks of the two Hanning functions were adjusted so that the transverse oscillation length λ_x in the pulse echo field was kept constant $\lambda_x = 1$ mm for the entire scanned area. Two beams were then beamformed, each separated a transverse distance of $\lambda_x/4 = 0.25$ mm using dynamic focusing. The beamforming was performed using a sound speed of $c = 1480$ m/s equal to the speed of sound in water. Echo canceling was applied on all beamformed data using the mean subtraction filter given by (27).

A. Measurement of lateral oscillation length

To verify that the TO method can produce a pulse-echo field where an oscillation is present in the transverse direction, a wire phantom was scanned using the RASMUS scanner and the linear array transducer described in Table IV. An active aperture consisting of 64 elements was moved over the transducer surface in steps of one element and a B-mode image was acquired without envelope detection. The wire was located in water at a depth of 40 mm and the distance between the maxima of the the two Hanning functions in the receive apodization function was adjusted to give a constant transverse wavelength $\lambda_x = 1.4$ mm.

The resulting PSFs for each beamformer can be seen in the top row of Fig. 16. Since the distance between each transducer element was 0.208 mm, the lateral resolution is poor, however, the transverse oscillation is clearly visible.

In the bottom of Fig. 16 the 2D-FFT power spectrum for the two PSFs is shown. The two clearly defined peaks on the y-axis is the center frequency of the emitted pulse. The center frequency on the x -axis corresponds to the transverse oscillation in the pulse-echo field. From the power spectrum the mean lateral wavelength is calculated to be $\lambda_x = 1.6$ mm, which is 16% more than the theoretical value of $\lambda_x = 1.4$ mm. Since the transverse velocity scales with the transverse spatial frequency $1/\lambda_x$, it is therefore expected that the velocity estimates will be slightly biased.

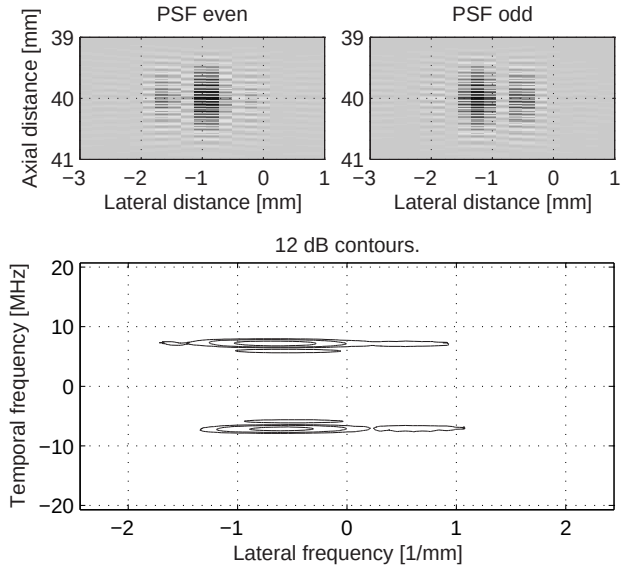

Fig. 16. Top: The PSFs from each beamformer. Bottom: the 2D power spectrum of $PSF_{even} + j\,PSF_{odd}$.

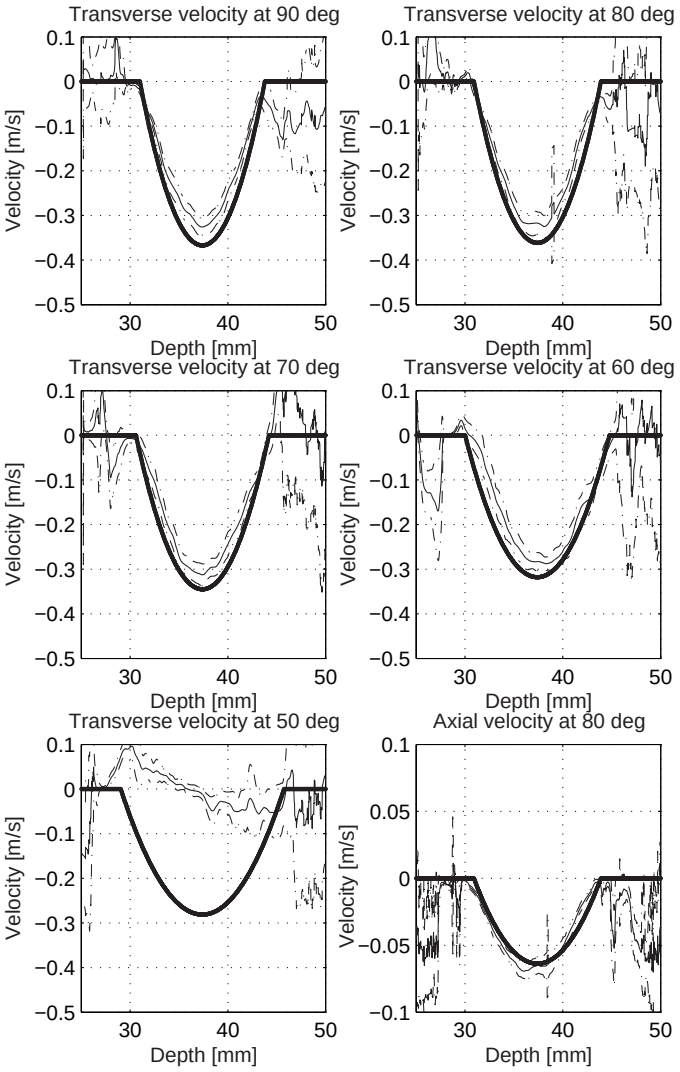

Fig. 17. The velocity as a function of depth for different angles of flow. The thick solid line is the theoretic parabolic velocity profile described by (26). The thin solid line is the mean of all the velocity estimates and the two dotted lines are the mean profile plus/minus 1 standard deviation. No attempt has been made to suppress false velocity estimates at the vessel wall and in the surrounding water.

V. Results for constant volume flow

The first set of measurements was performed on a flow where no acceleration was present. The volume flow rate Q was fixed at 23.6 ml/s, and since

$$Q = \overline{v}A \tag{35}$$

where $A = \pi R^2$ is the area of the cross section of the pipe, it follows from (34) that the Reynolds number is approximately 900. The flow can therefore be assumed laminar, and the flow velocity v as a function of distance r from the center of the pipe can be described by (26). The maximum velocity v_0 at the center of the pipe was, thus, $v_0 = 0.367$ m/s.

Five experiments were performed where the angle between the ultrasound beam and the flow velocity vector was varied between 50° and 90° in steps of 10°. The f_{prf} used was 4 kHz and the number of shots fired was 2000. Due to the interleaving procedure described in the previous section, this gives an effective f_{prf} of 2 kHz and 1000 beamformed lines, where 32 lines were used for each velocity estimate. In Fig. 17 the transverse velocity profiles and standard deviation as a function of depth are shown for the measured angles of flow. It can be seen that the estimated transverse velocities are approximately parabolic down to a flow angle of 60°. At 50° no parabolic velocity profile can be seen, even though the standard deviation still remains relatively small. The increase in bias at this angle is in agrement with the simulated results.

For comparison, the estimated axial velocity for 80° is also shown in Fig. 17 where the estimate is based on a conventional axial auto correlation estimator. The angle of 80° is the smallest of the measured angles where no aliasing occur in the axial estimate using $f_{prf} = 2$ kHz. It should be noted that the conventional axial estimate is based on the same channel data as the transverse velocity estimate at the same angle. Only the beamforming is different since no transverse oscillation in the

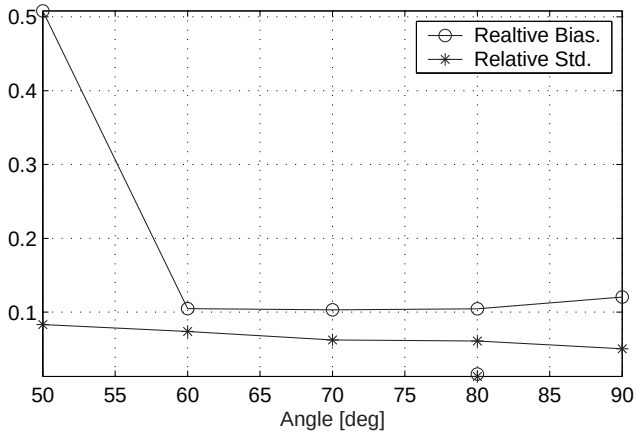

Fig. 18. The relative standard deviation and relative bias on the estimated velocity for different angles of flow.

pulse echo field has been introduced. Hamming apodization was used to suppress sidelobes in the receive beamforming, and 32 beamformed lines were used for each velocity estimate.

To quantitively compare the different velocity measurements, the relative standard deviation $\tilde{\sigma}_{v_x}$ and relative bias $\tilde{B}_{v_x}$ were estimated. In Fig. 18 $\tilde{\sigma}_{v_x}$ and $\tilde{B}_{v_x}$ are shown, and it can be seen that both $\tilde{B}_{v_x}$ and $\tilde{\sigma}_{v_x}$ remains approximately constant between $60°$ and $90°$. The two measurements at $80°$, which are not connected by a line, are the relative bias and relative standard deviation for the axial velocity estimate at this angle. Their values are $\tilde{\sigma}_{v_z} = 0.01$ and $\tilde{B}_{v_z} = 0.01$, i.e. approximately five times smaller than the corresponding $\tilde{\sigma}_{v_x}$ and $\tilde{B}_{v_x}$ for the transverse velocity at the same angle. This is in agreement with the corresponding simulations for constant flow.

VI. Results for pulsatile flow

Since the blood flow in the human body is not generally constant, the TO method has been tested for a pulsatile flow, which resembles flow in the femoral artery. The transverse flow velocity was estimated as a function of depth and time for 1.44 seconds of flow, and since the cycle period of the pump was 0.84 seconds, the measurements captured nearly two cycles of flow. At an f_{prf} of 6 kHz, 10080 beams were emitted from the transducer. Due to the interleaving procedure this gives an effective $f_{prf} = 3$ kHz and 5040 beamformed lines. The lines were divided into segments of 100 lines where consecutive segments had an overlap of 90%. The segments were then echocanceled using (27) and passed to the transverse velocity estimator.

In Fig. 19 the transverse velocity as a function of depth and time is shown for the angles $60°$ and $90°$. Also the axial velocity estimated at $60°$ is shown. The axial estimate at $60°$ is derived using a conventional axial estimator, and the data used are the same as the transverse velocity estimate at $60°$ is based on. Even though the transverse velocity estimates at $90°$ or $60°$ does not become as good and detailed as the axial estimate at $60°$, the transverse estimates still show the same overall flow.

The measurements can be more easily compared by deriving the corresponding volume flow as a function of time, by integrating the velocity over the vessel cross section area. Here the velocity profile is assumed circular symmetric around the center of the pipe. The volume flow rate is shown as a function of time in Fig. 20. When derived from the axial velocity, the measured volume flow at $60°$ clearly shows the characteristic profile of the flow in the femoral artery. Here a large positive peak in the flowrate is followed by a smaller negative peak and an even smaller positive peak. This pattern is also seen when the flow rate is derived from the transverse velocity profiles. The relative error between the two flowrate profiles at $60°$ is found to be 13.4%. The relative error between the flowrate derived from the transverse velocities at $90°$ and the flowrate derived from the axial velocity at $60°$ is found to be 27.8%. Here the relative error α between the two volume profiles $Q_{ref}(n)$ and $Q(n)$ of length N is defined as

$$\alpha = \frac{\sum_{n=1}^{N} |Q_{ref}(n) - Q(n)|}{\sum_{n=1}^{N} |Q_{ref}(n)|} \tag{36}$$

where the reference flowrate $Q_{ref}(n)$ is the flowrate derived from the axial velocity estimate at $60°$.

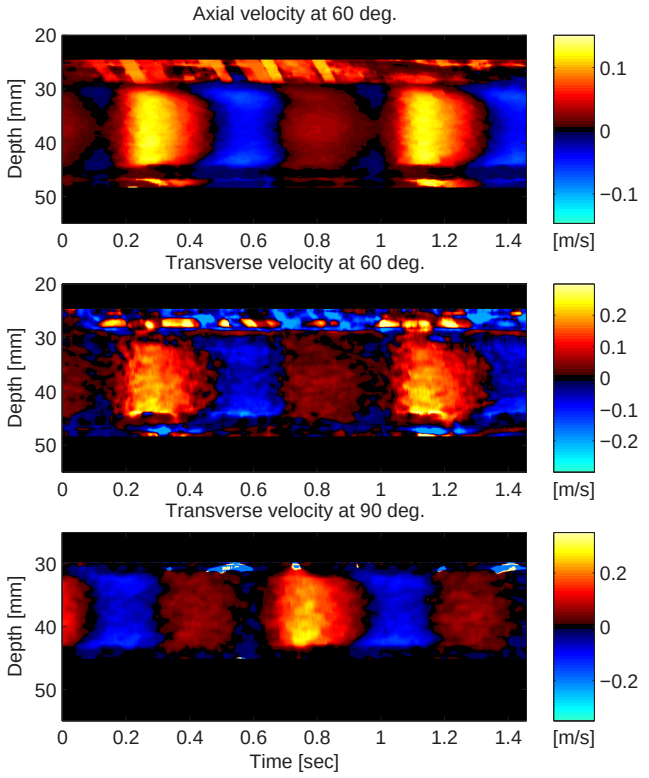

Fig. 19. Velocity as a function of time and depth. Top: Axial velocity at $60°$ flow angle. Center: Transverse velocity at $60°$ flow angle. Bottom: Transverse velocity at $90°$ flow angle. The flow resembles the flow in the human femoral artery. No attempt has been made to suppress false velocity estimates at the vessel wall and in the surrounding water.

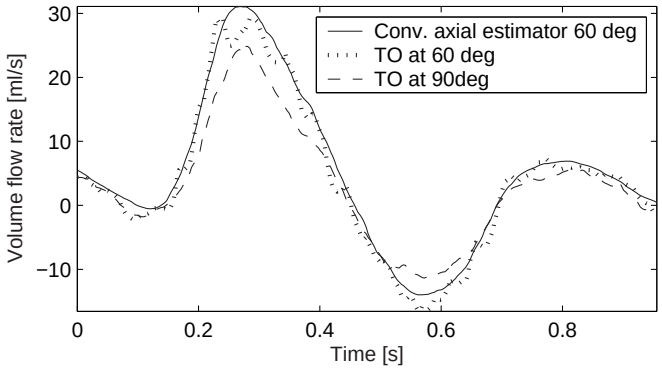

Fig. 20. The volume flow rate derived from the transverse velocity at $90°$, the transverse velocity at $60°$ and the axial velocity at $60°$.

VII. Discussion

A parameter study of the TO method has been performed and the resulting relative standard deviation and relative bias have been calculated for a number of points in the parameter space. The parameter study shows that the TO method is sensitive to the angle between the ultrasound beam and the flow direction. At angles more than approximately $45°$ the TO method can produce relatively good estimates of the transverse velocity. It is thus possible to estimate blood velocities at angles where a conventional scanner fails to detect any velocity at all.

Furthermore, it has been shown that the TO method is capable of measuring the transverse velocity in an experimental setup for angles between $60°$ and $90°$ for both constant and pulsatile flow. Parabolic velocity profiles are easily detectable down to an angle of $60°$ with a relative standard deviation and relative bias of approximately 10%. For pulsatile flow the characteristic profile of the flow in the femoral artery can be seen at both $90°$ and $60°$.

Future work should concentrate on the important issue of optimizing the echo-canceling filter. For small blood vessels the clutter signal will dominate the blood signal even in the center of the vessel, and the mean subtraction filter will presumably not be sufficient to remove all the clutter signal.

Also a clinical evaluation of the TO method has to be performed by an experienced sonographer. Different representative blood vessels have to be scanned and a reliable reference velocity estimate can be obtained by tilting the ultrasound beam. The TO method can then be evaluated by comparing the reference 1-D velocity to the 2-D vector estimate.

References

[1] M. D. Fox, "Multiple crossed-beam ultrasound Doppler velocimetry," *IEEE Trans. Son. Ultrason.*, vol. SU-25, pp. 281–286, 1978.

[2] G. E. Trahey, J. W. Allison, and O. T. von Ramm, "Angle independent ultrasonic detection of blood flow," *IEEE Trans. Biomed. Eng.*, vol. BME-34, pp. 965–967, 1987.

[3] V. L. Newhouse, D. Censor, T. Vontz, J. A. Cisneros, and B. B. Goldberg, "Ultrasound Doppler probing of flows transverse with respect to beam axis," *IEEE Trans. Biomed. Eng.*, vol. BME-34, pp. 779–788, 1987.

[4] O. Bonnefous, "Measurement of the complete (3D) velocity vector of blood flows," in *Proc. IEEE Ultrason. Symp.*, 1988, pp. 795–799.

[5] J. A. Jensen, "Directional velocity estimation using focusing along the flow direction: I: Theory and simulation," *IEEE Trans. Ultrason., Ferroelec., Freq. Contr.*, pp. 857–872, 2003.

[6] P. Munk, "Estimation of the 2-D flow vector in ultrasonic imaging: a new approach," M.S. thesis, Department of Information Technology, Technical University of Denmark, 1996.

[7] J. A. Jensen and P. Munk, "A new method for estimation of velocity vectors," *IEEE Trans. Ultrason., Ferroelec., Freq. Contr.*, vol. 45, pp. 837–851, 1998.

[8] J. A. Jensen, "A new estimator for vector velocity estimation," *IEEE Trans. Ultrason., Ferroelec., Freq. Contr.*, vol. 48, no. 4, pp. 886–894, 2001.

[9] M. E. Anderson, "Spatial quadrature: a novel technique for multi-dimensional velocity estimation," in *Proc. IEEE Ultrason. Symp.*, 1997, vol. 45, pp. 1233–1238.

[10] M. E. Anderson, "A heterodyning demodulation technique for spatial quadrature," in *Proc. SPIE - med. imag.*, 2000, pp. 1487–1490.

[11] J. Udesen and J. A. Jensen, "An in-vivo investigation of transverse flow estimation," in *Proc. SPIE - Progress in biomedical optics and imaging*, 2004, vol. 5373, pp. 307–314.

[12] J. Udesen and J. A. Jensen, "Experimental investigation of transverse flow estimation using transverse oscillation," in *Proc. IEEE Ultrason. Symp.*, 2003, pp. 1586–1589.

[13] J. A. Jensen and N. B. Svendsen, "Calculation of pressure fields from arbitrarily shaped, apodized, and excited ultrasound transducers," *IEEE Trans. Ultrason., Ferroelec., Freq. Contr.*, vol. 39, pp. 262–267, 1992.

[14] J. A. Jensen, "Field: A program for simulating ultrasound systems," *Med. Biol. Eng. Comp.*, vol. 10th Nordic-Baltic Conference on Biomedical Imaging, Vol. 4, Supplement 1, Part 1, pp. 351–353, 1996b.

[15] J. A. Jensen, O. Holm, L. J. Jensen, H. Bendsen, H. M. Pedersen, K. Salomonsen, J. Hansen, and S. Nikolov, "Experimental ultrasound system for real-time synthetic imaging," in *Proc. IEEE Ultrason. Symp.*, 1999, vol. 2, pp. 1595–1599.

[16] J. W. Goodman, *Introduction to Fourier optics*, McGraw Hill Inc., New York, second edition, 1996.

[17] C. Kasai, K. Namekawa, A. Koyano, and R. Omoto, "Real-time two-dimensional blood flow imaging using an autocorrelation technique," *IEEE Trans. Son. Ultrason.*, vol. 32, pp. 458–463, 1985.

[18] J. A. Jensen, *Estimation of Blood Velocities Using Ultrasound: A Signal Processing Approach*, Cambridge University Press, New York, 1996.

[19] D. H. Johnson and D. E. Dudgeon, *Array signal processing. Concepts and techniques.*, Prentice-Hall., Englewood Cliffs, New Jersey, 1993.

[20] K. V. Ramnarine, D. K. Nassiri, P. R. Hoskins, and J. Lubbers, "Validation of a new blood mimicking fluid for use in Doppler flow test objects," *Ultrasound Med. Biol.*, vol. 24, pp. 451–459, 1998.

[21] D. J. Acheson, *Elementary Fluid Dynamics*, Clarendon Press, Oxford, 1990.

Examples of in-vivo blood vector velocity estimation

Jesper Udesen[1,2], Michael Bachmann Nielsen[3], Kristina Rue Nielsen[3] and Jørgen Arendt Jensen[1]

1) Center for Fast Ultrasound Imaging, Ørsted•DTU,
Bldg. 348, Technical University of Denmark, DK-2800 Lyngby, Denmark.
2) B-K Medical A/S, Mileparken 34, DK-2730 Herlev, Denmark.
3) Department of Radiology, Section of Ultrasound,
Rigshospitalet. Blegdamsvej 9, DK-2100 Kbh. Ø, Denmark.

I. Abstract

In this paper examples of in-vivo blood vector velocity images of the carotid artery are presented. The transverse oscillation (TO) method for blood vector velocity estimation has been used to estimate the vector velocities and the method is first evaluated in a circulating flowrig where performance as function of flow angle is found. At 90° beam to flow angle the TO method can estimate the transverse velocity with a mean standard deviation of 2.8 % and with a mean absolute bias of 11.8 %.

A carotid artery is scanned in-vivo at three different positions by experienced sonographers. The scanning regions are: 1) The common carotid artery at 88° beam to flow angle, 2) The common carotid artery and the Jugular vein at $\sim 90^\circ$ beam to flow angle and 3) The bifurcation of the carotid artery. The resulting velocity estimates are displayed as vector velocity images where the velocity vector is superimposed on a B-mode image showing the tissue structures.

The volume flow is found for case 1) and when compared with MRI from the literature, a bias of approximately $\sim 20\%$ is found. The maximum flow velocities within the carotid artery is found to be 0.8 m/s, which is normal for a healthy person. In case 3) the estimated vector velocities are compared with numerical simulations. Qualitatively the same flow pattern can be seen in both simulations and in the vector velocity images. Furthermore a vortex is identified in the carotid sinus at the deceleration phase after the peak systole. This vortex is seen in all of the three acquired cardiac cycles.

II. Introduction

It is a well known limitation of conventional ultrasound scanners, that only the axial (i.e. towards or away from the transducer) velocity component of the blood can be estimated. This is a severe limitation especially in regions where blood vessels are curved or where different flow directions are present in e.g. bifurcations. In such regions the resulting CFM image will have a confusing appearance, since the axial velocity does not scale with the true speed of the blood. This is illustrated in Fig. 1, which shows the blood flow in the jugular vein, that carries the blood from the brain back to the heart. Even though the volume flow in the vein is constant throughout the image, different colors appear along the vessel, and at the center of the image the scanner fails to detect any blood flow at all. This is due to the angular dependence of the velocity estimates.

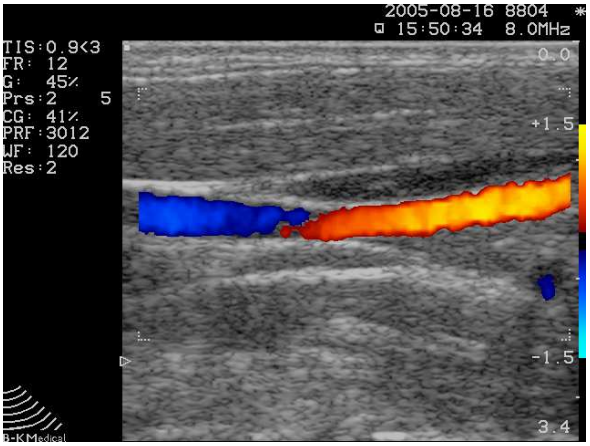

Fig. 1. Conventional CFM image of the flow in the Jugular vein acquired with a B-K medical 2102 scanner and a linear array BK-8804 transducer. The change in color and intensities in the blood vessel illustrates one of the fundamental problems with conventional flow estimation techniques.

Many authors have addressed the issue of extending the axial velocity estimate to a vector estimate, where both the speed and direction of the blood are found. Fox et al. [1] suggested a method where two transducers angled with respect to each other were used to find two independent axial velocity estimates from which the 2-D vector velocity could be found. Another variant of this method was suggested by Overbeck et al. [2]. Here the two angled ultrasound beams were constructed by having one transmitting aperture and two receiving apertures. The problem with both methods is that the angle between the two crossing beams decreases with depth. This implies that the standard deviation and bias on the vector estimates increases significantly for deeper lying vessels. Newhouse et al. [3] proposed a 2-D method where the spectral width of the Doppler spectrum was used to determine the lateral component of the velocity. For smaller vessels,

where large velocity gradients are present within a resolution volume, this method breaks down, since the lateral width of the spectrum also scales with the velocity spread within the volume. Trahey et al. [4] used 2-D cross-correlation on B-mode images of the blood flow to determine the vector velocity. This method is effective, especially close to the transducer where a high frame rate on the B-mode images can be obtained, but expensive in terms of computation power. Another method uses beamforming along the flow direction [5], [6], [7]. Here a normally focused ultrasound field is emitted and the data is beamformed along the direction of the flow. The acquired signals are then cross-correlated to find the shift in position and divided by the time between pulse emissions gives the velocity. The flow direction must, thus, be known before beamforming, or it can be determined by the method suggested by Kortbek and Jensen [8]. The directional beamforming method has also been employed in synthetic aperture flow imaging [9].

One promising method for finding the 2-D vector velocity is the method suggested by Jensen and Munk (Transverse Oscillation (TO)) [10], [11], [12] and by Anderson (Heterodyned Spatial Quadrature (HSQ)) [13], [14], [15]. The basic idea in both methods, is to introduce an additional oscillation in the lateral direction of the pulse-echo field and use an auto-correlation estimator to find the velocity. The TO method has been tested in both simulations and flow phantom experiments with promising results and preliminary in-vivo measurements have been performed at 90° beam to flow angle [16], [17].

This paper presents both experimental and clinical results from the TO method. First, in Section III, a brief discussion of the basic principle in the TO method is given. In Section IV the TO method is tested in a circulating flow rig scanned by the experimental scanner RASMUS [18], where the beam to flow angles are varied between $90^\circ - 50^\circ$. In Section V, clinical results are presented. Here the RASMUS scanner is used to scan the carotid artery at three different positions: 1) The common carotid artery at 88° beam to flow angle, 2) The common carotid artery and the Jugular vein at $\sim 90^\circ$ beam to flow angle and 3) The bifurcation of the carotid artery. Finally, in Section VI, the perspectives of the TO method are discussed.

III. Method

Ultrasound scanners for conventional Color Flow Map (CFM) imaging has a point spread function (PSF)[1] where a well defined oscillation is present along the ultrasound beam direction (the axial direction). This is illustrated in Fig. 2 which shows a simulation of a PSF for conventional CFM imaging[2]. Here the colors indicates the pressure received by the transducer. A well defined oscillation in the pressure along the axial direction can clearly be seen and the PSF has the shape of a bell curve along the lateral direction.

When blood scatterers are moving with an axial velocity v_z through the region of interest, the sampled signal recorded by the scanner[3] will oscillate with a frequency proportional to the axial velocity of the blood. The velocity is then found by estimating the mean frequency f_p in the sampled signal and the axial velocity can finally be found from

$$v_z = \frac{c}{2f_0} f_p \tag{1}$$

where $c = 1540$ m/s is the speed of sound in the human body and f_0 is the center frequency of the signal received by the transducer.

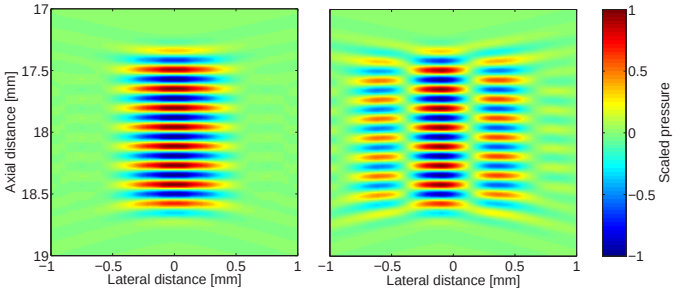

Fig. 2. A PSF obtained with a conventional CFM method using the Field II simulation program and the setup parameters given in Table II.

Fig. 3. A PSF where the TO method has been used to create an additional oscillation in the field transverse to the beam direction.

The reason why the conventional method fails to estimate the lateral component v_x of the velocity, is simply that the PSF does not oscillate in this direction but has the shape of a bell curve. When blood scatterers are moving along the lateral direction the resulting sampled signal has a frequency of $f_p = 0$ Hz and hence the the velocity is found from (1) to be $v_z = 0$ m/s. If the lateral component v_x of the velocity is to be found, it is therefore necessary to introduce an additional lateral oscillation in the PSF transverse to the beam direction as illustrated in Fig. 3.

The basic idea in the TO method is to create an additional oscillation in the PSF transverse to the beam direction. Qualitatively, this double oscillation field can be understood by the analogy of dropping two stones simultaneously into a pond as shown i Fig. 4. When the two wave patterns from each stone move outwards into the pond, they interfere with each other and at the region of interference the resulting wave pattern will oscillate in both the axial and lateral direction. The distance between the two stones will determine the lateral oscillation frequency and the size of the stones will determine the amplitude of the interference pattern and the bandwidth of the lateral frequency.

This principle can easily be applied on a ultrasound transducer. The sensitivity across the transducer surface (the apodization) can be adjusted, so that two distinct peaks resembling the two stones in the pond, are present, as illustrated

[1]The PSF is basicly an image of a single point scatterer as seen by the scanner.

[2]The PSF has been obtained using the ultrasound simulation program Field II [19], [20] where a 5 MHz linear array transducer and a point scatterer at a depth of 18 mm has been simulated.

[3]This signal is often called the *Doppler signal* or the *slow-time signal*

in Fig. 5. The resulting PSF will then oscillate both axially and laterally. The frequency of oscillation can be controlled by changing the distance between the two peaks and the bandwidth of the lateral oscillation can be controlled by the width of each peak[4].

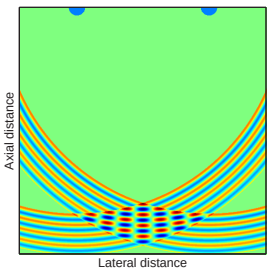

Fig. 4. The principle behind the creation of the double oscillating PSF can be understood by the analogy of dropping two stones simultaneously into a pond. The interference wave pattern in the pond will oscillate in two dimensions.

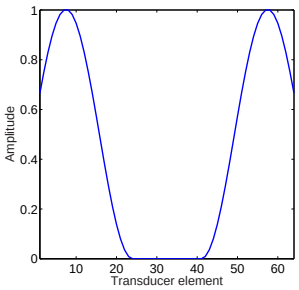

Fig. 5. The receive apodization function used to create the double oscillating PSF shown in Fig. 3.

In the TO method the apodization function shown in Fig. 5 is applied during reception of the ultrasound signals from the tissue and blood. The double oscillating field is therefore solely constructed in the receive beamforming and the transmitted signals from the transducer in the TO method is therefore identical to the transmitted signals from the conventional method for axial velocity estimation.

A schematic overview of the differences and similarities between the conventional method and the TO method is given in Table I and a comprehensive discussion about the theory behind the TO method can be found in [11], [12].

TABLE I

COMPARISON BETWEEN THE PROPERTIES OF THE CONVENTIONAL CFM METHOD AND THE TO METHOD.

	Conventional CFM method	TO method
Pulse-echo field	only axial oscillation	lateral and axial oscillation
Beams	one in transmit one in receive	one in transmit two in receive
In phase and quadrature signals	two	four
Echo canceling	FIR filter	polynomial regression [22], [23] of order 0-2
Velocity estimator	autocorrelation method [24]	extended auto-correlation method [12]

IV. SIMULATIONS AND EXPERIMENTS

The particular setup used for the in-vivo scanings presented in this paper, was evaluated in simulations and flow phantom experiments.

[4]The relation between the apodization and the lateral field component at the focal point is formally described by a Fourier transform [21]. This relation makes it possible to precisely shape the PSF by manipulating the apodization function of the transducer.

A. Resolution simulation

Due to the shape of the apodization function, one might expect a poor resolution of the PSF for the TO method compared to the conventional CFM method. This has been investigated using the Field II simulation program [19], [20] where a linear array transducer was simulated with the parameters given in Table II. This setup describes the transducer and scanner for all simulations, experiments, and in-vivo scannings performed in this paper. The axial and lateral resolution was found for both method (Fig. 6 and 7) using Hanning receive apodization on the conventional method. It can be seen that the axial resolution is identical for both methods. The apodization function for the TO method only affects the lateral intensity significantly in a 3 mm interval around the center of the PSF.

TABLE II

SCANNER AND TRANSDUCER SETUP USED FOR ALL EXPERIMENTS

Parameter	Value
Transducer	Linear array
Number of elements	128
Active number of elements	64
Pitch	0.3 mm
Kerf	0.035 mm
Center frequency	5 MHz
Number of cycles pr. pulse	8
f_{prf} in flow rig	0.6 kHz
f_{prf} in clinical scannings	6 kHz
Sampling frequency Field II	100 MHz
Sampling frequency RASMUS	40 MHz
Lateral wave length λ_x	1.0 mm
Apodization in transmit	Hanning
Apodization in receive	Two Hannings
Focus in transmit	18 mm
Focus in receive	Dynamic
F-number in transmit	3.3
F-number in receive	0.8
Number of firings pr. vel. est.	64
Lateral distance between velocity est.	4 pitch
$I_{spta \cdot is}$	293 mW/cm^2
MI	1.07
TIS	1.65

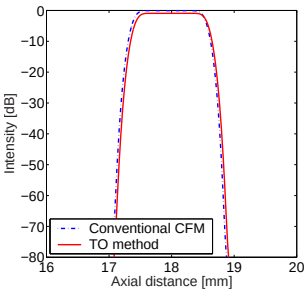

Fig. 6. The axial intensity for the conventional CFM method compared to the axial intensity for TO method. Simulation using the Field II program.

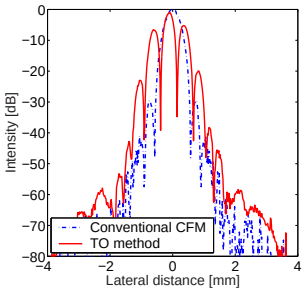

Fig. 7. The lateral intensity for the conventional CFM method compared to the lateral intensity for TO method.

B. Flow phantom experiments

The TO method was tested in a circulating flow rig scanned by the experimental scanner RASMUS [18] and a linear array transducer.

The function of the flow rig was to pump blood mimicking fluid around a closed circuit. Here all relevant parameters, like volume flow and ultrasound beam-to-flow angle, could be controlled. To avoid entrance effects in the flow, the fluid was first led through a 1.2 m long inflow pipe with radius $R = 6.0$ mm. At the end of the inflow pipe the fluid entered a heat shrink tube submerged in a water container. Here the scannings were performed. The tube had a internal radius of 6.0 mm and the walls were 0.5 mm thick. The fluid volume flow Q was measured using a Danfoss MAG 1100 (Sønderborg, Denmark) flow meter, which was situated after the heat shrink tube. A Cole Parmer (Vernon Hills, IL) 75211-60 centrifugal pump was used to pump the fluid around in the circuit at constant flow rate. The blood mimicking fluid consisted of water, glycerol, orgasol, Triton x-100, NaBenzoat and K_2EDTA diluted 10 to 1 with demineralized water. Temperature was $24°C$ and the viscosity was $2.6 \cdot 10^{-3}$ kg/(ms) (compared to $4 \cdot 10^{-3}$ kg/(ms) for blood).

The experimental scanner RASMUS was used for all experiments and the transmit setup was copied from a commercial scanner with a similar front end. This was done to ensure the optimal transmit pulse, in terms of both performance and the restrictions from the food and drug administration (FDA). Receive beamforming was done off-line in Matlab, and a lateral oscillation wavelength of 1 mm was applied in receive beamforming. All relevant parameters for the scanner and the transducer can be found in Table II.

Due to the geometry of the flow rig and the viscosity of the fluid, it was not possible to obtain velocities of more than ~ 0.3 m/s and still maintain laminar flow. I.e. the velocities were significantly less than the velocities in the carotid artery. To test the TO method at velocities comparable to the carotid artery, the maximum velocity in the flow rig was set to 0.1 m/s and the pulse repetition frequency (f_{prf}) was decreased from 6 kHz to 0.6 kHz. This gives a Reynolds number of 227 and hence the flow can be regarded as laminar [25]. Theoretically, the velocity profile through the tube can then be described by a parabola and the performance of the TO method is expected to be comparable to running at 1 m/s and $f_{prf} = 6$ kHz.

The distance from the transducer to the tube was adjusted, so that all fluid was situated less than 30 mm from the transducer surface. Due to the extend of the transducer, this results in a minimum beam-to flow angle of $50°$. The angle between the ultrasound beam and the flow was varied between $51.5° - 89.9°$ in steps of approximately $10°$. 64 pulse transmissions were used to find one velocity estimate and a total of 30 independent velocity estimates were found for each angle. The angle between the beam and the flow was found precisely from B-mode images acquired together with the velocity transmissions.

For each beam-to-flow angle, the mean velocity as a function of depth was found for both axial (v_z) and lateral (v_x) velocity estimates. The standard deviation on the estimates was found and the resulting curves can be seen in Fig. 9 together with curves for the theoretical parabolic profiles. The lateral velocity v_x is systematicly underestimated for all angles by approximately 10-20 %. Hence, compensation could be applied by multiplying the estimates with ~ 1.15. At flow angles of $51.5°$ and $61.8°$ aliasing is present in the axial flow estimates. In principle this could easily be removed by using a higher f_{prf}, but for the particular setup used the f_{prf} can not be raised above 6 KHz.

Fig. 8. The experimental RASMUS scanner. RASMUS has 128 transmitting channels and 64 receiving channels with 2:1 multiplexing. Arbitrary waveforms can be transmitted and the individual received channel data can be recorded for later processing.

To quantitatively validate the performance of the TO method, the relative mean standard deviation $\tilde{\sigma}_{v_x}$ and relative mean bias $\tilde{B}_{v_x}$ was calculated over the vessel for the estimates shown in Fig. 9. The non dimensional parameters $\tilde{\sigma}_{v_x}$ and $\tilde{B}_{v_x}$ are defined as

$$\tilde{\sigma}_{v_x} = \frac{1}{v_0(z_2 - z_1)} \int_{z_1}^{z_2} \sqrt{\frac{1}{M} \sum_{i=1}^{M} \left(\hat{v}_x^i(z) - \bar{v}_x(z)\right)^2} dz \quad (2)$$

$$\tilde{B}_{v_x} = \frac{1}{v_0(z_2 - z_1)} \int_{z_1}^{z_2} \left|\bar{v}_x(z) - v_x(z)\right| dz \quad (3)$$

where $v_0 = 0.1$ m/s is the velocity in the center of the tube, $\hat{v}_x^i(z)$ is one velocity estimate at a certain depth z, $\bar{v}_x(z)$ is the mean of the velocity estimates and $v_x(z)$ is the actual parabolic velocity profile. z_1 and z_2, are the depths to the beginning of the vessel and the end of the vessel, and $M = 30$ is the

number of velocity estimates $\hat{v}_x^i(z)$ used to calculate $\tilde{\sigma}_{v_x}$ and $\tilde{B}_{v_x}$. The resulting values can be found in Table III. It is seen that both the standard deviation and bias on the v_x estimate decreases with increasing angle and have a minima at $89.9°$. The axial performance is more difficult to evaluate due to the presence of aliasing at $51.5°$ and $61.8°$. For angles $> 61.8°$ axial standard deviation is approximately $2-4$ times smaller than lateral standard deviation and axial bias is approximately 10-20 times smaller than lateral bias. To solve the problems with low performance on the lateral velocity estimates, the TO method uses 64 pulse emissions for each velocity estimate. This is significantly higher than the number of emissions used in a conventional scanner for axial velocity estimation. Note that σ_x^2 is inversely proportional to the number of emissions N, and N can be lowered if a higher standard deviation can be accepted.

TABLE III

MEAN STANDARD DEVIATION $\tilde{\sigma}$ AND MEAN BIAS $\tilde{B}$ OVER THE TUBE FOR THE v_z AND v_x VELOCITY COMPONENTS IN PERCENT.

	$51.5°$	$61.8°$	$71.3°$	$80.0°$	$89.9°$
$\tilde{\sigma}_{v_x}$	4.8	4.6	4.3	3.0	2.8
$\tilde{B}_{v_x}$	14.4	15.0	20.3	13.8	11.8
$\tilde{\sigma}_{v_z}$	3.2	10.7	1.1	0.9	1.0
$\tilde{B}_{v_z}$	48.6	15.9	1.6	1.0	1.0

V. CLINICAL SCANNINGS

To clinically evaluate the performance of the TO method, the carotid artery was scanned at three different positions. This was done with the TO method used in a CFM fashion, where a vector velocity image (VVI) was superimposed on a conventional B-mode image.

A. Vector velocity image (VVI) setup

The RASMUS scanner and a linear array transducer described by the parameters from Table II was used for all clinical scannings. Since 64 pulse transmissions are used for each vector velocity estimate the frame-rate will be unacceptably low, if a full VVI is acquired at $f_{prf} = 6$ kHz. To increase frame-rate further, the TO method uses the time between emissions in a certain direction to transmit three other pulses at other spatial positions. This increases the actual f_{prf} to 24 kHz while maintaining the effective f_{prf} at 6 kHz. The result is that additional three velocity estimates can be acquired. However, the maximal scanning depth d will be limited by the time of flight for each pulse so that

$$d = \frac{c}{2f_{prf}} = \frac{1540\text{m/s}}{2 \cdot 24 \text{ kHz}} = 32 \text{ mm} \quad (4)$$

The used setup is therefore limited to depths less than 32 mm.

The vector velocities are found at 16 axial lines which are used to construct one VVI. This gives a lateral resolution of 1.2 mm on the velocity estimates and a frame-rate F of independent VVIs given by

$$F = \frac{24 \text{ kHz}}{64 \cdot 16 + 65} = 22 \text{ Hz}, \quad (5)$$

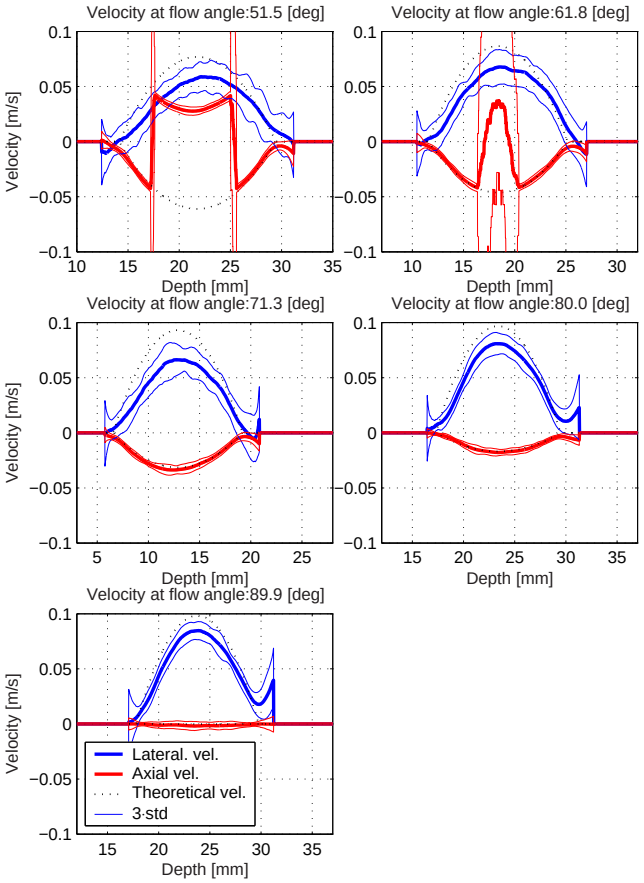

Fig. 9. The mean velocity (thick blue and red curves) and three times the standard deviation (thin blue and red curves) as a function of depth for flow angle $51.5°, 61.8°, 71.3°, 80.0°, 89.9°$. The theoretical parabolic velocity profiles (black dotted curves) are shown for comparison.

where the last term in the denominator is the number of emissions in the B-mode image, which is updated for each VVI. The scanner setup for B-mode emissions is identical to the setup for CFM emissions except for the number of cycles in each pulse, which is 1 for the B-mode emission. It should be noted that no filtering or averaging is performed on the VVI frames except from up-sampling to a size equal to the B-mode frames.

To differentiate between blood and tissue in each VVI frame a special technique is developed. A low resolution B-mode image is constructed from each B-mode image by first median filtering the image using a 1.5×0.5 mm kernel and thereafter low-pass filtering the image by convolving with a 3.8×0.5 mm square. All intensities below a certain threshold value in the low resolution B-mode image are then considered to be blood, where the velocity estimates are displayed. An example of this process is shown in Fig. 10 and 11.

B. The carotid artery at $88°$ beam to flow angle.

The carotid artery of a healthy 34 year old male was scanned for 1.81 seconds and data from approximately one and a half cardiac cycles was acquired. The beam-to-flow angle was

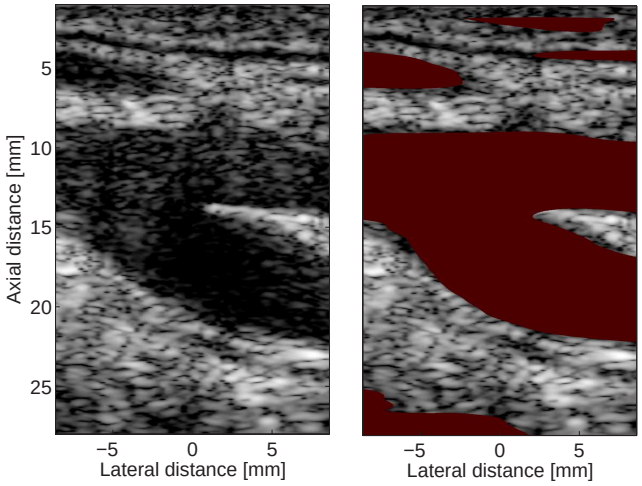

Fig. 10. B-mode image of the bifurcation of the carotid artery. Dynamic range is 40 dB.

Fig. 11. Same as Fig. 10 but with areas with potential blood presence colored in dark red. The threshold value is -29 dB.

found from the B-mode images to be approximately 88°, i.e. an angle where a conventional CFM method would not detect any movement of the blood. The B-mode sequence showed a clear intima, which indicates that the optimal scanning plane of the carotid artery was obtained.

To illustrate performance of the TO method when scanning the carotid artery, a number of VVI frames are shown in Fig. 13, 14 and 15. The acquisition time of each frame is illustrated by red circles in Fig. 12. It is seen that homogeneous vector estimates can be obtained and that the vector arrows follows the vessel walls in all frames. The maximum velocity at the time of peak systole is approximately 0.8 m/s. According to Evans et. al. [26] this is a normal value for a healthy person.

To further evaluate performance, the volume flow as a function of time was found. From each VVI frame the positions of the carotid vessel walls were automaticly identified. The velocity was integrated up over the vessel cross section area assuming circular symmetry. This was done in a 5 mm lateral wide strip in the center of the image to yield the volume flow. When averaging these estimates, the mean volume flow through the vessel as a function of time could be found as shown in Fig. 12. For comparison the data obtained by Marshall et. al. [27] using MRI is also depicted. There is a significant bias between the two measurements especially at the time of the first peak systole. A certain bias is expected since the flow rig measurements in Section IV showed a systematic under estimation of the theoretical lateral velocity of approximately 10-20 %. It should be noted that the volume flow from Marshall et. al. was based on measurements from 14 carotid arteries, where two of these showed abnormal flow-rates.

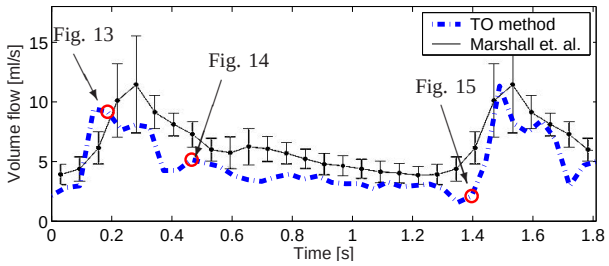

Fig. 12. The estimated volume flow as a function of time. For comparison the data obtained by Marshall et. al. [27] using MRI is also shown. The red circles indicates the acquisition time for the VVI frames shown in Fig. 13-15

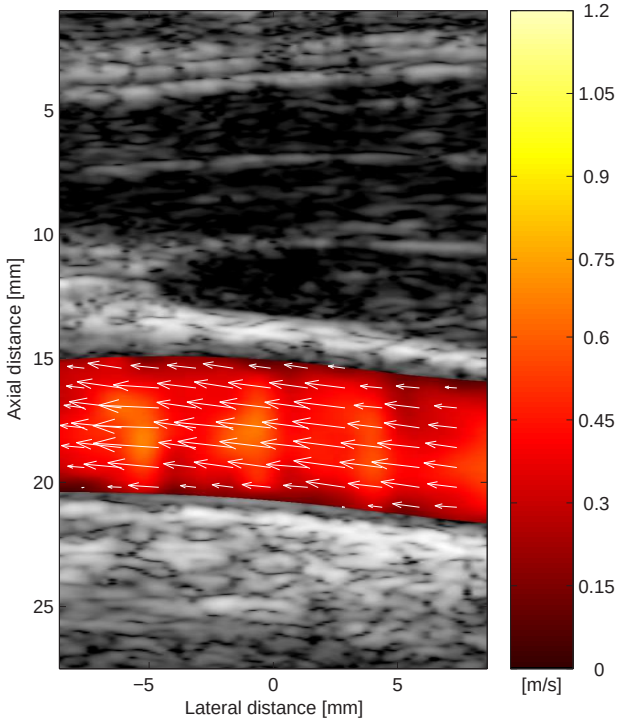

Fig. 13. The vector flow in the carotid artery at the time of the peak systole.

C. The carotid artery and jugular vein at 90° beam to flow angle.

A VVI sequence of 3.18 seconds using the TO method was acquired of the carotid artery and jugular vein. The volunteer was 30 year old and presumed healthy. A VVI frame at the time of the peak systole is shown in Fig. 16. The different directions of the blood velocity in the vein and the artery is clearly visible and the maximum velocity within the artery is approximately 0.8 m/s, i.e. a realistic value for a healthy person.

D. The bifurcation of the carotid artery

The bifurcation posses a challenge to the TO method due to the geometry of the vessels and hence the complicated flow pattern. This is especially the case at the time of the peak systole, where numerical simulations [28], [27], [29] have

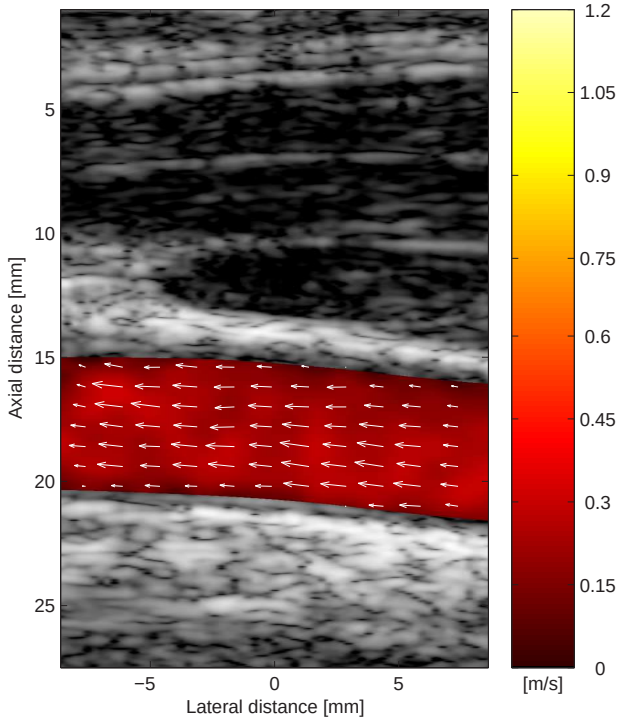

Fig. 14. The vector flow in the carotid artery at the time of the end systole.

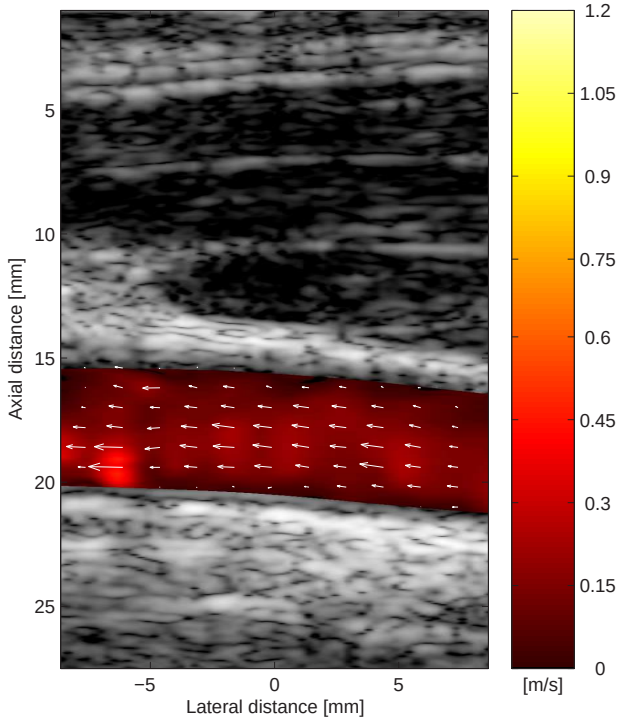

Fig. 15. The vector flow in the carotid artery at the time of the end diastole.

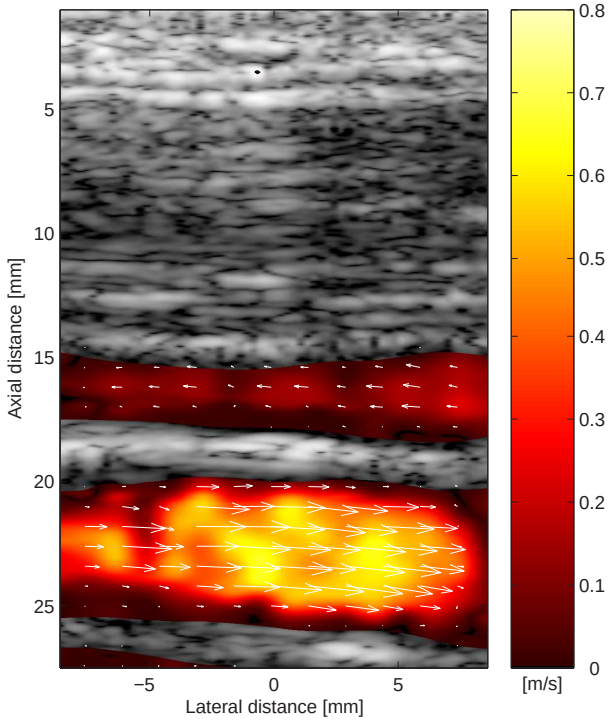

Fig. 16. The vector flow in the carotid artery and jugular vein at the time of the peak systole.

shown that a complicated flow pattern is present.

The carotid artery bifurcation of a healthy 30 year old male was scanned for 3.18 seconds yielding a sequence of 68 VVI frames covering three peak systoles. Fig. 17 shows the vector flow at the time of the second peak systole. Here a characteristic lack of flow is seen to be present in the lower part of the carotid sinus and a strong blood current is concentrated in the external carotid artery and the upper part of the internal carotid artery. This observation is confirmed by numerical studies [28], [27], [29] from where one simulated velocity image obtained from [29] is shown in Fig. 18. The same overall flow pattern is seen even though the geometry of the bifurcation in the simulation is significantly different from the ultrasound scanning bifurcation.

Numerical simulations predicts that a region with reversed flow will be present at the lower part of the carotid sinus shortly after peak systole. This is confirmed by the TO method. In Fig. 19 the vector flow 5 ms after peak systole is seen and a strong vortex can easily be identified in the lower part of the carotid sinus. This vortex is present in all of the three VVI frames obtained 5 ms after the three peak systoles. The corresponding simulation frame obtained from [29] is shown in Fig. 20. Here the vortex is not that dominant even though reversed flow can be seen in the lower part of carotid sinus.

This vortex can also be seen on the axial velocity estimate obtained with the conventional axial CFM technique. In Fig. 21 the axial velocity is shown. Each axial velocity estimate is found from 64 pulse emissions to obtain maximum perfor-

mance. The region with reversed flow is clearly visible as well as a region at the upper part of the carotid sinus with strong downwards flow.

Aliasing could potentially be confused with regions with reversed flow, but it is obvious from Fig. 21 that no axial aliasing is present even at flow angles of $\sim 45°$. Axial aliasing will happens when the Nyquist sampling theorem is violated, i.e. at axial velocities v_z^{max} larger than

$$v_z^{max} = \frac{c\, f_{prf}}{4 f_0} = \frac{1540 \text{ m/s} \cdot 6000 \text{ Hz}}{4 \cdot 5 \cdot 10^6 \text{ Hz}} = 0.46 \text{ m/s} \qquad (6)$$

Lateral aliasing will occur at purely transverse flow velocities v_x^{max} larger than

$$v_x^{max} = \frac{\lambda_x}{2} f_{prf} = \frac{0.001 \text{ m}}{2}\ 6000 \text{ Hz} = 3 \text{ m/s} \qquad (7)$$

It is, therefore, expected that no aliasing phenomenon will occur, when using the TO method on the carotid artery for this measurement setup.

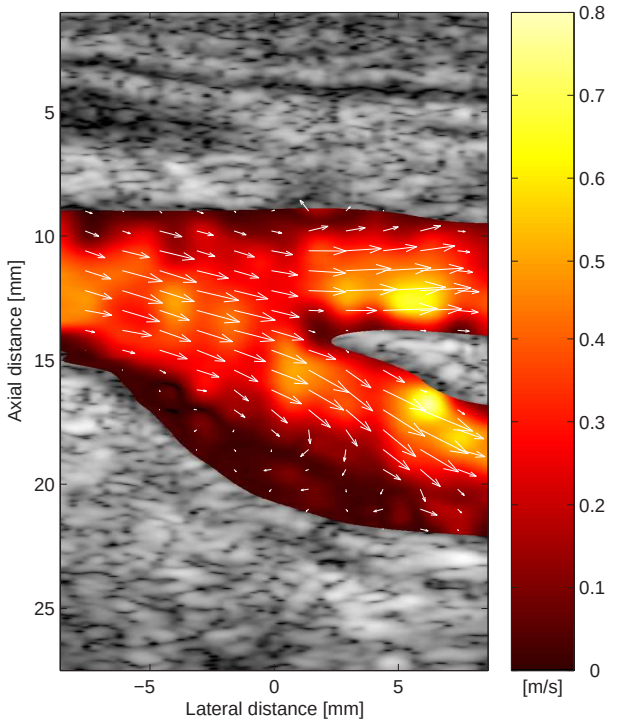

Fig. 17. The vector flow in the bifurcation of the carotid artery at the time of the peak systole.

VI. Discussion

When comparing the VVI frame in Fig. 19 with the conventional CFM frame in Fig. 21 it is evident that there is a huge potential in the TO method. The correct velocity magnitude and direction of the flow is displayed with the TO method. This is in contrast to the conventional CFM method, where only the axial component of the velocity is found.

Information which shows complicated vortex structures in the flow, can be gathered at regions where plaque might build

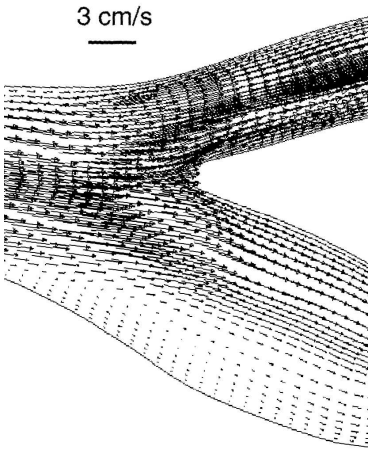

Fig. 18. A simulation of the vector flow in the bifurcation of the carotid artery at the time of the peak systole (reprinted with permission from Marshall et al. [29]).

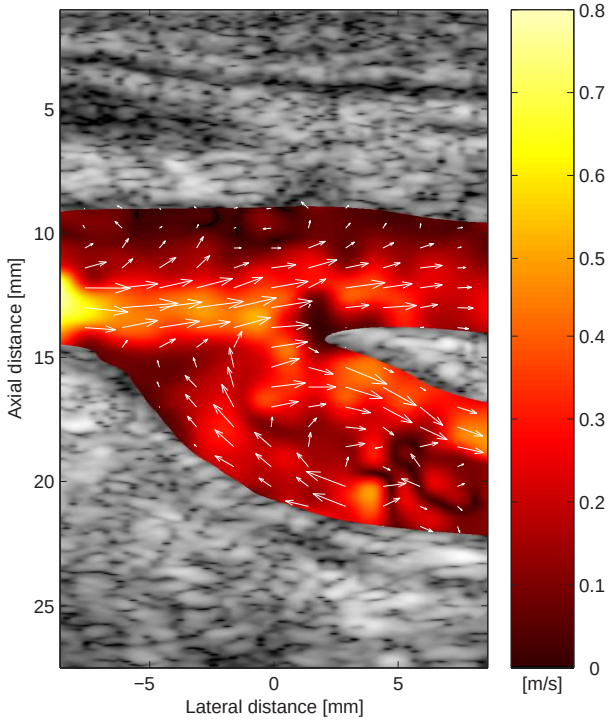

Fig. 19. The vector flow in the bifurcation of the carotid artery shortly after the peak systole.

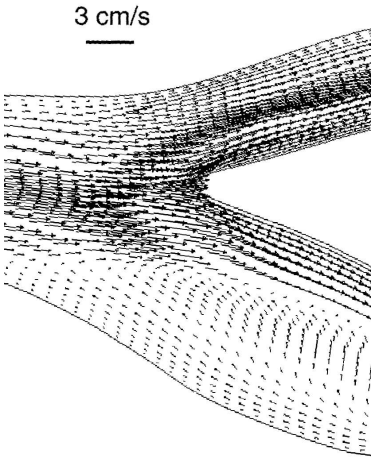

Fig. 20. A simulation of the vector flow in the bifurcation of the carotid artery at the time of the end systole (reprinted with permission from Marshall et al. [29]). In the lower part of carotid sinus a region with reversed flow is present (flow from right to left).

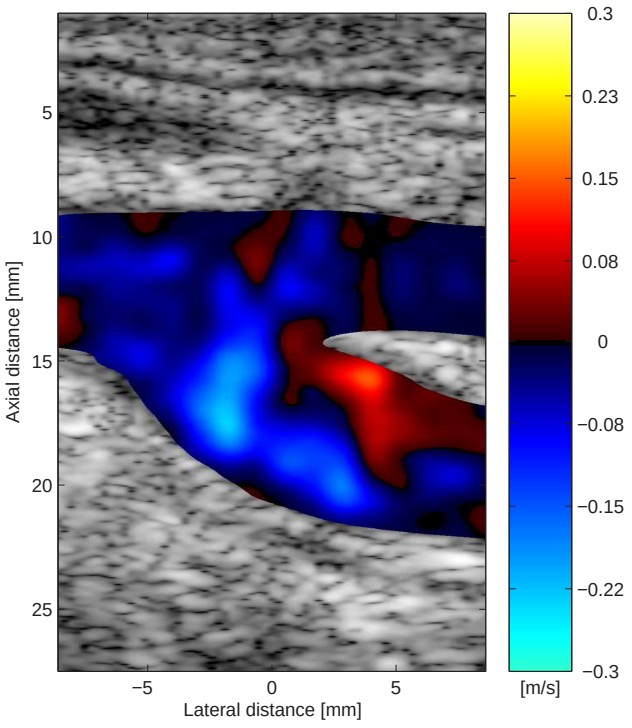

Fig. 21. The axial (towards or away from the transducer) velocity. The time instance is the same as for Fig. 19.

up. This could potentially lead to an early detection of stenosis. Further studies of the TO method should therefore concentrate on such regions, and the scannings should be performed on both healthy and stenosed carotid arteries. An experiment could then be performed, where a number of medical doctors should compare conventional CFM frames and VVI frames, and then determine which of the two methods would be preferable for detection of stenosis.

The draw back of using the TO method is the relative high number of pulses used for each velocity estimate. In the VVI frames presented in this paper the number of pulses used for each estimate was 64, which is ~ 6 times higher than what is used in most scanners for conventional CFM imaging. However, a lower number of pulses can be used, if a higher standard deviation and bias can be accepted.

The TO method could also be used for tissue motion estimation or elasticity imaging. When used on tissue, the signal-to-noise ratio will be $\sim 40 - 60$ dB higher than when used on blood. Consequently performance will be increased significantly.

ACKNOWLEDGMENT

Acknowledgement: This work was supported by grant 9700883, 9700563 and 26-01-0178 from the Danish Science Foundation, the Ministry of Science, Technology and Development, and by B-K Medical A/S, Denmark.

REFERENCES

[1] M. D. Fox, "Multiple crossed-beam ultrasound Doppler velocimetry," *IEEE Trans. Son. Ultrason.*, vol. SU-25, pp. 281–286, 1978.

[2] John R. Overbeck, Kirk W. Beach, and D. Eugene Strandness, "Vector Doppler: Accurate measurement of blood velocity in two dimensions," *Ultrasound Med. Biol.*, vol. 18, pp. 19–31, 1992.

[3] V. L. Newhouse, D. Censor, T. Vontz, J. A. Cisneros, and B. B. Goldberg, "Ultrasound Doppler probing of flows transverse with respect to beam axis," *IEEE Trans. Biomed. Eng.*, vol. BME-34, pp. 779–788, 1987.

[4] G. E. Trahey, J. W. Allison, and O. T. von Ramm, "Angle independent ultrasonic detection of blood flow," *IEEE Trans. Biomed. Eng.*, vol. BME-34, pp. 965–967, 1987.

[5] J. A. Jensen and I. R. Lacasa, "Estimation of blood velocity vectors using transverse ultrasound beam focusing and cross-correlation," in *Proc. IEEE Ultrason. Symp.*, 1999, pp. 1493–1497.

[6] J. A. Jensen, "Directional velocity estimation using focusing along the flow direction: I: Theory and simulation," *IEEE Trans. Ultrason., Ferroelec., Freq. Contr.*, pp. 857–872, 2003.

[7] J. A. Jensen and R. Bjerngaard, "Directional velocity estimation using focusing along the flow direction: II: Experimental investigation," *IEEE Trans. Ultrason., Ferroelec., Freq. Contr.*, pp. 873–880, 2003.

[8] J. Kortbek and J. A. Jensen, "Determination of velocity vector angles using the directional cross-correlation method," *IEEE Trans. Ultrason., Ferroelec., Freq. Contr.*, vol. x, pp. Accepted, 2005.

[9] J. A. Jensen and S. I. Nikolov, "Transverse flow imaging using synthetic aperture directional beamforming," in *Proc. IEEE Ultrason. Symp.*, 2002, pp. 1488–1492.

[10] P. Munk, "Estimation of the 2-D flow vector in ultrasonic imaging: a new approach," M.S. thesis, Department of Information Technology, Technical University of Denmark, 1996.

[11] J. A. Jensen and P. Munk, "A new method for estimation of velocity vectors," *IEEE Trans. Ultrason., Ferroelec., Freq. Contr.*, vol. 45, pp. 837–851, 1998.

[12] J. A. Jensen, "A new estimator for vector velocity estimation," *IEEE Trans. Ultrason., Ferroelec., Freq. Contr.*, vol. 48, no. 4, pp. 886–894, 2001.

[13] M. E. Anderson, "Spatial quadrature: a novel technique for multi-dimensional velocity estimation," in *Proc. IEEE Ultrason. Symp.*, 1997, vol. 45, pp. 1233–1238.

[14] M. E. Anderson, "Multi-dimensional velocity estimation with ultrasound using spatial quadrature," *IEEE Trans. Ultrason., Ferroelec., Freq. Contr.*, vol. 45, pp. 852–861, 1998.
[15] M. E. Anderson, "A heterodyning demodulation technique for spatial quadrature," in *Proc. SPIE - med. imag.*, 2000, pp. 1487–1490.
[16] J. Udesen and J. A. Jensen, "An in-vivo investigation of transverse flow estimation," in *Proc. SPIE - Progress in biomedical optics and imaging*, 2004, vol. 5373, pp. 307–314.
[17] J. Udesen and J. A. Jensen, "Experimental investigation of transverse flow estimation using transverse oscillation," in *Proc. IEEE Ultrason. Symp.*, 2003, pp. 1586–1589.
[18] J. A. Jensen, O. Holm, L. J. Jensen, H. Bendsen, H. M. Pedersen, K. Salomonsen, J. Hansen, and S. Nikolov, "Experimental ultrasound system for real-time synthetic imaging," in *Proc. IEEE Ultrason. Symp.*, 1999, vol. 2, pp. 1595–1599.
[19] J. A. Jensen and N. B. Svendsen, "Calculation of pressure fields from arbitrarily shaped, apodized, and excited ultrasound transducers," *IEEE Trans. Ultrason., Ferroelec., Freq. Contr.*, vol. 39, pp. 262–267, 1992.
[20] J. A. Jensen, "Field: A program for simulating ultrasound systems," *Med. Biol. Eng. Comp.*, vol. 10th Nordic-Baltic Conference on Biomedical Imaging, Vol. 4, Supplement 1, Part 1, pp. 351–353, 1996b.
[21] J. W. Goodman, *Introduction to Fourier optics*, McGraw Hill Inc., New York, second edition, 1996.
[22] A. P. G Hoeks, J. J. W. van de Vorst, A. Dabekaussen, P. J. Brands, and R. S. Reneman, "An efficient algorithm to remove low frequency Doppler signal in digital Doppler systems," *Ultrason. Imaging*, vol. 13, pp. 135–145, 1991a.
[23] S. Bjaerum and H. Torp, "Statistical evaluation of clutter filters in color flow imaging," *Ultrasonics*, vol. 38, pp. 376–380, 2000.
[24] C. Kasai, K. Namekawa, A. Koyano, and R. Omoto, "Real-time two-dimensional blood flow imaging using an autocorrelation technique," *IEEE Trans. Son. Ultrason.*, vol. 32, pp. 458–463, 1985.
[25] J. A. Jensen, *Estimation of Blood Velocities Using Ultrasound: A Signal Processing Approach*, Cambridge University Press, New York, 1996.
[26] D. H. Evans, W. N. McDicken, R. Skidmore, and J. P. Woodcock, *Doppler Ultrasound, Physics, Instrumentation, and Clinical Applications*, John Wiley & Sons, New York, 1989.
[27] I. Marshall, P. Papathanasopoulou, and K. Wartolowska, "Carotid flow rates and flow division at the bifurcation in healthy volunteers," *Physiological Measurement*, vol. 25, pp. 691–697, 2004.
[28] R. Botnar, G. Rappitsch, M. B. Scheidegger, D. Liepsch, K. Perktold, and P. Boesiger, "Hemodynamics in the carotid artery bifurcation: a comparison between numerical simulations and in vitro MRI measurements," *J. Biomech.*, vol. 33, pp. 137–144, 2000.
[29] I. Marshall, S. Zhao, P. Papathanasopoulou, P. Hoskins, and X. Y. Xu, "MRI and CFD studies of pulsatile flow in healthy and stenosed carotid bifurcation models," *J. Biomech.*, vol. 37, pp. 679–687, 2004.

Experimental Investigation of Transverse Flow Estimation using Transverse Oscillation

Jesper Udesen[1,2] and Jørgen Arendt Jensen[1]

1) Center for Fast Ultrasound Imaging, Ørsted•DTU,
Bldg. 348, Technical University of Denmark, DK-2800 Lyngby, Denmark.
2) B-K Medical A/S, Mileparken 34, DK-2730 Herlev, Denmark.

Abstract - Conventional ultrasound scanners can only display the blood velocity component parallel to the ultrasound beam. Introducing a laterally oscillating field gives signals from which the transverse velocity component can be estimated using 2:1 parallel receive beamformers. To yield the performance of the approach, this paper presents simulated and experimental results, obtained at a blood velocity angle transverse to the ultrasound beam.

The Field II program is used to simulate a setup with a 128 element linear array transducer. At a depth of 27 mm a virtual blood vessel of radius 2.4 mm is situated perpendicular to the ultrasound beam. The velocity profile of the blood is parabolic, and the speed of the blood in the center of the vessel is 1.1 m/s. An extended autocorrelation algorithm is used for velocity estimation for 310 trials, each containing 32 beamformed signals. The velocity can be estimated with a mean relative bias of 6.3 % and a mean relative standard deviation of 5.4 % over the entire vessel length.

With the experimental ultrasound scanner RASMUS the simulations are reproduced in a experimental flow phantom using a linear array transducer and vessel characteristics as in the simulations. The flow is generated with the Compuflow1000 programmable flow pump giving a parabolic velocity profile of the blood mimicking fluid in the flow phantom. The profiles are estimated for 310 trials each containing of 32 data vectors. The relative mean bias over the entire blood vessel is found to be 10.0 % and the relative mean standard deviation is found to be 9.8 %.

With the Compuflow1000 programmable flow pump a color flow mode image is produced of the experimental setup for a parabolic flow. Also the flow of the human femoralis is reproduced and it is found that the characteristics of the flow can be estimated.

I Introduction

In conventional ultrasound scanners the point spread function (PSF) only has an axial oscillation, and hence blood scatterers travelling through the acoustic field only gives signals from which the axial velocity of the blood can be determined. This is a severe limitation, since most blood vessels are parallel to the skin surface, and it is therefore a problem to achieve a sufficiently small angle between the flow and the beam. One way to overcome this problem is the introduction of two PSF's each with an oscillation both in the axial and in the lateral direction and each PSF transverse phase shifted 90° from each other (Fig. 2). This method has been suggested both by Jensen and Munk (Transverse Oscillation (TO)) [1, 2, 3] and by Anderson (Heterodyned Spatial Quadrature (HSQ)) [4, 5]. The major differences between the two methods is the way the two PSF's are constructed. Anderson is using two different apodizations in receive, where Jensen and Munk are using axicon focus in receive to create the 90° phase modulation. Furthermore the applied velocity estimators are different.

This paper investigates the performance of the TO method. The performance is determined using the ultrasound simulation program Field II [6], and phantom experiments using an experimental scanner and a flow phantom attached to a flow pump.

II Simulated setup and results

The Field II program is used to simulate a 128 element linear array transducer and a cylindrical blood vessel perpendicular to the beam direction. The acoustic field emitted from the transducer resembles that of a conventional Doppler system i.e hamming apodization and quadratic focusing is applied. The received signals are beamformed using axicon focusing and two sinc functions as apodization (see Fig. 1). This gives a PSF with an oscillation in both the axial and transverse direction. To have two PSF's, which are 90° transverse phase shifted from each other, two beamformers are applied, and the 90° phase modulation is created with two different axicon focuses. The exact setup parameters can be found in Table 1 and Table 2 and a detailed description of the theory for the transducer setup and the beamforming can be found in [2].

The corresponding PSF's can be seen in Fig. 2.

To make the simulation as simple as possible, and hence decrease computation time, no tissue was introduced around the vessel i.e. the only scatterers present in the simulation were the blood scatterers. They were moved transverse to the beam direction with a parabolic velocity profile v given by $v = v_0\left(1-\left(\frac{r}{R}\right)^2\right)$, where R is the radius of the vessel, r is the distance from the axis of the vessel, and v_0 is the maximum velocity. Since the vessel had a finite length, scatterers passing the end of the vessel were introduced in the other end.

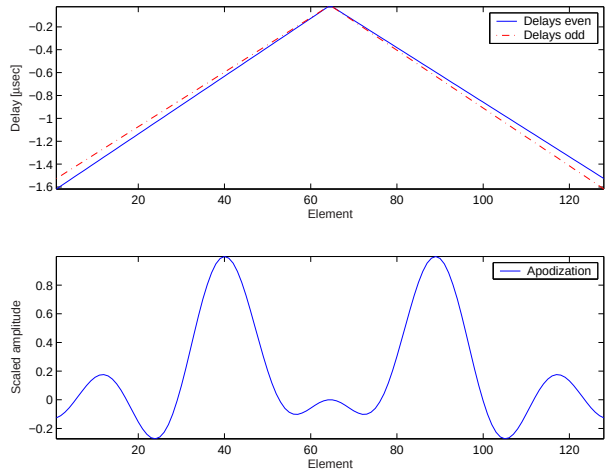

Figure 1: The delay times (top) and the apodization (bottom) used for the beamforming.

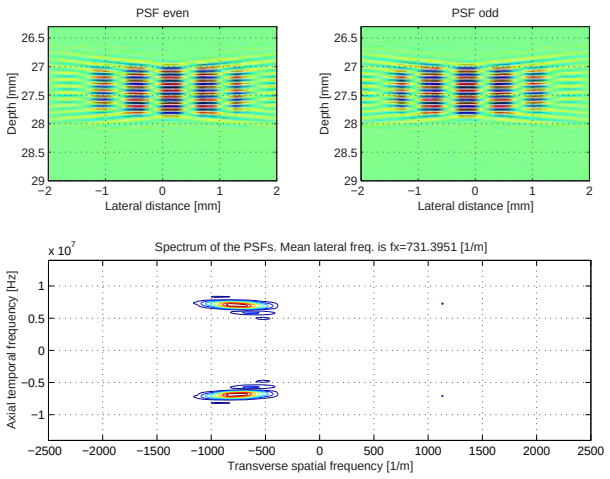

Figure 2: The two PSF's used for transverse velocity estimation and their corresponding spectra. The point scatterer is situated at a depth of 27mm.

The velocity estimation was performed using an extended autocorrelation algorithm for lag 1 described in [3]. For standard deviation estimation 310 data ensembles were used each containing 32 beamformed received signals. Echo canceling was applied using a highpass filter with a cut off frequency at $f = 80$ Hz and RF averaging over one pulse length was applied.

Transducer	Linear array
Number of elements	128
Pitch	0.208 mm
Kerf	0.035 mm
Center frequency	7 MHz
Number of cycles pr. pulse	8
fprf	8 kHz
Sampling frequency	100 MHz
Transverse wave length	1.2 mm
Apodization in transmit	Hamming
Apodization in receive	Two sinc's
Focus in transmit	54 mm
Focus in receive	Axicon at 27 mm

Table 1: Transducer setup

Depth to vessel	27 mm
Radius of vessel	2.4 mm
Length of vessel	20 mm
Number of scatterers	12,387
Maximum blood velocity	1.1 m/s
Blood velocity	Parabolic

Table 2: Parameters for the simulated blood vessel.

Since the velocity is scaled with the lateral oscillation length λ_x, a correct value for λ_x is desirable. In theory λ_x can be derived from the Fraunhofer approximation to be $\lambda_x = z/(\lambda_z \xi)$, where λ_z is the axial wave length, z is the depth and ξ is the spatial distance between the peaks of the two sinc functions used for the receive apodization [2, 7]. Since the Fraunhofer approximation is based on a number of assumptions, which are only approximately satisfied, a more correct estimate for λ_x can be derived using the PSF's for the transducer setup. Taking a 2D FFT of the PSF's and thereafter finding the mean value of the transverse frequencies gives a more correct value for λ_x, which then can be used in the velocity estimator. Typical the deviation between the theoretical value for λ_x and the one derived from the PSF's is around 10%. The resulting mean transverse velocity profile with corresponding standard deviations can be seen in Fig. 3. The velocity deviates from the theoretical velocity profile with a mean relative bias of 6.3 % and a relative mean standard deviation of 5.4 %, taken over the entire vessel profile relative to the maximum blood velocity. Near the vessel wall there is a significant deviation between the velocity estimate and the theoretical parabolic profile. This is because the PSF's

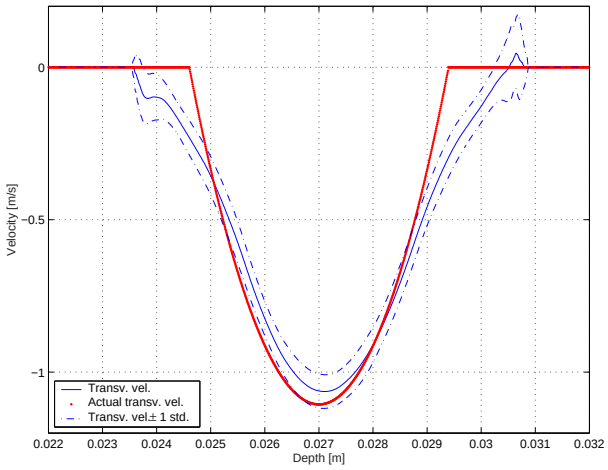

Figure 3: The mean velocity profile and corresponding standard deviation for the simulation using Field II.

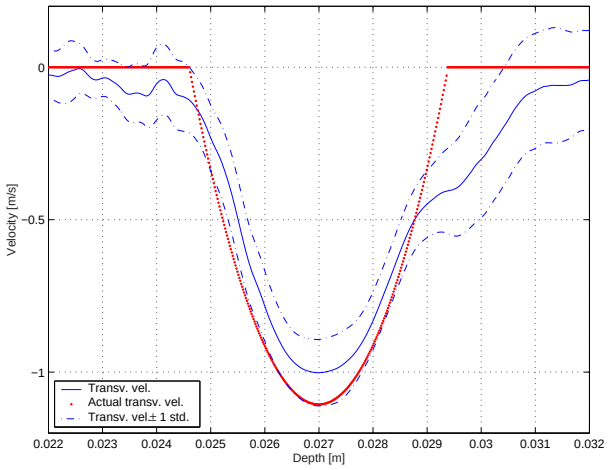

Figure 4: The mean velocity profile and corresponding standard deviation for the flow phantom experiment.

have an axial extend of approximately 1 mm, (see Fig. 2), and since every velocity estimate is an average over the velocities present inside the area of the PSF, the estimates will be "smooth" near the vessel walls.

III Experimental setup and results

A commercial linear array transducer with 128 elements was used to scan a flow phantom (SMI140 from Shelley Medical Imaging Technologies, London, Ontario, Canada) with blood mimicking fluid attached to a Shelley Compuflow1000 flow pump. The same setup parameters was used as in the simulation (see Table 1 and Table 2) except that matched filtering was performed on the acquired RF data to reduce noise. Furthermore the sampling frequency was decreased to 40 MHz, and tissue was present between the transducer and the vessel. The attenuation of the tissue was 0.7 dB/cm/MHz at 5 MHz and the blood mimicking fluid is described in [8]. The Reynolds number for the flow was approximately 10^3, hence the flow can be regarded as laminar with a parabolic velocity profile similar to the one in the simulation.

The scanner used for data acquisition was the experimental scanner RASMUS [9], which has 128 channels in transmit and 64 channels in receive. To acquire 128 elements in receive, two consecutive received data sets was sampled, respectively on the left hand side and the right hand side of the transducer and thereafter superimposed to each other (see Fig. 5). Again 310 data ensembles were acquired each containing 32 beamformed signals. The same echo canceling filter and velocity estimator was used as in the simulation, and the resulting mean velocity profile can be seen in Fig. 4. The velocity deviates from the theoretical velocity profile with a relative mean bias of 10.0 % and a relative mean standard deviation of 9.8 % taken over the entire vessel profile, where the values are relative to the maximum velocity. As mentioned in the previous section the velocity is scaled with λ_x, and hence a wrong choice of λ_x will result in a biased estimate. Therefore we believe, that the bias is a result of the choice of transverse oscillation length λ_x, which is determined from the 2D FFT of the PSF's.

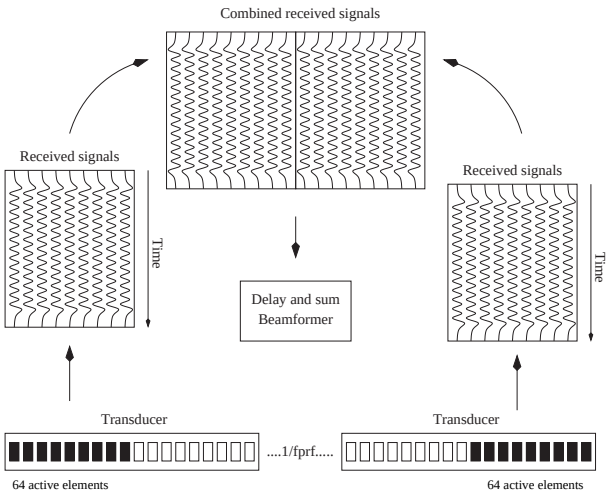

Figure 5: In order to acquire data from 128 elements in receive, signals from the left and right part of the aperture from two emissions are combined.

To demonstrate the algorithms capability of making color flow mode (CFM) images, the flow phantom was scanned using an aperture containing 64 transmitting and receiving elements, which moved across the transducer. The same trans-

ducer setup as in the simulation was used, except for the f_{prf} which was decreased to 4 kHz, in order to compensate for the reduction of the active number of transducer elements. Also the lateral wavelength λ_x was increased to $\lambda_x = 1.4$ mm. The resulting CFM image with a B mode image superimposed can be seen in Fig. 6. Only the velocities inside the vessel area have been shown. Some noise in the estimates is present, which presumably is a result of the echo canceling filter implemented.

In order to test the TO methods ability to work in dynamic conditions, the flow phantom was scanned when a pulsating flow resembling the human femoralis was present. The same setup parameters and velocity estimator was used as in the simulation, except that now the f_{prf} was set to 7 kHz. 10,000 beamformed signals were acquired, and 100 beamformed signals were used for each velocity estimation. The velocity estimates can be seen in Fig. 7. It is seen that the characteristics of the pulsatile flow can be estimated.

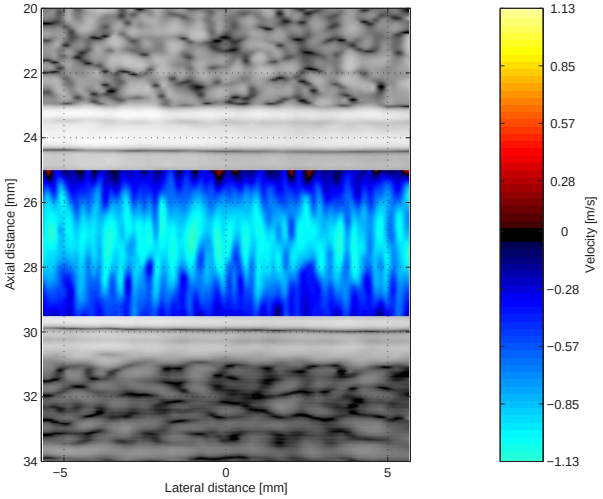

Figure 6: Transverse CFM image of the flow phantom. The dynamic range in the Bmode image is 45 dB.

IV Conclusion

The bias and standard deviation of the measured velocities was comparable with standard deviation and bias for conventional axial Doppler estimation. Therefore, it has been demonstrated that the method can estimate the blood velocity of a purely transverse flow in simulations and in flow phantom experiments.

Acknowledgment

Acknowledgement: This work was supported by grant 9700883, 9700563 and 26-01-0178 from the Danish Science Foundation, the Ministry of Science, Technology and Development, and by B-K Medical A/S, Denmark.

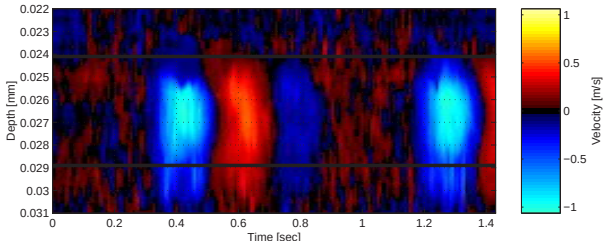

Figure 7: The velocity as a function of time for transverse flow in the flow phantom. The flow simulates the characteristics of the femoral artery. The thick lines indicate the vessel wall.

V References

[1] P. Munk. Estimation of the 2-D flow vector in ultrasonic imaging: a new approach. Master's thesis, Department of Information Technology, Technical University of Denmark, 1996.

[2] J. A. Jensen and P. Munk. A new method for estimation of velocity vectors. *IEEE Trans. Ultrason., Ferroelec., Freq. Contr.*, 45:837–851, 1998.

[3] J. A. Jensen. A new estimator for vector velocity estimation. *IEEE Trans. Ultrason., Ferroelec., Freq. Contr.*, 48(4):886–894, 2001.

[4] M. E. Anderson. Spatial quadrature: a novel technique for multi-dimensional velocity estimation. In *Proc. IEEE Ultrason. Symp.*, volume 45, pages 1233–1238, 1997.

[5] M. E. Anderson. A heterodyning demodulation technique for spatial quadrature. In *Proc. SPIE - med. imag.*, pages 1487–1490, 2000.

[6] J. A. Jensen. Field: A program for simulating ultrasound systems. *Med. Biol. Eng. Comp.*, 10th Nordic-Baltic Conference on Biomedical Imaging, Vol. 4, Supplement 1, Part 1:351–353, 1996b.

[7] P. Munk. *Estimation of blood velocity vectors using ultrasound*. PhD thesis, Department of Information Technology, Technical University of Denmark, Lyngby, Denmark, 2000.

[8] K. V. Ramnarine, D. K. Nassiri, P. R. Hoskins, and J. Lubbers. Validation of a new blood mimicking fluid for use in Doppler flow test objects. *Ultrasound Med. Biol.*, 24:451–459, 1998.

[9] J. A. Jensen, O. Holm, L. J. Jensen, H. Bendsen, H. M. Pedersen, K. Salomonsen, J. Hansen, and S. Nikolov. Experimental ultrasound system for real-time synthetic imaging. In *Proc. IEEE Ultrason. Symp.*, volume 2, pages 1595–1599, 1999.

An In-vivo investigation of transverse flow estimation

Jesper Udesen[a,b] and Jørgen Arendt Jensen[a]

[a]Center for Fast Ultrasound Imaging, Ørsted • DTU, Bldg. 348, Technical University of Denmark, DK-2800 Kgs. Lyngby, Denmark
[b]B-K Medical, Mileparken 34, DK-2730 Herlev, Denmark

ABSTRACT

Conventional ultrasound scanners are restricted to display the blood velocity component in the ultrasound beam direction. By introducing a laterally oscillating field, signals are created from which the transverse velocity component can be estimated. This paper presents velocity and volume flow estimates obtained from flow phantom and in-vivo measurements at 90° relative to the ultrasound beam axis.

The flow phantom experiment setup consists of a SMI140 flow phantom connected to a CompuFlow1000 programmable flow pump, which generates a flow similarly to that in the femoral artery. A B-K medical 8804 linear array transducer with 128 elements and a center frequency of 7 MHz is emitting 8 cycle ultrasound pulses with a pulse repetition frequency of 7 kHz in a direction perpendicular to the flow direction in the phantom. The transducer is connected to the experimental ultrasound scanner RASMUS, and 1.4 seconds of data is acquired. Using 2 parallel receive beamformers a transverse oscillation is introduced with an oscillation period 1.2 mm. The velocity estimation is performed using an extended autocorrelation algorithm. The volume flow can be estimated with a relative standard deviation of 13.0 % and a relative mean bias of 3.4 %. The in-vivo experiment is performed on the common carotid artery of a healthy 25 year old male. The same transducer and setup is used as in the flow phantom experiment, and the data is acquired using the RASMUS scanner. The peak velocity of the carotid flow is estimated to 1.2 m/s and the volume flow to 290 ml/min. This is within normal physiological range.

Keywords: Blood velocity, Doppler ultrasound, transverse velocity

1. INTRODUCTION

Over the past 30 years, extensive research has been carried out in the field of blood velocity estimation using ultrasound scanners. Today most scanners can display an image of the interior human body with a blood velocity image superimposed. The blood velocity image is calculated by determining the movement of the red blood cells in the direction of the ultrasound beam. The distance moved by the red blood cells, is calculated for each pulse emissions and dividing this distance by the time between pulse emissions, gives the velocity projected onto the ultrasound beam direction.[1] This method is illustrated in Fig. 1, where the blood supply to the brain is shown. The colors indicate the velocity of the blood projected onto the ultrasound beam, and the gray colors indicate the presence of the tissue in the neck. In the area near the dashed green line the angle between the ultrasound beam and the flow is close to 90° and the scanner fails to detect any movement of the red blood cells in the direction of the beam. Therefore no blood velocity is detected in this area. This lack of information about the blood velocity, when the angle between the ultrasound beam and the flow is close to 90°, is a severe limitation to conventional ultrasound systems. Many authors have addressed this issue, and different methods for calculating the vector velocity, has been suggested.[2–5]

One promising method for estimation of the full velocity vector, which has the potential of being implemented in a commercial scanner for realtime estimation, is the introduction of two double oscillating point spread functions (PSF), where an oscillation is present both in the transverse and the axial direction. This method has been suggested by both Jensen and Munk (Transverse Oscillation (TO))[6–8] and by Anderson (Heterodyned Spatial Quadrature).[9,10] It has previously been verified that the TO algorithm can estimate the transverse velocity in simulations as well as in flow phantom experiments, when the flow is steady and the flow is purely transverse, i.e. where the angle between the ultrasound beam and the flow is 90°.[8,11] The aim of this paper is to evaluate the performance of the TO algorithm for an accelerated purely transverse flow. This is first done in a flow phantom for a flow resembling the human femoral artery. Finally the algorithm is tested in-vivo, where the common carotid artery of a healthy 25 year old male is scanned.

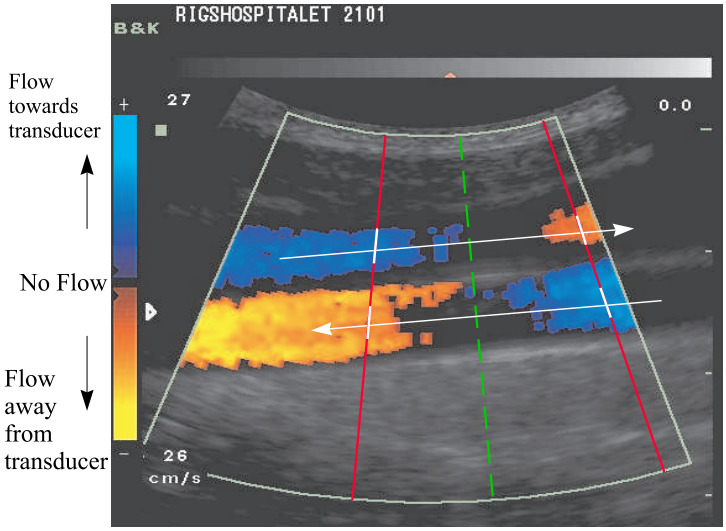

Figure 1. Conventional Color flow mode image of the blood supply to and from the brain. The upper blood vessel is the jugular vein leading the blood from the brain to the heart. The lower vessel is the common carotid artery leading the blood from the heart to the brain. Near the green dashed line the scanner fails to measure any movement of the blood between pulse emissions, and hence no velocity is detected (from Munk and Jensen, 1998).[12]

2. FIELD GENERATION

In a conventional ultrasound system the PSF only oscillates in the axial direction, i.e. along the direction of the ultrasound beam. Scatterers traveling through the acoustic field therefore produce a signal with a frequency proportional to their axial velocity. Hence, no information is acquired about the transverse velocity of the scatterers. The basic principle in the TO algorithm is the construction of a PSF, where an oscillation is present in both the axial and the transverse direction. Scatterers traveling through the acoustic field will thus produce a signal, where two frequency components are present; one for their axial velocity and one for their transverse velocity.

The double oscillating PSF is created using receive focusing and apodization. The receive apodization is related to the transverse field by a Fourier relation which states that the Fourier transform of the transducers apodization function $r(\xi)$ is proportional to the transverse field $R(x)$ in the focus point and the far field. Here x is transverse distance at the focus point, and ξ is the distance from the center of the transducer. The Fourier relation is then[13]

$$R(x) \quad = \quad k_1 \mathcal{F}\{r(\xi)\}. \tag{1}$$

In the following the constant of proportionality k_1 is omitted. A transversely oscillating field with a spatial frequency of f_x and a lateral width L

$$R(x) = \mathrm{rect}(L)\sin(2\pi f_x x), \tag{2}$$

thus yields an apodization function given by

$$\begin{aligned} r(\xi) &= \mathcal{F}^{-1}\{R(x)\} \\ &= \mathcal{F}^{-1}\{\mathrm{rect}(L)\} * \mathcal{F}^{-1}\{\sin(2\pi f_x x)\} \\ &= \frac{L}{2z\lambda}\left\{\mathrm{sinc}\left(\pi\left(\frac{\xi}{z\lambda}+f_x\right)L\right)+\mathrm{sinc}\left(\pi\left(\frac{\xi}{z\lambda}-f_x\right)L\right)\right\}. \end{aligned} \tag{3}$$

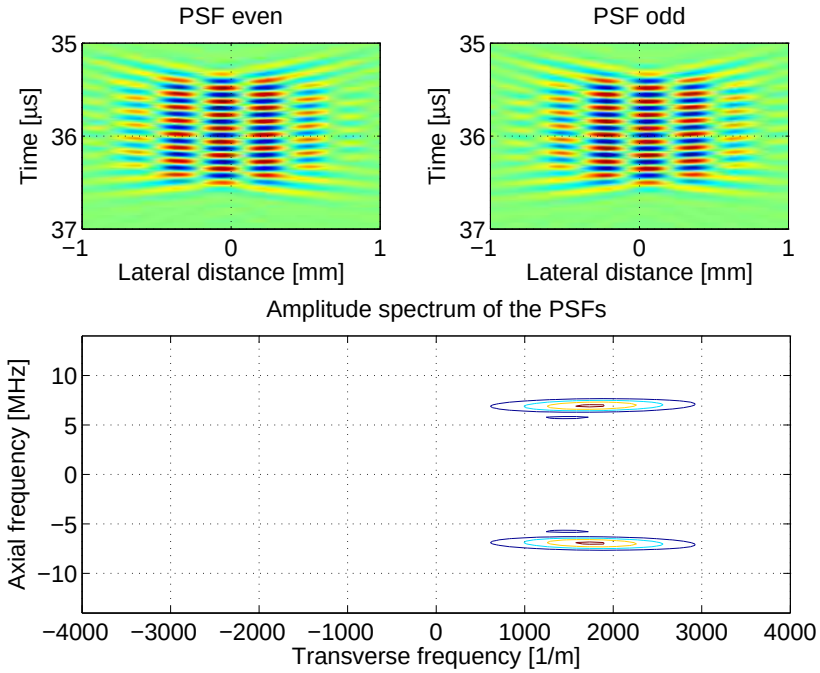

Figure 2. The two double oscillating PSF's (top) and their corresponding spectrum (bottom) created with the Field II program[14] for a point at 27 mm using the transducer defined in Tab. 1. The amplitude spectrum is calculated by taking the 2D Fourier transform of $\mathrm{PSF}_{\mathrm{even}} + j\mathrm{PSF}_{\mathrm{odd}}$. Note that the PSF's are 90° phase shifted with respect to each other and that the amplitude spectrum therefore is one sided.

Here the operator $*$ denotes spatial convolution, and the $\mathrm{sinc}(y)$ and the $\mathrm{rect}(L)$ functions are defined as

$$\mathrm{sinc}(y) = \begin{cases} 1 & \text{for} \quad y = 0 \\ \frac{\sin(y)}{y} & \text{otherwise} \end{cases} \tag{4}$$

$$\mathrm{rect}(L) = \begin{cases} 1 & \text{for} \quad -L/2 < y < L/2 \\ 0 & \text{otherwise} \end{cases} \tag{5}$$

The implementation of (3) into the transducers apodization function will, thus, yield a PSF, where an oscillation is present, both in the axial direction and in the transverse direction. To ensure that the transverse frequency f_x is constant at any depth, the apodization function should be dynamic.

In a conventional system the sign of the velocity is determined using a Hilbert transformation. The Hilbert transformation shifts the phase of the received RF signal with 90° in the axial direction and thus permits the construction of a complex signal whose frequency spectrum is one sided. The same strategy is applied in the TO algorithm, but now the 90° phase shift has to be applied both in the axial and transverse direction in order to separate the two frequency components. This is done by having two beamformers in receive. Each beamformer creates a double oscillating field using the apodization function given by (3), and each beamformer has a conventional quadratic dynamic focus in receive. The focus points for each beamformer are then separated a transverse distance corresponding to a 90° phase shift.[7] This is illustrated in the top of Fig. 2, where the two PSF's, $\mathrm{PSF}_{\mathrm{even}}$ and $\mathrm{PSF}_{\mathrm{odd}}$, corresponding to the two beamformers are shown. In the bottom of Fig. 2 the amplitude spectrum of the two PSF's is shown. It is calculated by taking the 2D Fourier transform of $\mathrm{PSF}_{\mathrm{even}} + j\mathrm{PSF}_{\mathrm{odd}}$. Since the two PSF's are 90° phase shifted in the transverse direction, the amplitude spectrum is one sided.

Transducer	Linear array
Number of elements	128
Pitch	0.208 mm
Kerf	0.035 mm
Height	4.5mm
Center frequency	7 MHz
Elevation focus	25.0 mm
Number of cycles pr. pulse	8
Sampling frequency	40 MHz

Table 1. Parameters for the transducer used in the experiments.

3. FLOW PHANTOM EXPERIMENTAL SETUP

To reveal the TO algorithms performance for a pulsatile flow, an experiment was conducted using a calibrated pulsatile flow pump. A flow phantom SMI140 (Shelley Medical Imaging Technologies, London, Ontario, Canada) containing blood mimicking fluid[15] was attached to a Shelley Compuflow1000 flow pump. The attenuation of the phantom was 0.7 dB/cm/MHz at 5 MHz. The cylindrical tube containing the blood mimicking fluid had a radius of 2.4 mm and was situated at a depth of 26.5 mm in the phantom.

The pump was programmed to produce a flow, which resembled the human femoral artery with a peak volume flow of 10 ml/s. A laminar parabolic peak flow of 10 ml/s gives a Reynolds number of approximately 10^3, hence the flow can be regarded as laminar.[1]

At the phantom surface a B-K medical 8804 transducer(Table 1) was placed, emitting 8 cycle 7 MHz ultrasound pulses perpendicular to the direction of the flow in the tube. A direction where a conventional ultrasound system would not be able to estimate any velocity. The transmit focus for the emitted pulses was set to 50mm - twice the depth to the center of the vessel. The transducer was attached to the RASMUS experimental scanner.[16] RASMUS has 128 channels in transmit and 64 channels in receive. It it thus possible to excite 128 transducer elements with different signals and to sample data from 64 transducer elements simultaneously. To acquire data from 128 elements in receive, two consecutive received data sets was sampled, respectively on elements 1-64 and 65-128 using two-to-one multiplexing. The two sets of data were thereafter combined, so the received data could be focused using 128 receive elements.

4. FLOW PHANTOM EXPERIMENTAL RESULTS

Data from the flow phantom was acquired for 1.43 seconds using a pulse repetition frequency of 7 kHz, thus yielding $10,000$ received signals, which was beamformed offline. The transverse oscillation length in the field was set to 1.2 mm and was created in the receive beamforming. The received signals were matched filtered to reduce noise. Stationary echo canceling was applied using a filter which fitted a straight line to the sampled data and subtracted this line from the data.[17] Selections of 100 consecutive signals were used in the velocity estimator, and the overlap between each selection was 50 %. The velocity was estimated using an extended autocorrelation algorithm which separates the frequency components in the signals and estimates the corresponding velocities. RF averaging was applied.[8]

In Fig. 3 the estimated velocities as a function of depth and time are shown, and the cyclic nature of the flow can clearly be recognized with a period of approximately 0.9 seconds.

In order to compare the velocity estimate with the true flow produced by the flow pump, the estimated velocities was integrated over the cross section of the vessel area to yield the volume flow. This is shown in Fig. 4, where the estimated volume flow is compared with the actual volume flow produced by the flow pump. The standard deviation is 1.30 ml/s, and the mean bias 0.34 ml/s, which gives a relative standard deviation of 13.0 % and a mean relative bias of 3.4 %, when scaled with the peak volume flow of 10 ml/s produced by the pump.

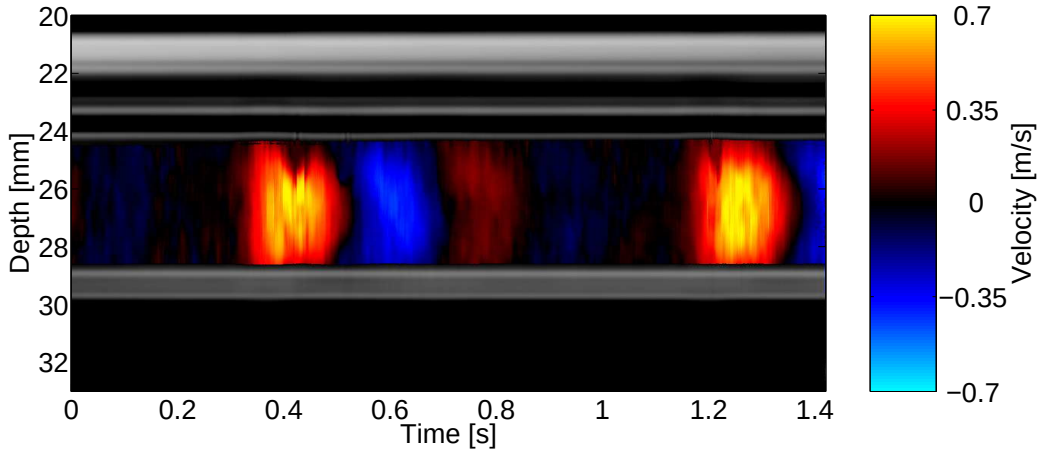

Figure 3. M-mode image of the estimated velocities as a function of depth and time for the flow phantom experiment. The gray colors indicates the presence of the vessel wall and the colors indicates the velocity.

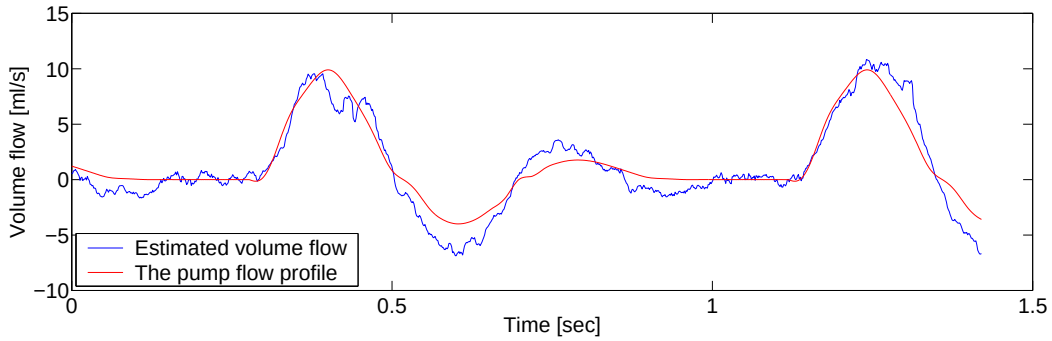

Figure 4. The estimated volume flow for the flow phantom experiment compared with the actual flow produced by the pump.

5. IN-VIVO EXPERIMENT

The common carotid artery of a healthy 25 year old male was scanned using the same transducer and experimental scanner as in the flow phantom experiment. To ensure that the blood flow was purely transverse to the emitted beam, a B-mode image was first acquired (Fig. 5). The transmit focus was set to 40 mm and 8 cycle ultrasound pulses were emitted with a center frequency of 7 MHz. The transverse oscillation length was set to 1.7 mm, the pulse repetition frequency was set to 5 KHz, and 2 seconds of data were acquired yielding 10,000 received signals, which were matched filtered and beamformed off line. Selections of 100 consecutive received signals with a overlap between each selection of 90 % were echo canceled. The echo canceling filter multiplied each selection of signals with a hamming window and thereafter zero padded them to a total length of 200 samples, which were transformed into the frequency domain using a fast Fourier transform. In the frequency domain the signals were band pass filtered with cutoff frequencies at 200 Hz and 1500 Hz and thereafter transformed back into the time domain using an inverse fast Fourier transform. Finally, the extended autocorrelation velocity estimator described in the previous section was applied.[8]

In Fig. 6 the velocity estimates in the common carotid artery as a function of time and depth are shown as a color image together with a gray scale image of the vessel walls. The vessel diameter is approximately 8 mm depending on where in the cardiac cycle it is measured. For a healthy person the diameter of the common carotid artery is 2-8 mm.[1] The pulsatile nature of the blood flow can be recognized with a period of approximately 0.9 seconds, and it is seen that the velocity is nearly symmetric around the center of the vessel.

In Fig. 7 the velocity in the center of the vessel is shown, and it is seen that the maximum velocity present in the flow is approximately 1.2 m/s. The peak velocity was also found to be approximately 1.2 m/s, when a commercial scanner (2102 from BK-Medical) in spectral Doppler mode with tilted beam, was used on the same volunteer.

The corresponding volume flow of the blood in the common carotid artery is calculated assuming a circular cross section of the vessel. The volume flow is shown in Fig. 8, where the maximum value is approximately 30 ml/s and the integrated volume flow is 290 ml/min. In the literature the corresponding value for a healthy person is 387 ml/min.[18] Note that the volume flow is approximately positive at all times during the scanning, which is characteristic for the flow in the common carotid artery.[18]

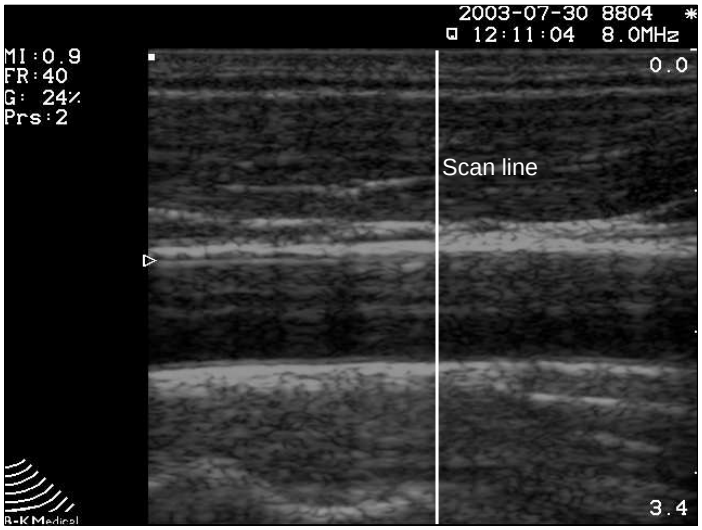

Figure 5. B mode image of the common carotid artery scanned for the in-vivo experiment using a commercial scanner (2102 BK-Medical). The transverse velocity was estimated along the white line.

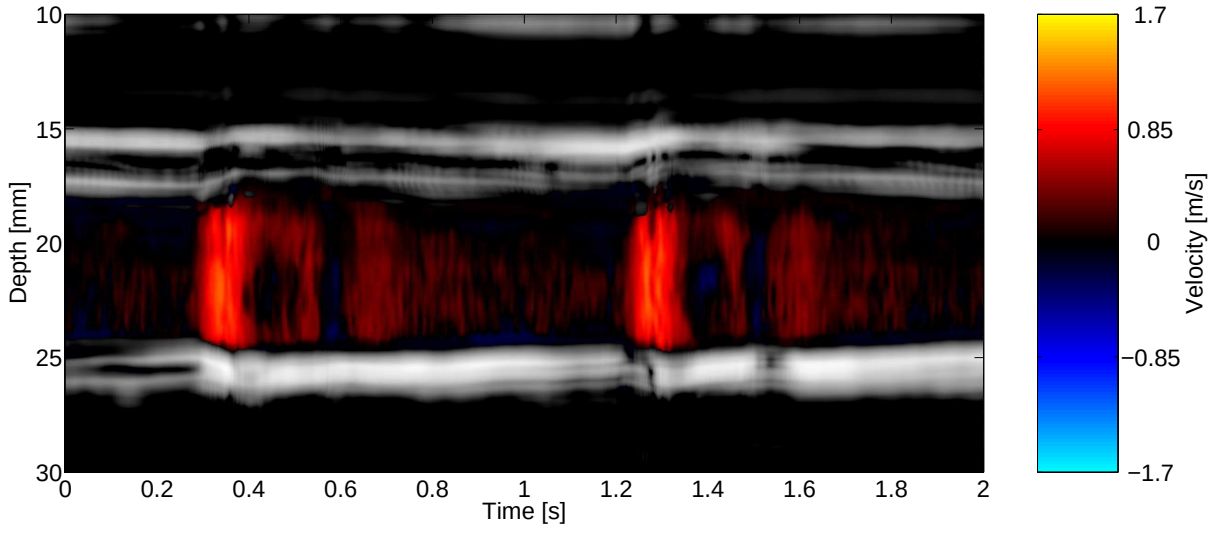

Figure 6. M-mode image of the estimated velocities in the common carotid artery at purely transverse flow. The gray colors indicates the presence of the vessel wall and the colors indicates the velocity. Red colors indicates velocities towards the brain.

6. CONCLUSION

The TO method has been evaluated on a flow phantom for a purely transverse flow, and the method estimated the volume flow with a relative standard deviation of 13.0 % and a mean relative bias of 3.4 %. Furthermore, the method has been tested on the common carotid artery of a healthy male for purely transverse flow. The estimated peak velocity of 1.2 m/s agreed with the value measured in a commercial scanner using spectral Doppler estimation. Furthermore the integrated volume flow of 290 ml/min is within normal physiological range.

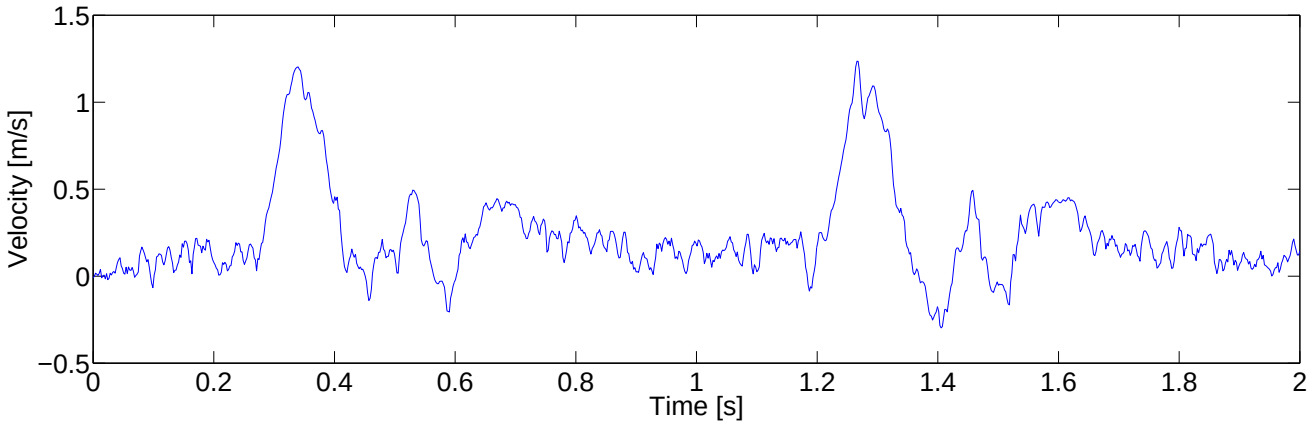

Figure 7. The velocity in the center of the common carotid artery as a function of time.

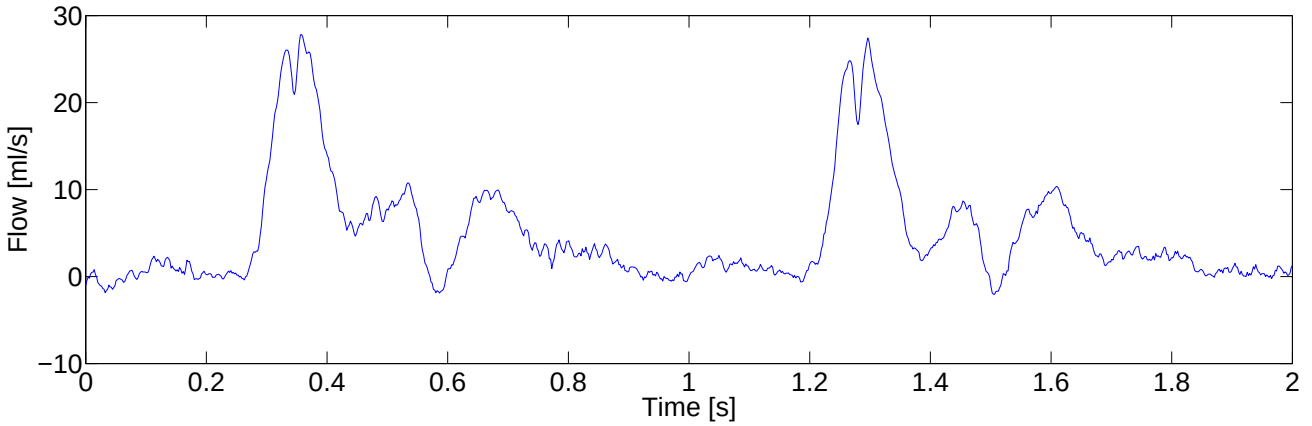

Figure 8. The estimated volume flow in the common carotid artery as a function of time.

REFERENCES

1. J. A. Jensen, *Estimation of Blood Velocities Using Ultrasound: A Signal Processing Approach*, Cambridge University Press, New York, 1996.
2. M. D. Fox, "Multiple crossed-beam ultrasound Doppler velocimetry," *IEEE Trans. Son. Ultrason.* **SU-25**, pp. 281–286, 1978.
3. G. E. Trahey, J. W. Allison, and O. T. von Ramm, "Angle independent ultrasonic detection of blood flow," *IEEE Trans. Biomed. Eng.* **BME-34**, pp. 965–967, 1987.

4. V. L. Newhouse, D. Censor, T. Vontz, J. A. Cisneros, and B. B. Goldberg, "Ultrasound Doppler probing of flows transverse with respect to beam axis," *IEEE Trans. Biomed. Eng.* **BME-34**, pp. 779–788, 1987.
5. O. Bonnefous, "Measurement of the complete (3D) velocity vector of blood flows," in *Proc. IEEE Ultrason. Symp.*, pp. 795–799, 1988.
6. P. Munk, "Estimation of the 2-D flow vector in ultrasonic imaging: a new approach," Master's thesis, Department of Information Technology, Technical University of Denmark, 1996.
7. J. A. Jensen and P. Munk, "A new method for estimation of velocity vectors," *IEEE Trans. Ultrason., Ferroelec., Freq. Contr.* **45**, pp. 837–851, 1998.
8. J. A. Jensen, "A new estimator for vector velocity estimation," *IEEE Trans. Ultrason., Ferroelec., Freq. Contr.* **48**(4), pp. 886–894, 2001.
9. M. E. Anderson, "Spatial quadrature: a novel technique for multi-dimensional velocity estimation," in *Proc. IEEE Ultrason. Symp.*, **45**, pp. 1233–1238, 1997.
10. M. E. Anderson, "A heterodyning demodulation technique for spatial quadrature," in *Proc. SPIE - med. imag.*, pp. 1487–1490, 2000.
11. J. Udesen and J. A. Jensen, "Experimental investigation of transverse flow estimation using transverse oscillation," in *Proc. IEEE Ultrason. Symp.*, pp. 1586–1589, 2003.
12. P. Munk and J. A. Jensen, "Performance of a vector velocity estimator," in *Proc. IEEE Ultrason. Symp.*, pp. 1489–1493, 1998.
13. J. W. Goodman, *Introduction to Fourier optics*, McGraw Hill Inc., New York, second ed., 1996.
14. J. A. Jensen, "Field: A program for simulating ultrasound systems," *Med. Biol. Eng. Comp.* **10th Nordic-Baltic Conference on Biomedical Imaging, Vol. 4, Supplement 1, Part 1**, pp. 351–353, 1996b.
15. K. V. Ramnarine, D. K. Nassiri, P. R. Hoskins, and J. Lubbers, "Validation of a new blood mimicking fluid for use in Doppler flow test objects," *Ultrasound Med. Biol.* **24**, pp. 451–459, 1998.
16. J. A. Jensen, O. Holm, L. J. Jensen, H. Bendsen, H. M. Pedersen, K. Salomonsen, J. Hansen, and S. Nikolov, "Experimental ultrasound system for real-time synthetic imaging," in *Proc. IEEE Ultrason. Symp.*, **2**, pp. 1595–1599, 1999.
17. A. P. G. Hoeks, J. J. W. van de Vorst, A. Dabekaussen, P. J. Brands, and R. S. Reneman, "An efficient algorithm to remove low frequency Doppler signal in digital Doppler systems," *Ultrason. Imaging* **13**, pp. 135–145, 1991a.
18. D. H. Evans, W. N. McDicken, R. Skidmore, and J. P. Woodcock, *Doppler Ultrasound, Physics, Instrumentation, and Clinical Applications*, John Wiley & Sons, New York, 1989.

Blood vector velocity estimation using an autocorrelation approach: In vivo Investigation.

Jesper Udesen[1,2], Michael Bachmann Nielsen[3], Kristina Rue Nielsen[3] and Jørgen Arendt Jensen[1]

1) Center for Fast Ultrasound Imaging, Ørsted•DTU,
Bldg. 348, Technical University of Denmark, DK-2800 Lyngby, Denmark.
2) B-K Medical A/S, Mileparken 34, DK-2730 Herlev, Denmark.
3) Department of Radiology, Section of Ultrasound,
Rigshospitalet. Blegdamsvej 9, DK-2100 Kbh , Denmark.

***Abstract*— In conventional techniques for blood velocity estimation, only the axial component of the velocity vector is found. We have previously shown that it is possible to estimate the 2-D blood velocity vector both in simulations and in flow phantom experiments using a fast and inexpensive method (the transverse oscillation (TO) method) based on an autocorrelation approach. The TO method makes use of a double oscillating pulse-echo field which is created by manipulating the receive apodization function. Two receive beams are beamformed, where the lateral distance between the two beams corresponds to a 90° phase shift in the lateral direction. The TO method works at angles where conventional methods fails to estimate any blood movement, i.e. when the angle between the ultrasound beam and the velocity vector is approximately 90°. In this paper the first in-vivo color flow map (CFM) images are presented using the TO method. A 128 element 5 MHz linear array transducer was used together with the experimental ultrasound scanner RASMUS operating at a sampling frequency of 40 MHz with a pulse repetition frequency of 24 kHz. After sampling the received channel data were beamformed off-line, and a transverse oscillation period of 1 mm was created in the lateral pulse-echo field by manipulating the receive apodization function. Echo-canceling was performed by subtracting a line from the sampled data, where the line was a linear fit to the sampled data. Three different scan areas were selected: 1) The common carotid artery, 2) the common carotid artery and the jugular vein, 3) the bifurcation of the common carotid artery. In all three cases the angle between the ultrasound beams and the blood velocity vector is larger than 60° i.e. the conventional Doppler velocity estimator degrades significantly in terms of standard deviation and bias. The velocity direction and magnitude could be estimated for all cases and it was found that the blood flow is within the values given by the literature.**

I. Introduction

In conventional ultrasound scanners the pulse echo field only has an axial oscillation, and hence blood scatterers traveling through the acoustic field gives signals from which only the 1-D axial velocity of the blood can be determined. Many authors have addressed the problem of extending the 1-D velocity estimator to a 2-D vector velocity estimator which potentially could give valuable information about the blood flow One promising method for finding the 2-D vector velocity is the method suggested by Jensen and Munk (Transverse Oscillation (TO)) [1], [2], [3] and by Anderson (Heterodyned Spatial Quadrature (HSQ)) [4], [5]. The basic principle in both methods is to use the receive apodization function to create a lateral oscillation in the pulse echo field and use an autocorrelation estimator to find the 2-D vector velocity.

This paper presents the first in-vivo color flow map (CFM) images using the TO method. The experimental scanner RASMUS has been used to scan the carotid artery at three different positions: 1) The carotid artery at transverse flow, 2) The carotid artery and the Jugular vein at transverse flow, 3) The bifurcation of the carotid artery.

II. Method

The basic principle in the TO method is the extension of the conventional 1-D autocorrelation method [6] to 2-D[1]. Since the 1-D method makes use of an axial oscillation in the pulse echo field, an additional oscillation in the lateral direction is implemented in the TO method by manipulating the receive apodization function. This is possible since a Fourier relationship exists between the apodization function and the lateral component of the pulse echo field in the focal point [7]. To distinguish between forward and backward flow, the conventional 1-D method makes use of a quadrature signal which is a 90° phase shifted version in the axial direction of the in-phase signal. This principle is also implemented in the TO method but in both the axial and lateral direction. This can be done by having two receive beams each shifted a lateral distance in space, which corresponds to a 90° phase shift. Echo canceling is done by removing the mean value of the slow-time samples, and velocity vectors are found from an extended autocorrelation estimator [3].

The performance of the TO method has previously been tested in simulations using Field II, and in flow-phantom experiments using the RASMUS scanner [8], [9]. It has been found that acceptable vector velocities could be estimated when the angle between the blood flow and the ultrasound

[1]A complete discussion of the TO method is given in [2], [3]

beam was within the interval $90^\circ - 50^\circ$. To increase performance and get velocity estimates with a diagnostic value, the TO method uses a larger number of transmitted pulses pr. velocity estimate than conventional 1-D estimation. This can be done if the pulse repetition frequency f_{prf} is increased to its maximum value, which for a scanning depth of 30 mm is $f_{prf} = 24$ kHz. In all the cases presented in this paper aliasing only occurs when f_{prf} is below 6 kHz. It is therefore possible to transmit consecutive pulses in four different direction at $f_{prf} = 24$ kHz before returning to the initial direction. It should be noted that the scanning sequence used in all measurements is within the limits of the Food and Drug Administration (FDA). A complete description of the measurement setup can be found in Table I.

TABLE I

TRANSDUCER SETUP

Parameter	Value
Transducer	Linear array
Number of elements	128
Active number of elements	64
Pitch	0.3 mm
Kerf	0.035 mm
Center frequency	5 MHz
Number of cycles pr. pulse	8
fprf	24 kHz
Sampling frequency	40 MHz
Transverse wave length	1.0 mm
Apodization in transmit	Hanning
Apodization in receive	Two Hannings
Focus in transmit	18 mm
Focus in receive	Dynamic
F-number in transmit	3.3
F-number in receive	0.8
Number of firings pr. vel. est.	64
Lateral distance between velocity est.	4 pitch
$I_{spta \cdot is}$	293 mW/cm^2
MI	1.07

The scanner used for all experiments was the RASMUS scanner [10] which can store 16 GB of data for off-line processing. Data was beamformed off-line using MATLAB, and a CFM movie was constructed over the entire scanning sequence. The frame rate of the movie was 20.8 Hz, which is comparable to CFM frame rates on most commercial scanners. All scannings were performed by the author and by two experienced medical doctors and the human volunteers were all healthy and below the age of 40 years.

To compare the TO method to conventional CFM images, B-mode images were also acquired during the scanning. The B-mode images were resized using a lateral sampling of $\lambda/5$ and bicubic interpolation in Matlab, and the velocity images were resized to the same size as the B-mode images. To differentiate between blood and tissue, low resolution B-mode images were constructed by median filtering the B-mode images using a 1.5×0.5 mm kernel and thereafter low-pass filtering the images by convolving with a 3.8×0.5 mm square. Values under a certain threshold value in the low resolution B-mode images were considered to be blood and all other values were considered to be tissue. This approach gives a smooth appearance of the blood vessels and work well especially for larger vessels.

III. RESULTS

A. The common carotid artery

The common carotid artery of a healthy 34 year old male was scanned for 1.81 s, where the angle between the flow and the ultrasound beam was found from the B-mode image to be approximately 88°, i.e. an angle where a conventional axial velocity estimator would not detect any blood movement. Fig. 1 shows the 2-D vector velocity at the time shortly after peak systole where the velocity is most homogeneous over the vessel. It is seen that the maximum velocities occurs in the center off the vessel and that the whole vessel area is detected as blood by the discriminator. The maximum peak velocity over the scanning period was approximately 0.8 m/s, which is a normal value for a healthy person [11]. For each CFM frame the mean volume flow over lateral distance was estimated from the vector velocity assuming circular symmetry of the vessel, and the resulting mean volume flow as a function of time is shown in Fig. 2. The maximum value of approximately 300 ml/min is a normal value for a healthy person [11].

B. The common carotid artery and jugular vein

The common carotid artery and jugular vein of a healthy 30 year old male was scanned for 3.18 seconds with an angle between the flow and the ultrasound beam of approximately 90° for both vessels. Fig. 3 shows the flow at the time of the peak systole in the carotid artery, where the maximum flow in the carotid artery is approximately 0.8 m/s. The flow in the artery is moving in opposite direction of the flow in the vein and again the maximum velocities are found at the center of both vessels. Due to the positions of the vessels compared to the scanning plane, the maximum velocity occurs around the lateral center of all the CFM image.

C. The bifurcation of the common carotid artery.

The carotid artery bifurcation of a healthy 30 year old male was scanned for 3.18 seconds yielding data from three peak systoles. The vector flow at the time of the second peak systole in the CFM movie can be seen in the top of Fig. 4 together with the corresponding axial velocity image estimated from the same data (Fig. 4 bottom). The vector velocity image is clearly seen to contain information about the turbulent nature of the flow which is not present in the conventional image. In particular, a large eddie is seen to be present in the internal carotid artery.

IV. DISCUSSION

The CFM images presented in this paper are the first 2-D blood vector velocity estimates using the TO method, and the velocity estimates are, according to the literature, within acceptable limits. The estimated vector velocities have previously been shown to have low bias and standard deviation in flow phantom experiments where a precise reference velocity exists. However, further research should concentrate on getting

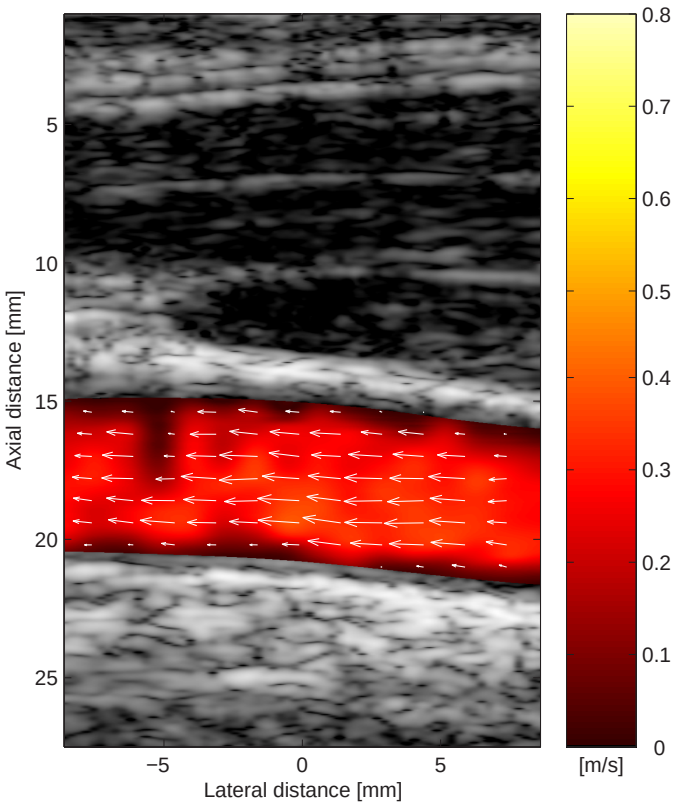

Fig. 1. The vector velocity in the carotid artery shortly after the peak systole.

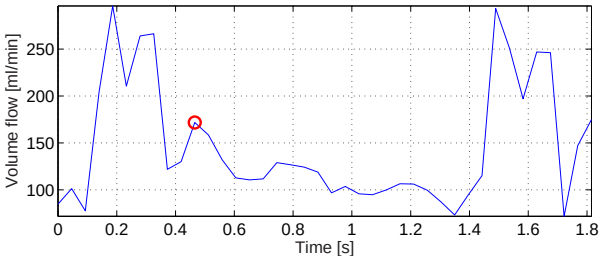

Fig. 2. The mean volume flow in the common carotid artery estimated using the TO method. The vector flow in Fig. 1 is estimated at the time indicated by the red circle.

a precise in-vivo reference velocity obtained with a independent method, e.g. speckle tracking so that the performance of the TO method can be more precisely evaluated during in-vivo scanning.

The TO method gives the ability to show blood flow information which is not present in conventional flow imaging. This huge amount of information introduces the challenge of choosing an optimal way to show the velocity, and the 2-D vector arrows used in the images in this paper is only one way to do this. Another way to display the vector velocity is to use a 2-D color-map, where the colors indicates the direction of flow and the intensity indicates the speed. Seeking optimal ways to present the velocity is subject for further research.

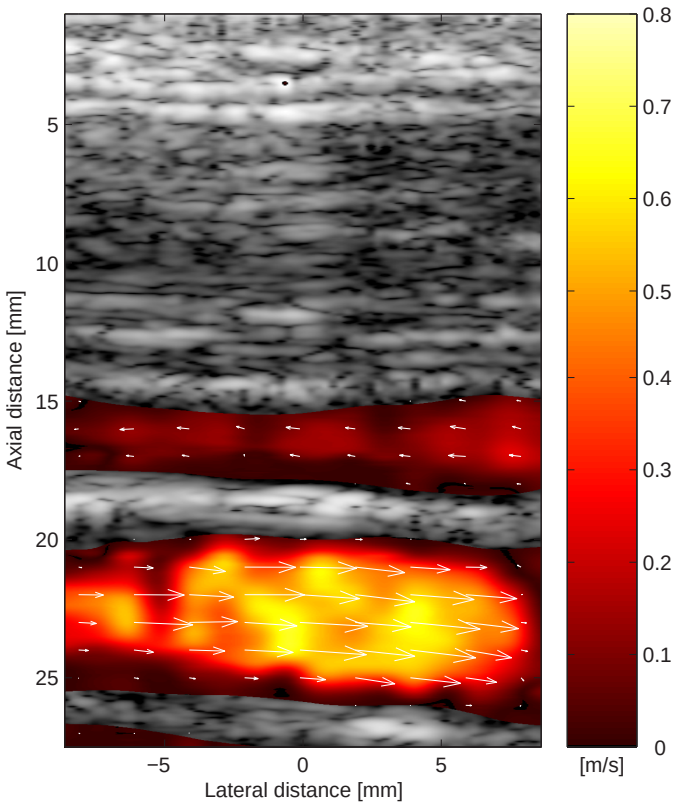

Fig. 3. The vector velocity in the carotid artery (bottom) and jugular vein (top) at the time of the peak systole.

REFERENCES

[1] P. Munk. Estimation of the 2-D flow vector in ultrasonic imaging: a new approach. Master's thesis, Department of Information Technology, Technical University of Denmark, 1996.

[2] J. A. Jensen and P. Munk. A new method for estimation of velocity vectors. *IEEE Trans. Ultrason., Ferroelec., Freq. Contr.*, 45:837–851, 1998.

[3] J. A. Jensen. A new estimator for vector velocity estimation. *IEEE Trans. Ultrason., Ferroelec., Freq. Contr.*, 48(4):886–894, 2001.

[4] M. E. Anderson. Spatial quadrature: a novel technique for multi-dimensional velocity estimation. In *Proc. IEEE Ultrason. Symp.*, volume 45, pages 1233–1238, 1997.

[5] M. E. Anderson. A heterodyning demodulation technique for spatial quadrature. In *Proc. SPIE - med. imag.*, pages 1487–1490, 2000.

[6] C. Kasai, K. Namekawa, A. Koyano, and R. Omoto. Real-time two-dimensional blood flow imaging using an autocorrelation technique. *IEEE Trans. Son. Ultrason.*, 32:458–463, 1985.

[7] J. W. Goodman. *Introduction to Fourier optics*. McGraw Hill Inc., New York, second edition, 1996.

[8] J. Udesen and J. A. Jensen. Experimental investigation of transverse flow estimation using transverse oscillation. In *Proc. IEEE Ultrason. Symp.*, pages 1586–1589, 2003.

[9] J. Udesen and J. A. Jensen. An in-vivo investigation of transverse flow estimation. In *Proc. SPIE - Progress in biomedical optics and imaging*, volume 5373, pages 307–314, 2004.

[10] J. A. Jensen, O. Holm, L. J. Jensen, H. Bendsen, H. M. Pedersen, K. Salomonsen, J. Hansen, and S. Nikolov. Experimental ultrasound system for real-time synthetic imaging. In *Proc. IEEE Ultrason. Symp.*, volume 2, pages 1595–1599, 1999.

[11] D. H. Evans, W. N. McDicken, R. Skidmore, and J. P. Woodcock. *Doppler Ultrasound, Physics, Instrumentation, and Clinical Applications*. John Wiley & Sons, New York, 1989.

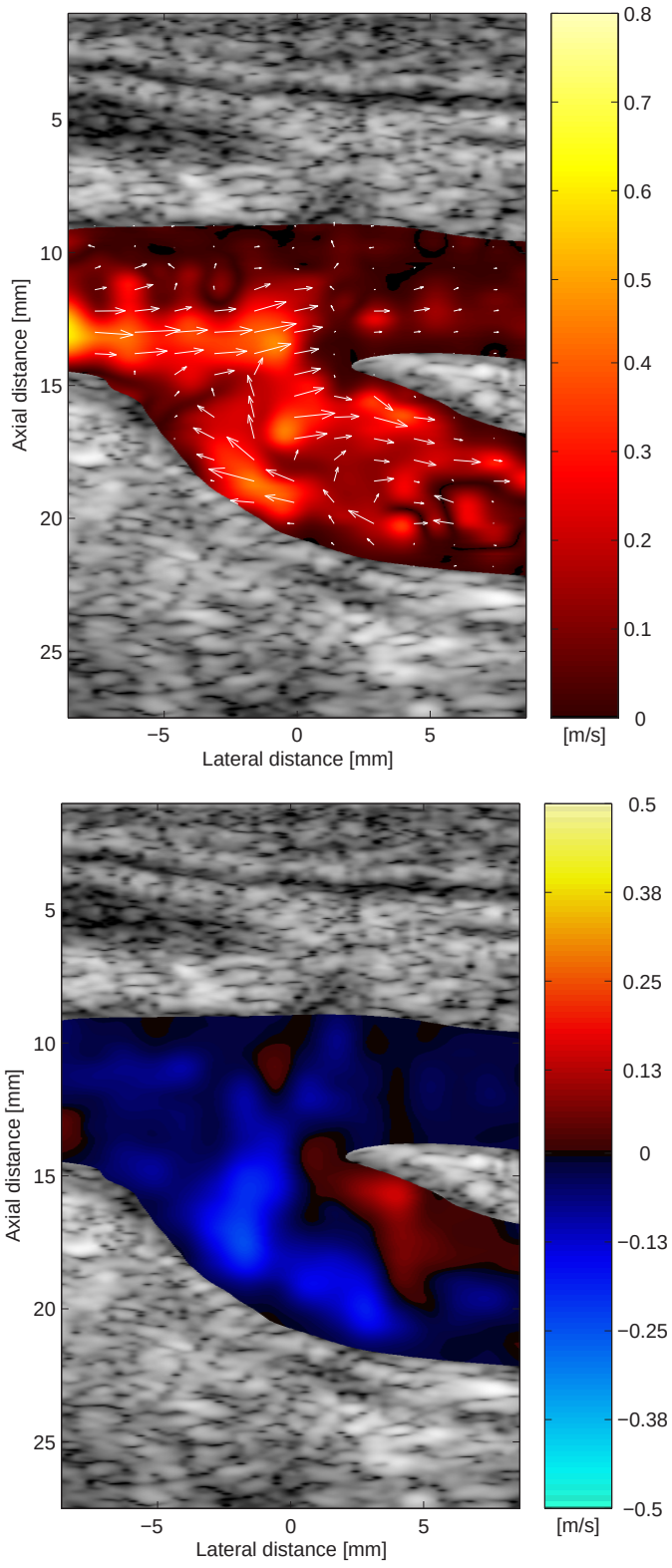

Fig. 4. Top: The vector velocity in the bifurcation of the carotid artery at the time of the peak systole. Bottom: The axial velocity estimated from the same data.

A simple method to reduce aliasing artifacts in color flow mode imaging.

Jesper Udesen[1,2], Svetoslav Nikolov[1] and Jørgen Arendt Jensen[1]

1) Center for Fast Ultrasound Imaging, Ørsted•DTU,
Bldg. 348, Technical University of Denmark, DK-2800 Lyngby, Denmark.
2) B-K Medical A/S, Mileparken 34, DK-2730 Herlev, Denmark.

***Abstract*— It is a well known limitation in conventional blood velocity estimation using a phase estimation approach, that aliasing artifacts are present, when the blood velocities exceed a value determined by half the pulse repetition frequency (the Nyquist frequency). This paper proposes a simple anti-aliasing discriminator (AAD) method based on using two different pulse repetition frequencies to increase the aliasing limit to twice the Nyquist frequency. The method is evaluated in simulations using the Field II program. The axial velocity in a virtual blood vessel is found along one axial line, where N=10 emissions are used for each velocity estimate. Mean standard deviation and mean absolute bias are** 4.9% **and** 23.8%**, respectively, when no attempt is done to suppress the aliasing. When the AAD is used the corresponding values are** 3.4% **and** 1.0%**. When median filtering is applied, the values are** 1.1% **and** 0.6%**. The method is evaluated experimentally using the ultrasound scanner RASMUS and a circulating flowrig with parabolic flow. The mean standard deviation and mean absolute bias are** 4.0% **and** 20.3%**, respectively, when no attempt is done to suppress the aliasing. When the anti-aliasing discriminator is used the corresponding values are** 3.6% **and** 1.2%**. The values are** 1.0% **and** 0.8%**, when median filtering is performed.**

I. Introduction

One of the drawbacks of conventional ultrasound imaging used for blood flow estimation, is the presence of aliasing in the velocity estimates, when the slow-time frequency f_p exceeds half the pulse repetition frequency $1/(2T_{prf})$. This problem becomes most pronounced, when both the blood velocity and the pulse repetition time T_{prf} is high, e.g. when scanning the human heart. Here false velocity estimates will often create a confusing velocity image with a variety of different colors, and medical doctors may potentially loose important information about the real blood flow. One way to overcome the aliasing problem is to use a time shift technique where consecutive received signals are cross-correlated [1]. However, this method is expensive in terms of computation power and even though aliasing will not occur, a similar problem may be seen especially if the emitted pulse is too narrow banded. Another way to overcome the aliasing problem is to use multiple transmit frequencies [2] or use continuity constraints on the spatial and temporal velocity [3]. However, these method are all expensive in terms of computer power.

This paper proposes a simple anti-aliasing discriminator (AAD), which can raise the aliasing frequency to twice the Nyquist frequency for a system using a phase shift estimator. The AAD method is evaluated in computer simulations using the Field II program [4], [5], where a virtual blood vessel is scanned. Furthermore the method is tested in a circulating flowrig which is scanned by the experimental RASMUS scanner [6].

II. Method

The basic idea in the AAD method is to use two different pulse repetition times T_{prf} and $1.5T_{prf}$ to acquire two data sequences. The first sequence sampled at T_{prf} is used to estimate the velocity from an autocorrelation estimator [7] and the second sequence is used to raise the aliasing limit in the velocity estimate to twice the Nyquist frequency. This can be done even though aliasing is present in both sequences.

Assume that N_1 narrow band ultrasound pulses have been emitted from an ultrasound transducer focused into a blood vessel, and that each pulse has center frequency f_0, and the time between consecutive pulses is T_{prf}. After $1.5\,T_{prf}$ N_2 similar focused pulses are emitted towards the blood vessel with a pulse repetition time $1.5\,T_{prf}$ resulting in a shot sequence as shown in Fig. 1. When all the echo signals are received by the transducer, they are delay-and-sum beamformed. In-phase and quadrature signals are then constructed to form analytical signals from which it is possible to distinguish between forward and backward flow.

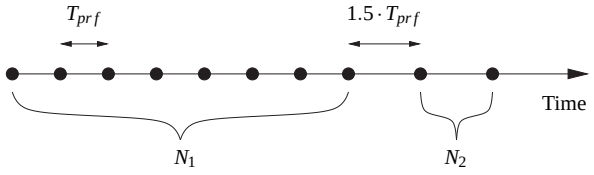

Fig. 1. The shot sequence for the AAD method. First N_1 pulses are emitted from the transducer at a pulse repetition time T_{prf} followed by N_2 pulses at $1.5 \cdot T_{prf}$

Let the $N = N_1 + N_2$ analytical beamformed signals sampled at the position of the focal point be denoted by $r(n)$, where n enumerates the emitted pulse, and assume that the analytical signals are monocromatic and have unit amplitude. I.e.

$$r(n) = \begin{cases} e^{j2\pi f_p T_{prf} n} & n = 1,2,..,N_1 \\ e^{j2\pi f_p T_{prf}(\frac{3}{2}n - \frac{1}{2}N_1)} & n = N_1+1,..,N \end{cases} \quad (1)$$

where the frequency f_p is related to the axial velocity v_z through the relation [1],

$$f_p = \frac{2v_z f_0}{c}, \tag{2}$$

with c being the speed of sound in the medium. The problem is now to determine the axial velocity of the blood without aliasing from the signal $r(n)$.

The mean phase difference between the first N_1 samples separated T_{prf} in time will be the phase of the vector $P1$ given by the autocorrelation in lag 1 of $r(n)$ for $n = 1,2,..,N_1$. I.e.,

$$\begin{aligned} P1 &= \frac{1}{N_1 - 1}\sum_{n=1}^{N_1-1} r^*(n)r(n+1) \\ &= e^{j2\pi f_p T_{prf}}, \end{aligned} \tag{3}$$

where $*$ denotes complex conjugation. This is the vector whose phase is estimated in a conventional autocorrelation estimator [7], where aliasing is present, when the phase becomes less than $-\pi$ or larger than π.

The phase difference between the last N_2+1 samples in $r(n)$ separated $1.5\,T_{prf}$ in time will be given by the phase of the vector $P2$,

$$\begin{aligned} P2 &= \frac{1}{N_2}\sum_{n=N_1}^{N-1} r^*(n)r(n+1) \\ &= e^{j2\pi f_p T_{prf} 3/2}, \end{aligned} \tag{4}$$

and the phase difference between $P1$ and $P2$ will, thus, be given by the phase to the vector $P3$,

$$\begin{aligned} P3 &= P1^* P2 \\ &= e^{j2\pi f_p T_{prf}/2} \end{aligned} \tag{5}$$

From (3) and (5) it follows that

$$P1 = P3^2, \tag{6}$$

and the phase of $P1$ will, thus, always be double the phase of $P3$. Therefore the sign of the phase of $P3$ can be used as a discriminator to determine the direction of the flow even though aliasing is present in the first N_1 samples of $r(n)$.

Now let the phase θ_1 and θ_3 to $P1$ and $P3$ be determined by an *arctan* operator as it is done in a real scanner and note that both θ_1 and θ_3 are bounded by the interval between $\pm\pi$. Due to signal noise (6) will generally never be satisfied. Instead the weaker formulation can be used:

Aliasing is present in $r(n), \quad n = 1,2,..,N_1$

$$\Updownarrow$$

The signs of θ_1 *and* θ_3 *are opposite and* $|\theta_1 - \theta_3| > \pi/2$

The first constraint "*The signs of* θ_1 *and* θ_3 *are opposite*" is basicly a weaker formulation of (6). The last constraint "$|\theta_1 - \theta_3| > \pi/2$" handles the special case where θ_1 is close to zero and θ_3 therefore is likely to change sign, if noise is present in the signal $r(n)$.

When the discriminator discovers aliasing in $r(n)$, the sign of the aliased velocity is changed and the velocity magnitude is corrected. The discriminator is valid until the phase of $P3$ exceeds the aliasing limit at $\pm\pi$, where all information of the flow direction is lost. This happens when $f_p = 1/T_{prf}$, i.e. at twice the frequency of a normal autocorrelation estimator. The method is illustrated in Fig. 2, where an example of the vectors $P1, P2, P3$ is shown.

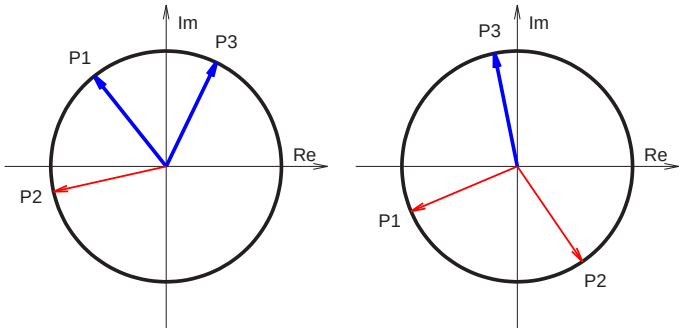

Fig. 2. Examples of the complex vectors $P1, P2, P3$ where thick blue arrows indicates no-aliasing and thin red arrows indicates aliasing. Left: here no aliasing is present in the first N_1 samples of $r(n)$, hence $P1$ has not crossed the border at π. Right: Here aliasing is present and $P1$ has crossed the border at π. However, the angle to $P3$ has not crossed the border at π and the sign of the phase of $P3$ can be used to determine the direction of flow eventhough aliasing is present.

To improve signal-to-noise ratio, it is necessary to perform RF-averaging on $r(n)$, i.e the complex value of the vectors $P1, P2, P3$ are found as a mean value over one pulse length in the axial direction. Median filtering can also be applied on the velocity estimates, since single aliased velocity estimates are likely to pass through the discriminator, if noise or turbulence is present. Filtering makes good sense from a physical point of view, since the blood flow will not allow large velocity gradients unless full turbulence is present in the flow.

In all ultrasound systems for blood velocity estimation, signals from stationary tissue have to be removed before the velocity can be estimated. Usually this is done by using a high pass filter on $r(n)$. However, since the last N_2 samples have been acquired at a different sampling frequency compared to the rest of $r(n)$, this approach is not straight forward. Instead a simple mean value removal algorithm can be implemented, which simply subtracts the mean value of $r(n)$ from each value in $r(n)$. Another approach could be to use a line fitting algorithm [8], which approximates a straight line to all the data in $r(n)$ taking into account that the last N_2 samples are acquired with a sampling time of $1.5\,T_{prf}$.

III. Simulation

The Field II ultrasound simulation program [4], [5] was used to simulate a M-mode scan of a virtual blood vessel. All the relevant parameters concerning the transducer, the beamforming, and the blood vessel can be found in Table I.

The velocity was chosen so that aliasing would occur in the center of the vessel within a radius of 3.15 mm, when a conventional autocorrelation estimator was used. Using $N = 10$ emissions and a conventional autocorrelation estimator with

RF-averaging, 24 estimates of the axial velocity through the virtual vessel was obtained. From the same data the velocity was found using the AAD method and the anti-aliased estimates were median filtered over axial depth and estimate number (time), with a 3×3 pixel kernel to remove false estimates. The mean axial velocity and the standard deviation as a function of depth for all three cases can be seen in Fig. 3. To quantify the performance into single numbers the mean standard deviation and mean absolute bias over the vessel was calculated. The mean standard deviation and mean absolute bias are 4.9% and 23.8%, respectively, when no attempt is made to suppress the aliasing. When the AAD is used the corresponding values are 3.4% and 1.0%. When 3×3 median filtering is performed, the values are 1.1% and 0.6%. It is seen that the AAD method significantly improves the estimates.

TABLE I

FIELD II SIMULATION SETUP

Parameter	Value
Transducer	Linear array
Number of elements	128
Active number of elements	64
Pitch	0.208 mm
Kerf	0.035 mm
Height	5 mm
Center frequency	7 MHz
Number of cycles pr. pulse	8
T_{prf}	0.5 ms
Sampling frequency	100 MHz
Transmit and receive apodization	Hanning
Focus in transmit	40 mm
Focus in receive	Dynamic
Blood vessel	straight tube
Length	10 mm
Radius	6.752 mm
Axial center position	40 mm
Angle between beam and vessel	70°
Type of flow	parabolic
Center velocity	0.4 m/s
Number of scatters pr. m^3	$9.4 \cdot 10^{10}$
Number of shots used to est. $P1$	$N_1 = 8$
Additional shots used to est. $P2$	$N_2 = 2$

IV. EXPERIMENTAL INVESTIGATION

The experimental ultrasound scanner RASMUS [6] was used to scan a tube with blood mimicking fluid in a circulating flow-rig. The Reynolds number of the flow in the tube was below 1000, hence the flow was assumed laminar and parabolic. The same setup parameters were used as in the simulation except from the scanner sampling frequency, which was 40 MHz and the axial distance to the center of the tube containing the blood was 42.5 mm (compared to 40 mm in the simulations). The mean velocity from 24 estimates together with the corresponding curves for ± 1 standard deviation can be seen in Fig. 4. The mean standard deviation and mean absolute bias are 4.0% and 20.3%, respectively, when no attempt is made to suppress the aliasing. When the AAD is used without the median filtering the corresponding values are 3.6% and 1.2%. When 3×3 median filtering is performed the values are 1.0% and 0.8%. As in the simulations it is seen that the AAD significantly improves the estimates.

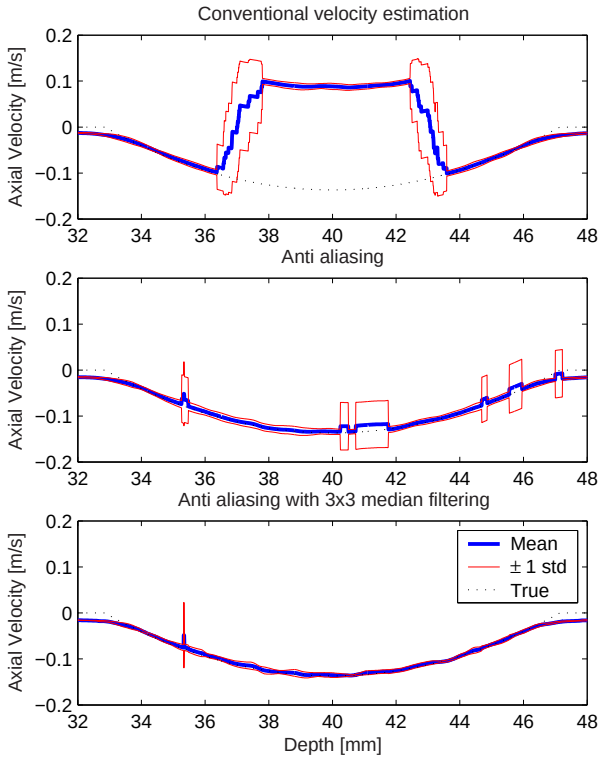

Fig. 3. Simulation using Field II. The axial velocity in a virtual blood vessel as a function of depth is estimated. The dotted black curve is the true velocity, the thick blue curve is the estimated mean velocity and the thin red curves indicate ± 1 standard deviation on the estimates. Top: axial velocity for a conventional estimator. Center) axial velocity using AAD. Bottom: the same as the center figure, but with 3×3 median filtering.

V. DISCUSSION

The AAD method has been seen to perform well in simulations as well as flow phantom experiments using additional $N_2 = 2$ emissions to compensate for aliasing. For a full evaluation of the method the next step is to test it under in-vivo conditions. Here it must be expected that a worse signal-to-noise ratio will demand additional emissions to compensate for aliasing, which for some applications could be problematic. However, the axial velocity could also be estimated from the additional N_2 emissions, i.e., from the phase of the vector $P2$, so that the total number of emissions is kept the same as a conventional estimator and, at the same time, aliasing in the estimates is removed.

REFERENCES

[1] J. A. Jensen. *Estimation of Blood Velocities Using Ultrasound: A Signal Processing Approach.* Cambridge University Press, New York, 1996.

[2] H. J. Nitzpon, J. C. Rajaonah, C. B. Burckhardt, B. Dousse, and J. J. Meister. A new pulsed wave Doppler ultrasound system to measure blood velocities beyond the Nyquist limit. *IEEE Trans. Ultrason., Ferroelec., Freq. Contr.*, 42:265–279, 1995.

[3] J. Jackson. Automatic velocity anti-aliased ultrasound methods and systems, US Patent US2004254467, 2004.

[4] J. A. Jensen and N. B. Svendsen. Calculation of pressure fields from arbitrarily shaped, apodized, and excited ultrasound transducers. *IEEE Trans. Ultrason., Ferroelec., Freq. Contr.*, 39:262–267, 1992.

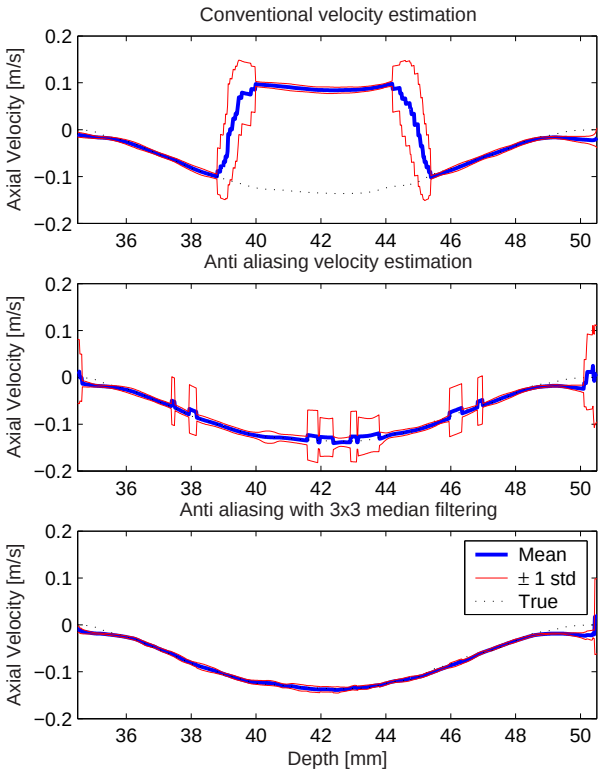

Fig. 4. Experiments using the RASMUS scanner. The axial velocity in a tube as a function of depth is estimated. The dotted black curve is the true velocity, the thick blue curve is the estimated mean velocity and the thin red curves indicate ± 1 standard deviation on the estimates. Top: axial velocity for a conventional estimator. Center: axial velocity using AAD. Bottom: the same as the center figure, but with 3×3 median filtering.

[5] J. A. Jensen. Field: A program for simulating ultrasound systems. *Med. Biol. Eng. Comp.*, 10th Nordic-Baltic Conference on Biomedical Imaging, Vol. 4, Supplement 1, Part 1:351–353, 1996b.

[6] J. A. Jensen, O. Holm, L. J. Jensen, H. Bendsen, H. M. Pedersen, K. Salomonsen, J. Hansen, and S. Nikolov. Experimental ultrasound system for real-time synthetic imaging. In *Proc. IEEE Ultrason. Symp.*, volume 2, pages 1595–1599, 1999.

[7] C. Kasai, K. Namekawa, A. Koyano, and R. Omoto. Real-time two-dimensional blood flow imaging using an autocorrelation technique. *IEEE Trans. Son. Ultrason.*, 32:458–463, 1985.

[8] A. P. G Hoeks, J. J. W. van de Vorst, A. Dabekaussen, P. J. Brands, and R. S. Reneman. An efficient algorithm to remove low frequency Doppler signal in digital Doppler systems. *Ultrason. Imaging*, 13:135–145, 1991a.

Fast color flow mode imaging using plane wave excitation and temporal encoding

Jesper Udesen[a,b], Fredrik Gran[a] and Jørgen Arendt Jensen[a]

[a]Center for Fast Ultrasound Imaging, Ørsted • DTU, Bldg. 348, Technical University of Denmark, DK-2800 Kgs. Lyngby, Denmark
[b]B-K Medical A/S, Mileparken 34, DK-2730 Herlev, Denmark

1. ABSTRACT

In conventional ultrasound color flow mode imaging, a large number ($\sim$ 500) of pulses have to be emitted in order to form a complete velocity map. This lowers the frame-rate and temporal resolution. A method for color flow imaging in which a few ($\sim$ 10) pulses have to be emitted to form a complete velocity image is presented. The method is based on using a plane wave excitation with temporal encoding to compensate for the decreased SNR, resulting from the lack of focusing. The temporal encoding is done with a linear frequency modulated signal. To decrease lateral sidelobes, a Tukey window is used as apodization on the transmitting aperture. The data are beamformed along the direction of the flow, and the velocity is found by 1-D cross correlation of these data. First the method is evaluated in simulations using the Field II program. Secondly, the method is evaluated using the experimental scanner RASMUS and a 7 MHz linear array transducer, which scans a circulating flowrig. The velocity of the blood mimicking fluid in the flowrig is constant and parabolic, and the center of the scanned area is situated at a depth of 40 mm. A CFM image of the blood flow in the flowrig is estimated from two pulse emissions. At the axial center line of the CFM image, the velocity is estimated over the vessel with a mean relative standard deviation of 2.64% and a mean relative bias of 6.91%. At an axial line 5 mm to the right of the center of the CFM image, the velocity is estimated over the vessel with a relative standard deviation of 0.84% and a relative bias of 5.74%. Finally the method is tested on the common carotid artery of a healthy 33-year-old male.

2. INTRODUCTION

In conventional ultrasound imaging used for blood flow estimation (CFM) an image of the flow velocities is formed by focusing a number ($\sim$ 500) of beams. Each beam has a certain time of flight, since the sound has to travel forward and back through the tissue. Hence, the frame rate of a conventional CFM system is often low ($\sim$ 10 Hz) and the temporal resolution in the velocity estimates is therefore poor. The problem becomes even more significant, when structures deep in the human body (e.g. the heart) are scanned. Here, fine temporal details in the blood flow will not be estimated due to the low frame rate. It is therefore of interest to develop methods, which combine a high frame rate with a relatively good performance in terms of bias and standard deviation on the velocity estimates.

The limiting factors on the frame rate can mainly be divided into two types. The first type is the factors connected to the electronics of the scanner. Here, the problem is the trade off between having fast expensive electronics and at the same time producing a scanner which is competitive on the scanner market. The second type of limitations, is the factors connected to the physics of the method implemented in the scanner. This paper addresses the latter type of limitations.

The method called plane wave excitation (PWE) presented in this paper uses different techniques to achieve a high frame rate ($\sim f_{prf}/10$) and a good performance on the velocity estimates.

- A chirp is used as excitation pulse to increase the signal to noise ratio (SNR)
- A plane wave is transmitted from the transducer. One image of the speckle pattern in the region of interest (ROI) is constructed from each transmitted plane wave. This method has previously been suggested for elastography,[1] but has not been used for blood velocity estimation. Mo et al.[2] have suggested a technique where a zone based imaging is performed, but this method does not use a single planewave in transmit, and the velocity estimation is performed using an autocorrelation method.

- Blood velocities are estimated using cross correlation along the lines of flow. This method has previously shown promising results for conventional and synthetic aperture flow.[3–5]

The paper is organized as follows: In Section 3 the theory behind the PWE method is introduced. In Section 4 the spatial resolution for the method is investigated and also the performance in terms of the intensities of the beamformed signals is compared to conventional focused flow imaging. In Section 5 the method is tested using the ultrasound simulation program Field II,[6,7] where a virtual blood vessel with a parabolic velocity profile is scanned. In Section 6 the PWE method is tested on a circulating flowrig using the experimental ultrasound scanner RASMUS.[8] Finally, in Section 7 the method is tested in-vivo on the carotid artery of a healthy 33-year-old male.

3. THEORY

3.1. Excitation

The fundamental idea in the PWE method is to acquire an image of the whole ROI using only one transmission. This can be done, if the transmitted field is generated by a plane wave, where all transducer elements are excited at the same time. The acoustic energy will then be spread out in the tissue rather than be focused in one specific point. This enables the beamformation over several lines per transmission, but lowers the signal to noise ratio (SNR). To compensate for this degradation of SNR, a linear frequency modulated signal (chirp) is used which increases the (peak) SNR. The theoretical gain in SNR after matched filtration (in dB) is given by[9]

$$G = 10\log_{10}\Big(\frac{E_{chirp}}{E_{ref}}\Big), \tag{1}$$

where E_{chirp} is the energy of the chirp and E_{ref} is the energy of the waveform which is used as a reference. The theoretical gain calculated from (1) will be 20.8 dB. However, due to tapering of the chirp and the compression filter the actual gain will be 14 dB.[10] The excitation waveform is defined as

$$s(t) = a(t)\sin\Big\{2\pi(f_0 - \frac{B}{2})t + 2\pi\frac{B}{2T}t^2\Big\},\ 0 \le t \le T. \tag{2}$$

where $a(t)$ is a temporal weighting function, f_0 is the center frequency, B is the bandwidth, and T is the duration of the excitation waveform. The center frequency is 7 MHz, the bandwidth is 75% of the center frequency and the duration is 20 μs. The temporal weighting function is chosen to be a Tukey window with 10% tapering. The compression filter is the corresponding matched filter version of the excitation waveform mismatched using a Chebyshev window with relative sidelobe attenuation of 70 dB. The temporal window applied to derive the mismatched filter is used in order to suppress axial sidelobes.[9]

To decrease lateral sidelobe level, apodization is applied on the transmitting aperture. A Tukey apodization with 70% tapering is used in order to get an acceptable contrast.

3.2. Receive beamforming

The basic principle in the receive beamforming is to beamform every point as a weighted sum of the received echoes. The echoes are delayed such that the delay for a specific receiving element corresponds to the shortest distance from the transducer surface to the point of interest and back to the receiving element. The beamforming principle can be seen in Fig. 1. The beamformed signal to a specific point for an array with Q receiving elements is given by

$$H(\vec{r}_p) = \sum_{q=1}^{Q} w_q s_q(t_q), \tag{3}$$

where $s_q(t)$ is the received echo on the q:th receiving element and w_q is the applied weighting function (apodization) on this element. The sample chosen from the filtered received signals corresponds to the time t_q which is given by

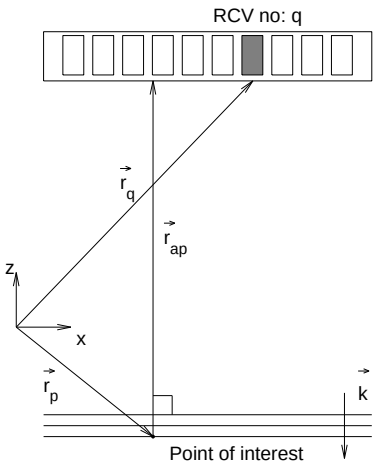

Figure 1. The principles of the beamforming method. Note that the applied delay for a specific received echo for a point in the image, is the shortest distance from the array to the point (which corresponds to the depth of the point) and back to the receiving element in question.

$$t_q = \frac{||\vec{r}_{ap}||}{c} + \frac{||\vec{r}_p - \vec{r}_q||}{c}, \tag{4}$$

where c is the speed of sound in the propagating medium, $\vec{r}_p - \vec{r}_q$ is the vector from the q:th receiving element and out to the field point. The vector $\vec{r}_{ap}$ is the vector which corresponds to the shortest distance from the array to the point. This vector is parallel to the wavevector $\vec{k}$ of the generated plane wave.

3.3. Velocity Estimation

Echo canceling is performed using a mean subtraction algorithm over a number of the acquired images. To estimate the velocity, the data are beamformed along the direction of the blood flow in the ultrasound plane. It has previously been shown that it is possible to find the direction of the flow automatically using one dimensional cross correlation.[5] It is therefore assumed, that the angle of the flow is known. The blood velocity is estimated using a one dimensional cross correlation method,[3] which estimates the velocity of the flow in the direction chosen. The number of plane wave beams used for one velocity frame is two for the simulations and flow rig experiments and 11 for the in-vivo experiments. It is thus possible to estimate a whole frame of independent velocity estimates with a rate of $\sim f_{prf}/10$ Hz.

4. RESOLUTION AND MAXIMUM INTENSITIES

Due to the broad lateral extend of the transmitted field, it is expected that the PWE method will perform worse than conventional flow imaging in terms of resolution. To quantify the resolution a simulation was performed using the ultrasound simulation program Field II.[6,7] A 7 MHz linear array transducer was simulated with 128 elements and the excitation pulse was a plane wave chirp as described in the previous section. The data for the transducer setup can be found in Table 1. The position of the transducer relative to the coordinate system is defined in Fig. 2 In Fig. 3 a point spread function for the PWE method is shown for a point at depth $z = 40$ mm and at lateral position $x = 0$ mm. The lateral and axial widths of the point spread functions are determined by estimating the maximum intensities in the lateral and axial directions. For comparison the corresponding PSF was simulated using a conventionally focused linear array approach (Fig. 4) with a one cycle pulse excitation, and the resolution was calculated. For the conventional linear array PSF the transmit and receive apodizations were changed to a boxcar function, and the transmit focus was situated at 40 mm. The number of elements used

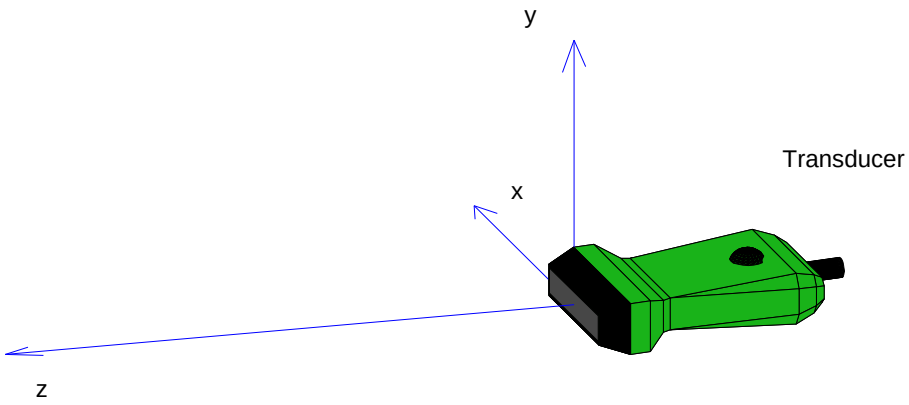

Figure 2. Definition of xyz-coordinate system.

Parameter	Value
Transducer	Linear array
Number of elements	128
Pitch	0.208 mm
Kerf	0.035 mm
Height	4.5 mm
Center frequency	7 MHz
Sampling frequency simulation	100 MHz
Sampling frequency experiments	40 MHz
Apodization in transmit	Tukey
Apodization in receive	Hamming

Table 1. Transducer set-up

for the conventional case are 64. In Fig. 4 it can be seen that the lateral width of the mainlobe is approximately the same for the PWE method compared to the conventional scan.

To get a quantitative measure of the resolution at different depths, the simulation was repeated for point scatters placed at depth between 5 mm and 100 mm, where consecutive points were separated by 2.5 mm. The lateral positions of the points were respectively $x = -5$ mm and $x = 0$ mm. Lateral and axial widths of the 3 dB contours were then determined by estimating the maximum intensities in the lateral and axial directions. The resolution for the PWE method was then compared to a conventional scan with transmit focus at 40 mm, dynamic receive focus and boxcar apodization. The result can be seen in Fig. 5. It can be seen that the lateral resolution is decreased by approximately a factor two at all depths when transmit focusing is not present, i.e. when using the PWE method. However, the axial resolution does not seem to be affected by the lack of transmit focusing in the PWE method.

Due to the broad lateral extend of the transmitted beam in the PWE method it is expected that the maximum intensities in the beam will be significantly lower compared to a focused beam. To quantify the intensities of the PWE method a simulation was performed using the transducer setup from Table 1, but with a one cycle sinusoid as excitation pulse. The maximum intensities in the resulting PSFs were compared to the corresponding case, when the beam was focused in transmit at the point of interest. In Fig. 6 the intensities for the two cases are shown. It is seen that the intensities are approximately 15 dB lower for the PWE method at 40 mm. However, when a chirp is used as excitation pulse in the PWE the intensities will be increased by 14 dB. It should therefore be expected that the signal intensities, and hence the signal to noise ratio, in the PWE method is comparable to normal focused imaging, when a chirp is used as excitation pulse.

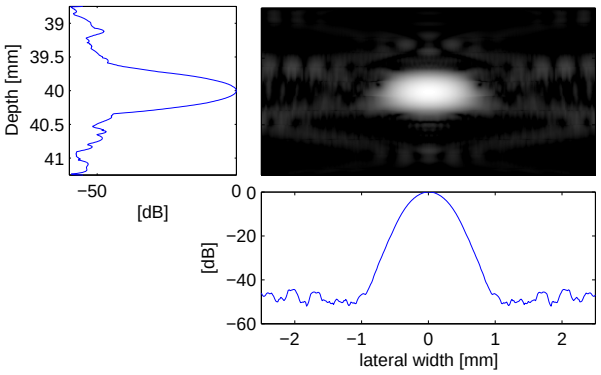

Figure 3. Point spread function (PSF) for the PWE method. Dynamic range is 60 dB.

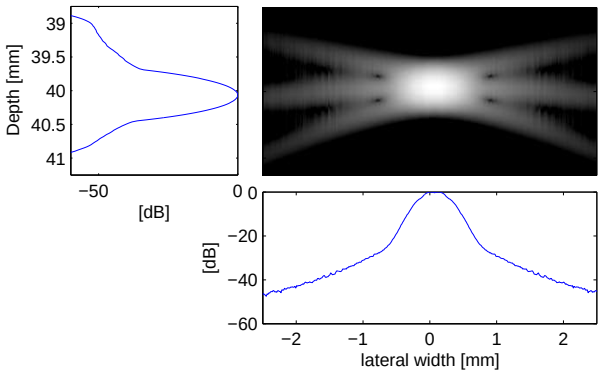

Figure 4. Point spread function (PSF) for conventional focused imaging. Dynamic range is 60 dB.

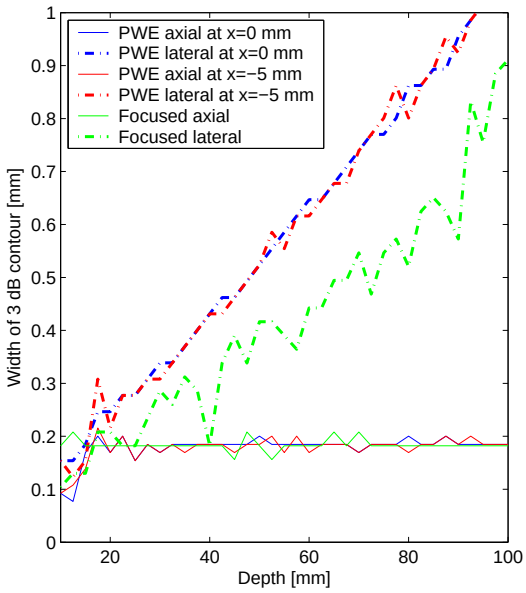

Figure 5. The resolution for the PWE method compared to conventional focused imaging. The axial and lateral widths at -3 dB are shown when a point scatter is located at $x = 0$ mm or $x = -5$ mm. For comparison, the corresponding resolution for a conventional focused scan with transmit focus at 40 mm is also shown.

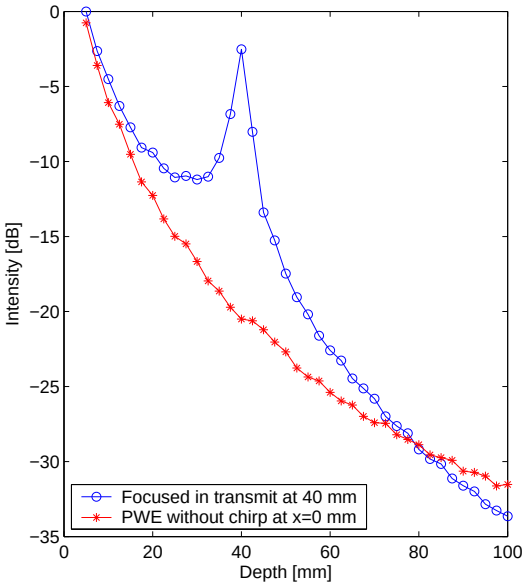

Figure 6. The maximum intensity in the PSFs for the conventional focused beam with transmit focus at 40 mm and for the PWE method without using chirp. The chirp gives an additional 14 dB to the PWE method.

5. FLOW SIMULATIONS

A cylindrical virtual blood vessel situated at a depth of 40 mm with a length of 45 mm and radius of 5 mm was simulated using the Field II program[6,7] and the transducer described in Table 1. The number of point scatters used to model the vessel was 66,384, to ensure fully developed speckle signals. A beamformed B-mode image of the vessel using the PWE method is shown in Fig. 8. Note that this is acquired using only one pulse emmision. All scatters were moved between consecutive pulse emissions with $f_{prf} = 8$ kHz using a parabolic velocity profile with maximum velocity of 0.5 m/s in the center of the vessel (Fig. 7). The flow angle with respect to the emitted beam was 45°. Two images were acquired using the beamforming described in Section 3.2 and the resulting images were divided into a grid of 250×250 points. At these points cross correlation was performed along the lines of flow, where each line to be cross corelated had a length of 10 times the wavelength of the emitted pulse at the center frequency. The spatial sampling interval was 0.1 times the wavelength of the emitted pulse at the

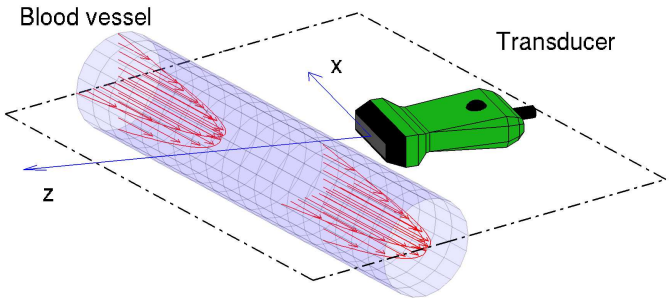

Figure 7. The setup of the virtual blood vessel.

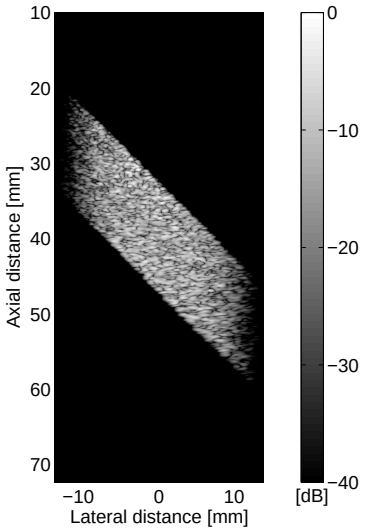

Figure 8. B-mode image of 66,384 point scatters using the Field II program and a single transmission (PWE method).

center frequency, i.e each line to be correlated consisted of 100 samples. The resulting CFM image is shown in Fig. 9 and the velocity at the line $x = 0$ mm is shown in Fig. 10 . Note that these images are acquired using only two pulse emissions.

6. FLOW PHANTOM EXPERIMENTS

The PWE method was evaluated on a circulating flowrig, which pumps blood mimicking fluid around a closed circuit. To avoid entrance effects in the flow, the fluid was first led through a 1.2 m long inflow pipe with radius $R = 6.4$ mm. At the end of the inflow pipe the fluid was led through a heat shrink tube submerged in a water container and scanned. The tube had an internal radius of 6.7 mm and the walls were 0.5 mm thick. The fluid volume flow Q was measured using a Danfoss MAG 1100 flow meter, which was situated after the heat shrink tube.

To drive the fluid around the closed circuit, a Cole Parmer (Vernon Hills, IL) 75211-60 centrifugal pump was used. The blood mimicking fluid consisted of water, glycerol, orgasol, Triton x-100, NaBenzoat and K_2EDTA diluted 10 to 1 with demineralized water. Viscosity was $\mu = 2.6 \cdot 10^{-3}$ kg/(m s), density $\rho = 10^3$ kg/m^3, and temperature during scanning was $T_0 = 24°C$.

The experimental ultrasound scanner RASMUS[8] and a 7 MHz linear array transducer characterized by the parameters in Table 1 and $f_{prf} = 2$ kHz, was used to scan the blood mimicking fluid and store the data for off-line processing. The Reynolds number of the flow was below 2000, hence the flow was assumed laminar and parabolic.[11] The maximum velocity in the center of the pipe was 0.32 m/s.

The blood vessel was situated at a depth of 40 mm at an angle of 60° with respect to the ultrasound beam. For each pulse emission a beamformed image of the ROI was created and echo canceling was performed by subtracting the mean value of all the 50 images acquired. The echo canceled images were divided into 150×150 points where the velocity was estimated at each point using 1D cross correlation along the direction of flow. Each line to be cross correlated had a spatial sampling interval of 0.15 times the wavelength of the emitted pulse at the center frequency and a length of 15 times the wavelength of the emitted pulse at the center frequency.

Using two echo canceled images a CFM mode image was created (Fig. 11). Due to the low number of correlated data (two images), false peaks are present in the CFM image. The image can be improved by using more pulse transmissions. In Fig. 12 the CFM image is made from 11 pulse transmissions.

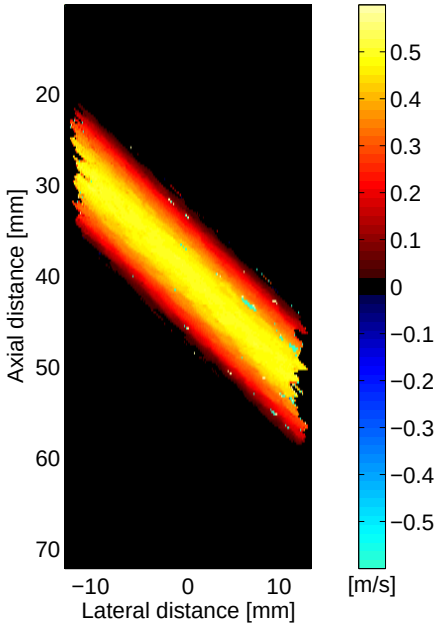

Figure 9. CFM-mode image of a virtual blood vessel. Two emissions with a plane wave chirp was simulated using the Field II program. The velocity was estimated using 1D cross correlation along the direction of flow. The direction of the flow is from the upper left corner to the lower right.

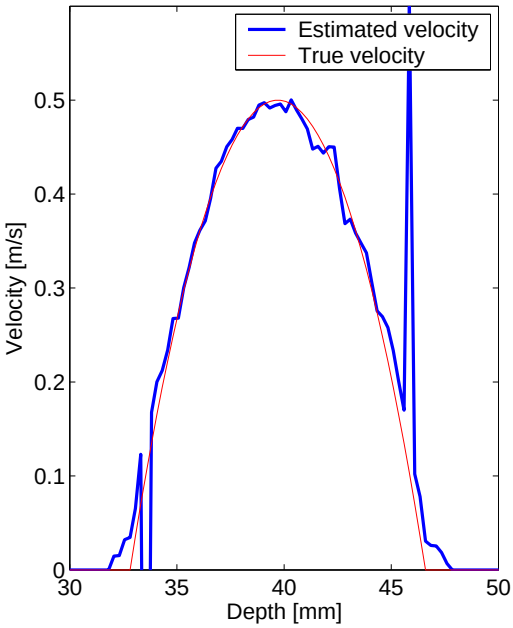

Figure 10. The velocity estimated at the line given by x=0 mm.

To verify that the derived CFM image is in agreement with the actual flow in the pipe, the velocity was estimated at two cross sections through the scanned area, where the lateral position x was $x = 0$ mm and $x = 5$ mm. 50 CFM images were used to find the mean velocity and standard deviation. The resulting mean velocity profile and standard deviation for $x = 0$ mm is shown in Fig. 13 together with the theoretical parabolic velocity profile. The velocity is estimated over the vessel with a mean relative standard deviation of 2.64% and a mean relative bias of 6.91%.

In Fig. 14 the profiles for $x = 5$ mm are shown. The velocity is estimated over the vessel with a relative standard deviation of 0.84% and a relative bias of 5.74%. This performance is comparable to conventional flow imaging.[12]

7. IN VIVO MEASUREMENT

An in vivo experiment was performed on a healthy 33-year-old male using the RASMUS scanner connected to the transducer defined by the parameters from Table 1 and with a pulse repetition frequency of $f_{prf} = 2$ kHz. The common carotid artery was scanned for two seconds and data were saved for off-line beamforming.

Echo canceling was performed by subtracting the mean value from 11 consecutive images. The echo canceled images were then divided into 150×150 points where the velocity was estimated at each point using 1D cross correlation along the direction of flow. Each line to be cross correlated had a spatial sampling interval of 0.3 times the wavelength of the emitted pulse at the center frequency and a length of 15 times the wavelength of the emitted pulse at the center frequency. To decrease the standard deviation on the estimates 11 lines were cross correlated and averaged before the maximum was estimated. This means that completely independent velocity images of the artery are acquired every $11/f_{prf} = 5.5$ ms.

In Fig. 15 the resulting CFM image is shown when data are acquired at the peak systolie. The B-mode image is estimated from one plane wave pulse transmission and no filtration of the velocity image has been performed.

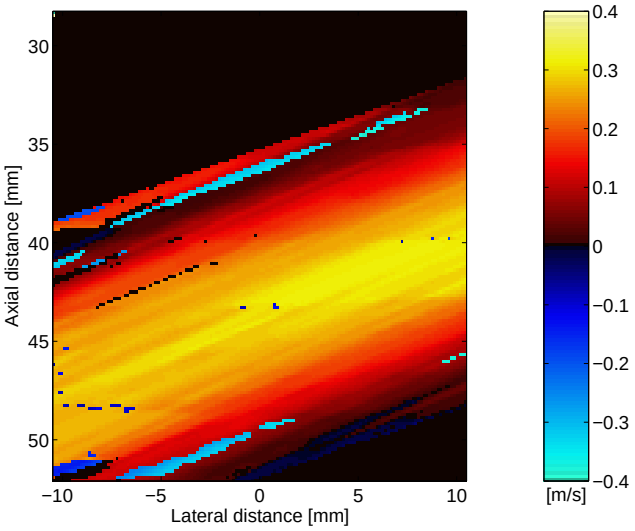

Figure 11. Data from two pulse emissions were used to make a CFM-mode image of flow in an experimental flowrig. The experimental RASMUS scanner was used to acquire data. The velocity is only estimated in the tube containing the blood mimicking fluid.

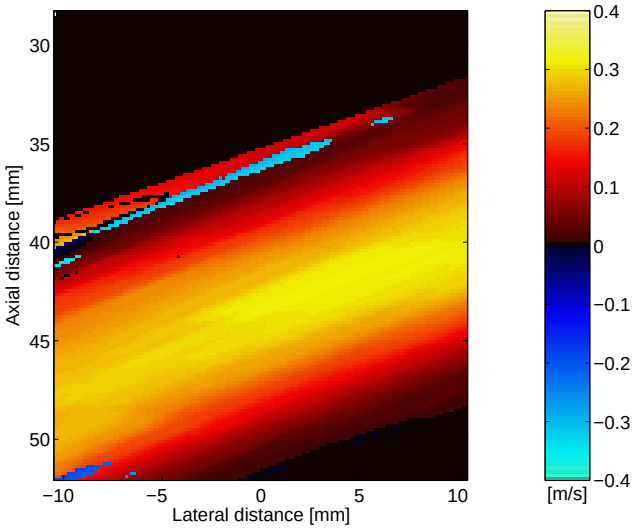

Figure 12. Data from 11 pulse emissions were used to make a CFM-mode image of flow in an experimental flowrig. The velocity is only estimated in the tube containing the blood mimicking fluid.

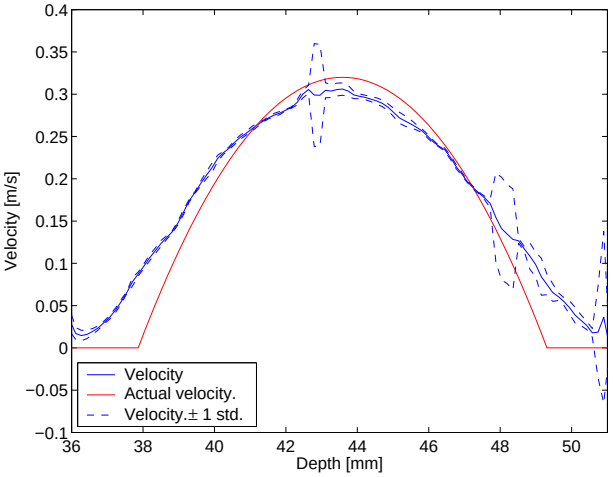

Figure 13. The mean velocity and standard deviation as a function of depth for the line defined at $x = 0$ mm from Fig. 11. Two pulse emissions used for each estimate.

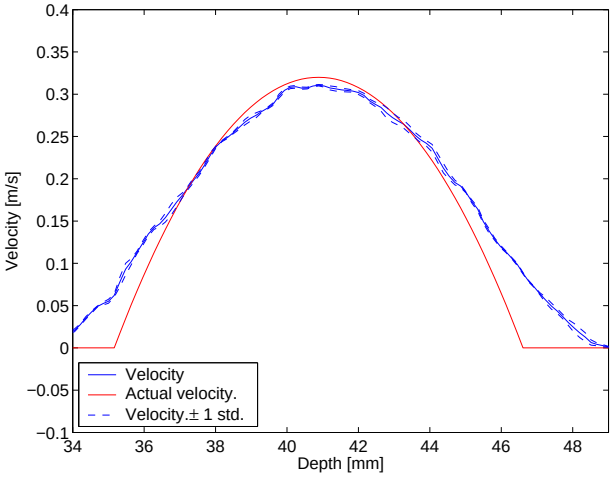

Figure 14. The mean velocity and standard deviation as a function of depth for the line defined at $x = 5$ mm from Fig. 11. Two pulse emissions used for each estimate.

8. DISCUSSION

It has been verified in simulations and experiments, that it is possible to obtain a CFM-mode image using less than 12 pulse emissions, when plane wave chirps are used as excitation pulses. If fast accelerating flow (e.g. in the heart) is to be estimated, the PWE method, thus, has the potential of showing temporal variations in the flow, which could not be estimated using a conventional method.

Furthermore, we believe that the PWE method also has potentials for 3D flow estimation using a 2D linear array transducer. Conventional methods for 3D flow based on focused transmit beams will have to compromise performance if a high frame rate is desired. This is due to the high (> 100) number of beams needed to cover the

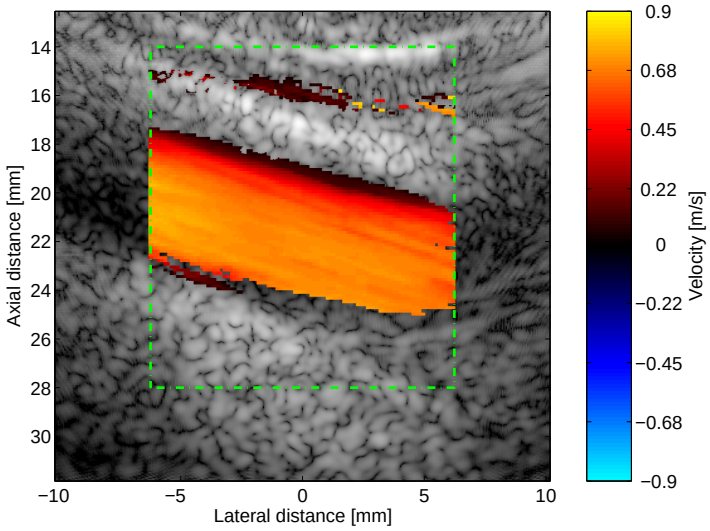

Figure 15. In vivo measurement of the common carotid artery of a healthy 33-year-old male at the time of the peak systolie. The velocity image is estimated from 11 plane wave pulse transmissions and the B-mode image is estimated from one plane wave pulse transmission. The B-mode image has a dynamic range of 40 dB and no filtration of the velocity data has been performed other than echo canceling. The velocity is only estimated within the green dashed line.

whole 3D ROI. The PWE method can cover the 3D ROI in only one pulse emission and in principle maintain the same performance as in the 2D case.

REFERENCES

1. M. Tanter, J. Bercoff, L. Sandrin, and M. Fink, "Ultrafast Compound Imaging for 2-d Motion Vector Estimation: application to Transient Elastography," *IEEE Trans. Ultrason., Ferroelec., Freq. Contr.* **49**, pp. 1363–1374, 2002.
2. L. Y. L. Mo, T. L. Ji, C. H. Chou, D. Napolitano, G. W. McLaughlin, and D. DeBusschere, "Zone-based color flow imaging," in *Proc. IEEE Ultrason. Symp.*, pp. 29–32, 2003.
3. J. A. Jensen, "Directional velocity estimation using focusing along the flow direction: I: Theory and simulation," *IEEE Trans. Ultrason., Ferroelec., Freq. Contr.* , pp. 857–872, 2003.
4. J. A. Jensen and R. Bjerngaard, "Directional velocity estimation using focusing along the flow direction: II: Experimental investigation," *IEEE Trans. Ultrason., Ferroelec., Freq. Contr.* , pp. 873–880, 2003.
5. J. A. Jensen, "Velocity vector estimation in synthetic aperture flow and B-mode imaging," in *IEEE International Symposium on Biomedical imaging from nano to macro*, pp. 32–35, 2004.
6. J. A. Jensen and N. B. Svendsen, "Calculation of pressure fields from arbitrarily shaped, apodized, and excited ultrasound transducers," *IEEE Trans. Ultrason., Ferroelec., Freq. Contr.* **39**, pp. 262–267, 1992.
7. J. A. Jensen, "Field: A program for simulating ultrasound systems," *Med. Biol. Eng. Comp.* **10th Nordic-Baltic Conference on Biomedical Imaging, Vol. 4, Supplement 1, Part 1**, pp. 351–353, 1996b.
8. J. A. Jensen, O. Holm, L. J. Jensen, H. Bendsen, H. M. Pedersen, K. Salomonsen, J. Hansen, and S. Nikolov, "Experimental ultrasound system for real-time synthetic imaging," in *Proc. IEEE Ultrason. Symp.*, **2**, pp. 1595–1599, 1999.

9. T. Misaridis, *Ultrasound imaging using coded signals.* PhD thesis, Ørsted•DTU, Technical University of Denmark, Lyngby, Denmark, 2001.
10. T. X. Misaridis and J. A. Jensen, "An effective coded excitation scheme based on a predistorted FM signal and an optimized digital filter," in *Proc. IEEE Ultrason. Symp.*, **2**, pp. 1589–1593, 1999.
11. D. J. Acheson, *Elementary Fluid Dynamics*, Clarendon Press, Oxford, 1990.
12. J. A. Jensen, *Estimation of Blood Velocities Using Ultrasound: A Signal Processing Approach*, Cambridge University Press, New York, 1996.

A frequency splitting method for blood flow estimation.

Jesper Udesen[a,b], Fredrik Gran[a] and Jørgen Arendt Jensen[a]

[a]Center for Fast Ultrasound Imaging, Ørsted • DTU, Bldg. 348, Technical University of Denmark, DK-2800 Kgs. Lyngby, Denmark

[b]B-K Medical, Mileparken 34, DK-2730 Herlev, Denmark

1. ABSTRACT

A new method for axial blood velocity estimation is introduced that uses a linear frequency modulated signal (chirp) as excitation pulse. In receive, the channel signals are matched filtered to compress the chirp, and then delay-and-sum beamformed. The resulting broad band signal is separated into narrow band signals using appropriate band pass filters. Each narrow band signal is then used in an conventional autocorrelation estimator to find one velocity estimate for each frequency band. Finally the velocity estimates are averaged to find an improved axial velocity estimate.

The method is tested in simulations using the program Field II where a significant improvement is found on the standard deviation compared to a conventional autocorrelation method. Furthermore the method is tested in the experimental RASMUS scanner using a linear array 7 MHz transducer on a circulating flowrig. Compared to a conventional autocorrelation method, the standard deviation is found to decrease with a factor of approximately two for the proposed method.

2. INTRODUCTION

In conventional blood velocity estimation using ultrasound, a number of consecutive pulses are transmitted from the transducer. After a number of transmissions (usually > 3) the axial velocity can be estimated along a line perpendicular to the transducer surface. The process can thereafter be repeated for other directions and finally a whole color flow image of the blood velocity can be constructed.

The bias and standard deviation on the velocity estimates decreases with the number of transmissions used for each estimate. To obtain high quality blood velocity images, it is therefore necessary to have as many transmissions as possible for each velocity estimate. However, due to the time of flight for each ultrasound pulse, this is often not possible, if vessels deep in the human body is to be scanned. It is therefore of interest to develop methods, which have low bias and standard deviation, even when only a few transmissions are used for each velocity estimate.

Currently the two main methods for color flow map (CFM) imaging are

1. The cross-correlation approach (or time shift estimation) is based on the transmission of broad band pulses with good time resolution. Consecutive beamformed signals are cross correlated to find the lag of maximum correlation from which the velocity is estimated. This method has good performance in terms of standard deviation and bias, but it is very expensive in terms of computation power and does not perform well when the signals are corrupted with noise. The SNR problem can, however, be significantly reduced if a frequency modulated signal (chirp) is used as excitation pulse.

2. The autocorrelation approach (or phase shift estimation) developed by Kasai [1] is implemented in nearly all commercial scanners. This method is based on the transmission of narrow banded pulses with good resolution in the frequency domain. An axial velocity estimate is found by calculating the mean phase shift in the slow-time domain. The method is very fast and robust but does not perform as good as the cross correlation method in terms of standard deviation on the velocity estimates. Also it is not possible to use a chirp, since the signals have to be narrow band.

The frequency band method presented in this paper uses some of the advantages from both methods to improve the conventional autocorrelation approach. In Section 3, the method will be explained. In Section 4 simulated results will be presented together with flow phantom experiments obtained with the experimental RASMUS scanner.

3. METHOD

The basic principle of the frequency band method introduced in this paper is as follows:

- A linear chirp is used as excitation signal.
- The beamformed received signals are compressed using matched filtration. After filtration the signals are still broad banded.
- Each broad band signal is divided into a number of narrow band signals by filtering with a number of narrow band filters.
- Each narrow band signal is echo canceled and the velocity is estimated with a conventional autocorrelation approach.
- Finally the velocity estimates from each narrow-band signals are averaged to form a single improved estimate.

Each step of the transmission, filtration and estimation process will now be discussed.

3.1. The chirp

A linear chirp is used for transmission. This improves the SNR compared to using a single oscillation pulse while maintaining resolution. The theoretical gain in SNR after matched filtration (in dB) is given by [2]

$$G = 10\log_{10}\Big(\frac{E_{chirp}}{E_{ref}}\Big), \tag{1}$$

where E_{chirp} is the energy of the chirp and E_{ref} is the energy of the waveform, which is used as a reference.

The excitation waveform is defined as

$$s(t) = a(t)\sin\Big\{2\pi(f_0 - \frac{B}{2})t + 2\pi\frac{B}{2T}t^2\Big\},\ 0 \le t \le T. \tag{2}$$

where $a(t)$ is a temporal weighting function, f_0 is the center frequency, B is the bandwidth, and T is the duration of the excitation waveform. The center frequency is 7 MHz, the bandwidth is 75% of the center frequency and the duration is 20 μs. The temporal weighting function is chosen to be a Tukey window with 10% tapering. It should be noted that the chirp is a broad band signal compared to the signals used in an conventional autocorrelation approach.

The theoretical gain calculated from (1) will be 20.8 dB when the reference waveform is a single oscillation pulse. However, due to tapering of the chirp and the compression filter the actual gain will be 14 dB [3].

3.2. Receive filtration

After the signals have been received by the transducer, each channal signal is matched filtered using the excitation waveform mismatched with a Chebyshev window with relative sidelobe attenuation of 70 dB. The temporal window applied to derive the mismatched filter is used in order to suppress axial sidelobes [2]. In theory the matched filtration has to be performed before beamforming. However, it has been shown that no significant degeneration of resolution and contrast results from doing the matched filtering after the delay and sum beamforming [4].

After matched filtration the broad band signals are divided into a number of narrow band signals. This can be done in numerous ways. If the implementation has to be simple and fast, an easy way is to convolve the signal with a filter $y(n)$ given by

$$y_{m,p_m}(n) = \cos(2\pi n\frac{f_m}{f_s}), \quad n = 1, 2, ..., p_m\frac{f_s}{f_m} \tag{3}$$

where f_m is the center frequency of each frequency band, f_s is the sampling frequency and p_m determines the width of each frequency band.

To decrease side-lobe levels further the filter $y_{m,p}$ is shaped by a Hanning window and the resulting filter is convolved with itself. Since the bandwidth of each frequency band determines the axial resolution, special care should be taken such that each band does not become to narrow. For all results presented in this paper the axial resolution of the frequency band method is comparable to the axial resolution of a 7 MHz 8 cycle pulse.

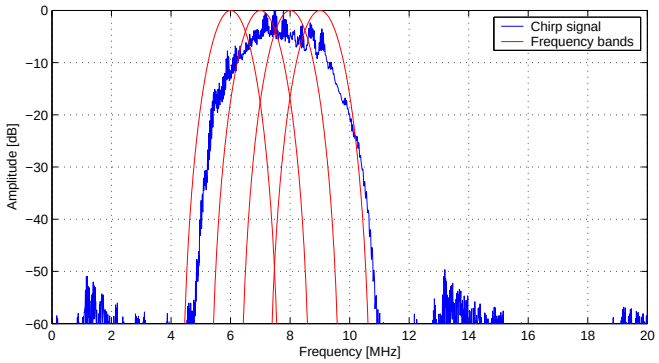

Figure 1. The principle of the method. Blue curve: the amplitude spectrum of the received beamformed chirp signal from a flow rig. Red curve: the frequency bands used to split the broad band spectrum of the chirp into narrow band signals.

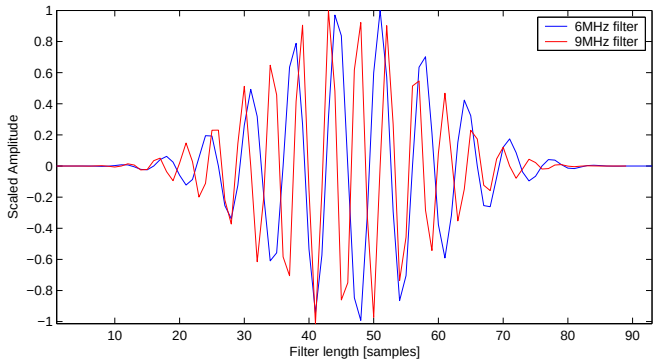

Figure 2. The filters for the 6MHz and 9MHz band.

For the chirp given by (2) used on a 7 MHz 60% bandwidth transducer (B-K 8804) f_m can be chosen to be $f_m \in \{6 \text{ MHz}, 7 \text{ MHz}, 8 \text{ MHz}, 9 \text{ MHz}\}$ and the corresponding p_m is $p_m \in \{7, 8, 9, 10\}$. After Hanning windowing and convolution, these values gives frequency bands of approximately 1 MHz of width. It should be noted that the frequency bands do not have to be disjoint. If overlap occurs between the bands the velocity estimates will not be independent and the standard deviation and bias on the estimates will increase, but the filters implemented will be much more simple to construct. The frequency bands which corresponds to (3) can be seen in Fig. 1 and two of the band-pass filters are shown in Fig. 2.

3.3. Velocity estimation

So far the filtration of the signals has been performed in the so called fast time domain, where the sampling frequency is f_s. When consecutive pulse transmissions are performed, data can be sampled at a certain depth with a sampling frequency of the pulse repitetion frequency (f_{prf}). The data is then sampled in the so called slow time domain. When no aliasing is present the transformation between the fast time (f_0) domain and the

slow time (f_p) frequency domain is given by

$$f_p = \frac{2v_z}{c} f_0, \tag{4}$$

where v_z is the velocity of the blood, c is the speed of sound in the tissue, and f_0 is the center frequency of the narrow band signal.

After filtration the signals from each frequency band is echo canceled in the slow time domain. For optimal echo canceling the cut-off frequency of the echo canceling filter should change with the frequency band of each signal. This is due to the fact that the frequency f_p of the tissue signal will scale with the center frequency f_0 of each band according to (4). So that for a frequency band signal with a center frequency of 10 MHz the tissue will be located at twice the frequency as for the tissue signal from a 5 MHz band signal.

When echo canceling is performed an axial velocity estimate can be found for each frequency band signal using an conventional autocorrelation estimator [1]. Finally these velocity estimates are averaged to find an improved axial velocity estimate. Alternatively the individual velocity estimates could be scaled with the energy in the respective frequency band, thereby reducing noise.

4. RESULTS

Two set of results are presented in this section: one set of simulated results using the Field II program and one set of measured results using the RASMUS ultrasound scanner. In both cases the same transducer (B-K 8804) is used.

4.1. Simulation

The Field II ultrasound simulation program [5, 6] was used to simulate the ultrasound response from a virtual blood vessel situated at a depth of 30 mm at an angle of 45° with respect to the ultrasound beam. The transducer used was a 7 MHz virtual linear array B-K 8804 transducer where 64 elements were used in transmit and receive. The number of transmissions was 120 using a chirp given by (2) and 120 transmissions using a 7 MHz 8 cycle sinusoid. Pulse repetition frequency (f_{prf}) was 10kHz.

White Gaussian noise was added to each received signal. The mean SNR was 0 dB over the vessel for the 8 cycle pulse and noise with the same power was added to the received chirp signals. The received echos from the chirp signal was matched filtered, beamformed and divided into frequency bands according to (3). However the band at center frequency of 9 MHz was omitted due to high attenuation by the transducer at these frequencies. Also the received signals from the 8 cycle pulse were matched filtered.

The resulting velocity estimates for 2 and 4 transmissions respectively, can be seen in Fig. 3 and 4. It is seen that the standard deviation is significantly lower for the frequency band method compared to a conventional 8 cycle pulse.

4.2. Experiment

The experimental ultrasound scanner RASMUS [7] was used together with a B-K Medical 8804 transducer to scan a circulating flowrig with a tube radius of 6.725 mm. The flow in the flowrig was assumed to be laminar, since the Reynolds number was kept at approximatelly 2000. The number of transmit and receive elements was 64, the pulse repetition frequency was f_{prf}=4 kHz and 400 transmissions were acquired using either a chirp, a 6 MHz 8 cycle pulse, a 7 MHz 8 cycle pulse or a 8 MHz 8 cycle pulse.

In receive, each channel signal was matched filtered and delay-and-sum beamformed. The received signal from the chirp was separated into frequency bands as described in the previous section and the velocity was found for each frequency band and averaged. It should be noted that no echo canceling or rf-averaging [8] was performed on the signals.

The resulting velocity estimates for 2 and 4 transmissions respectively, can be seen in Fig. 5 and 6. Again it is seen that the standard deviation is significantly lower for the frequency band method compared to a conventional 8 cycle pulse. Also the mean standard deviation is calculated over the vessel and scaled with the maximum velocity

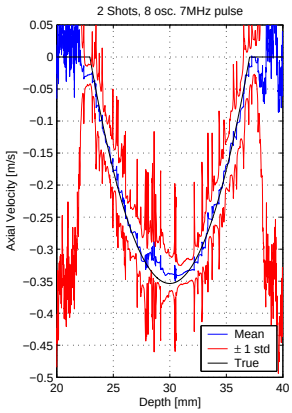

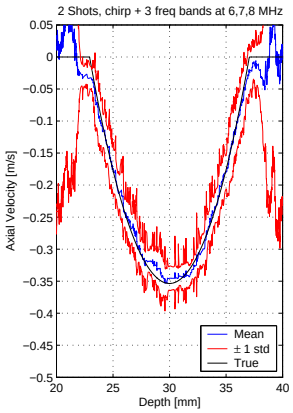

Figure 3. The mean velocity and standard deviation as a function of depth simulated with Field II and a virtual B-K 8804 transducer. The angle between the flow and the ultrasound beam was 45° and the maximum velocity was 0.5 m/s. Two pulse emissions used for each estimate and different transmission pulses. Left: estimates from a 8 cycle pulse at 7 MHz. Right: estimates from the frequency band method described in this paper.

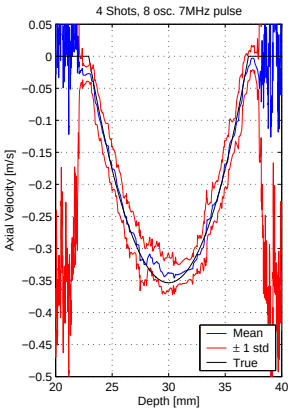

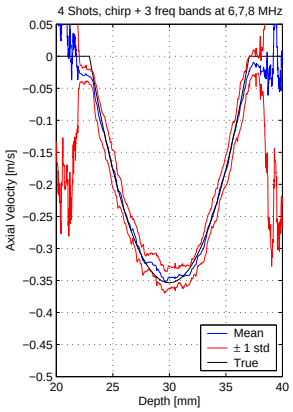

Figure 4. Same as Fig. 3 but with four transmissions for each estimate.

and shown in Table 1. It is seen that the mean standard deviation on the velocity estimates from the frequency band method, is approximately half of the mean standard deviation of the conventional method.

The reference curve for the true velocity is calculated from 400 transmissions with a 7 MHz 8 cycle pulse. After reception each beamformed signal was rf-averaged and the axial velocity was estimated in a conventional autocorrelation estimator. The reference velocity is shown as a black curve in all plots in Fig. 5 and 6.

	2 transmissions	4 transmissions
6 MHz pulse	10.89	5.52
7 MHz pulse	9.79	4.73
8 MHz pulse	10.47	4.64
Frequency bands	5.19	2.64
Chirp	10.84	8.45

Table 1. Mean standard deviation in percent relative to the center velocity.

5. CONCLUSION

A frequency band method for estimating blood velocity using ultrasound has been presented. In terms of mean standard deviation on the velocity estimates the frequency band method outperforms conventional autocorrelation methods. We believe that further investigations should focus on the emitted energy in the chirp compared to the FDA limits. Also improved performance using more advanced filters to divide the signals into frequency bands as well as weighting the velocity estimates from each band, could be an area of investigation. Further more we believe that the frequency band method has potentials for other flow estimators, which uses the autocorrelation technique, e.g. the TO vector velocity estimator for 2D blood velocity estimation.

REFERENCES

1. C. Kasai, K. Namekawa, A. Koyano, and R. Omoto, "Real-time two-dimensional blood flow imaging using an autocorrelation technique," *IEEE Trans. Son. Ultrason.* **32**, pp. 458–463, 1985.

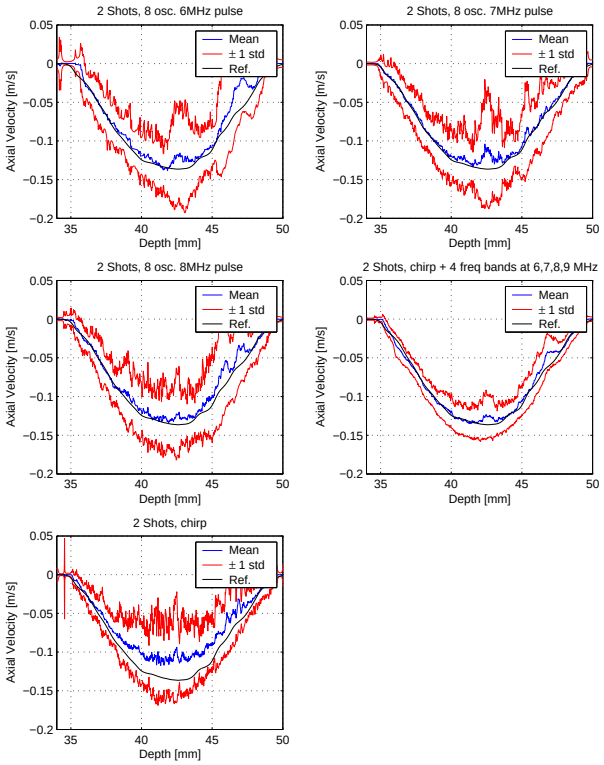

Figure 5. The mean velocity and standard deviation as a function of depth measured with the RASMUS using a B-K 8804 transducer on a flow phantom. The angle between the flow and the ultrasound beam was 70°. Two pulse emissions used for each estimate and different transmission pulses. Upper left: estimates from a 8 cycle pulse at 6 MHz. Upper right: estimates from a 8 cycle pulse at 7 MHz. Center left: estimates from a 8 cycle pulse at 8 MHz. Center right: estimates from the frequency band method described in this paper. Lower left: estimates from a chirp with no band-pass filtering. The black curve in each plot indicates the reference velocity estimate using 400 transmissions of a 7 MHz 8 cycle pulse and rf-averaging.

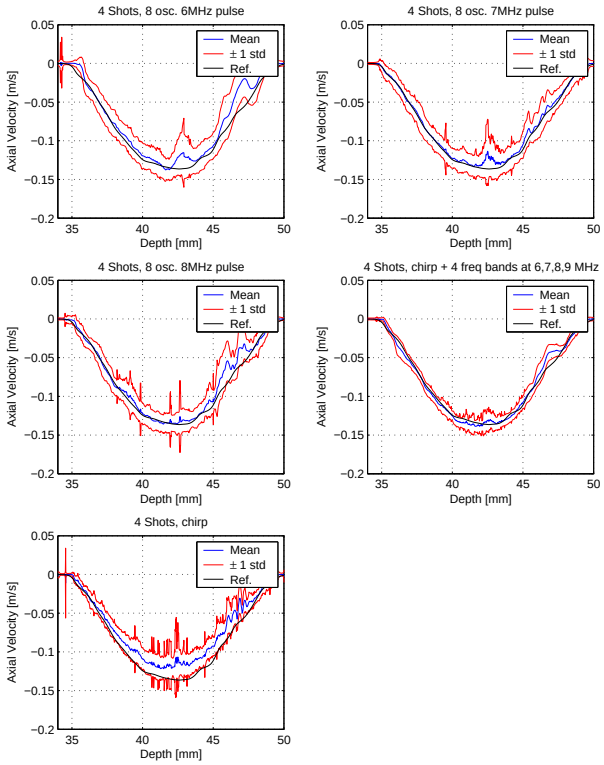

Figure 6. Same as Fig. 5 but with four transmissions for each estimate.

2. T. Misaridis, *Ultrasound imaging using coded signals.* PhD thesis, Ørsted•DTU, Technical University of Denmark, Lyngby, Denmark, 2001.
3. T. X. Misaridis and J. A. Jensen, "An effective coded excitation scheme based on a predistorted FM signal and an optimized digital filter," in *Proc. IEEE Ultrason. Symp.*, **2**, pp. 1589–1593, 1999.
4. R. Bjerngaard, "Transverse blood flow estimation and effective coded excitation," Master's thesis, Ørsted•DTU, Technical University of Denmark, Lyngby, Denmark, 2001.
5. J. A. Jensen and N. B. Svendsen, "Calculation of pressure fields from arbitrarily shaped, apodized, and excited ultrasound transducers," *IEEE Trans. Ultrason., Ferroelec., Freq. Contr.* **39**, pp. 262–267, 1992.
6. J. A. Jensen, "Field: A program for simulating ultrasound systems," *Med. Biol. Eng. Comp.* **10th Nordic-Baltic Conference on Biomedical Imaging, Vol. 4, Supplement 1, Part 1**, pp. 351–353, 1996b.
7. J. A. Jensen, O. Holm, L. J. Jensen, H. Bendsen, H. M. Pedersen, K. Salomonsen, J. Hansen, and S. Nikolov, "Experimental ultrasound system for real-time synthetic imaging," in *Proc. IEEE Ultrason. Symp.*, **2**, pp. 1595–1599, 1999.

8. J. A. Jensen, "A new estimator for vector velocity estimation," *IEEE Trans. Ultrason., Ferroelec., Freq. Contr.* **48**(4), pp. 886–894, 2001.

Bibliography

[1] J. A. Jensen and P. Munk, "A new method for estimation of velocity vectors," *IEEE Trans. Ultrason., Ferroelec., Freq. Contr.*, vol. 45, pp. 837–851, 1998.

[2] J. A. Jensen, "A new estimator for vector velocity estimation," *IEEE Trans. Ultrason., Ferroelec., Freq. Contr.*, vol. 48, no. 4, pp. 886–894, 2001.

[3] P. Munk, "Estimation of the 2-D flow vector in ultrasonic imaging: a new approach," M.S. thesis, Department of Information Technology, Technical University of Denmark, 1996.

[4] P. Munk, *Estimation of blood velocity vectors using ultrasound*, Ph.D. thesis, Department of Information Technology, Technical University of Denmark, Lyngby, Denmark, 2000.

[5] J. A. Jensen, O. Holm, L. J. Jensen, H. Bendsen, H. M. Pedersen, K. Salomonsen, J. Hansen, and S. Nikolov, "Experimental ultrasound system for real-time synthetic imaging," in *Proc. IEEE Ultrason. Symp.*, 1999, vol. 2, pp. 1595–1599.

[6] J. A. Jensen and N. B. Svendsen, "Calculation of pressure fields from arbitrarily shaped, apodized, and excited ultrasound transducers," *IEEE Trans. Ultrason., Ferroelec., Freq. Contr.*, vol. 39, pp. 262–267, 1992.

[7] J. A. Jensen, "Field: A program for simulating ultrasound systems," *Med. Biol. Eng. Comp.*, vol. 10th Nordic-Baltic Conference on Biomedical Imaging, Vol. 4, Supplement 1, Part 1, pp. 351–353, 1996b.

[8] T. L. Szabo, *Diagnostic ultrasound imaging inside out*, Elsevier, 2004.

[9] J. A. Jensen, *Estimation of Blood Velocities Using Ultrasound: A Signal Processing Approach*, Cambridge University Press, New York, 1996.

[10] D. H. Evans, W. N. McDicken, R. Skidmore, and J. P. Woodcock, *Doppler Ultrasound, Physics, Instrumentation, and Clinical Applications*, John Wiley & Sons, New York, 1989.

[11] H. B. Meire, D. O. Cosgrove, K. C. Dewbury, and P. Farrant, *Abdominal and General Ultrasound*, vol. 1, Churchill Livingstone, 2001.

[12] C. Kasai, K. Namekawa, A. Koyano, and R. Omoto, "Real-time two-dimensional blood flow imaging using an autocorrelation technique," *IEEE Trans. Son. Ultrason.*, vol. 32, pp. 458–463, 1985.

[13] M. D. Fox, "Multiple crossed-beam ultrasound Doppler velocimetry," *IEEE Trans. Son. Ultrason.*, vol. SU-25, pp. 281–286, 1978.

[14] John R. Overbeck, Kirk W. Beach, and D. Eugene Strandness, "Vector Doppler: Accurate measurement of blood velocity in two dimensions," *Ultrasound Med. Biol.*, vol. 18, pp. 19–31, 1992.

[15] V. L. Newhouse, D. Censor, T. Vontz, J. A. Cisneros, and B. B. Goldberg, "Ultrasound Doppler probing of flows transverse with respect to beam axis," *IEEE Trans. Biomed. Eng.*, vol. BME-34, pp. 779–788, 1987.

[16] G. E. Trahey, J. W. Allison, and O. T. von Ramm, "Angle independent ultrasonic detection of blood flow," *IEEE Trans. Biomed. Eng.*, vol. BME-34, pp. 965–967, 1987.

[17] B. H. Friemel, L. N. Bohs, K. R. Nightingale, and G. E. Trahey, "Wall filtering challenges in two-dimensional vector velocity estimation," *Proc. IEEE Ultrason. Symp.*, vol. 2, pp. 1031–1034, 1993.

[18] M. E. Anderson, "Vector flow estimator isomorphism and wall filter requirements," in *Proc. SPIE - med. imag.*, 2001, vol. 4325, pp. 215–226.

[19] L. Løvstakken, S. Bjærum, M. Ditlef, and H. Torp, "Real-time blood motion imaging a 2d blood flow visualization technique," in *Proc. IEEE Ultrason. Symp.*, 2004.

[20] J. A. Jensen, "Directional velocity estimation using focusing along the flow direction: I: Theory and simulation," *IEEE Trans. Ultrason., Ferroelec., Freq. Contr.*, pp. 857–872, 2003.

[21] J. Kortbek and J. A. Jensen, "Determination of velocity vector angles using the directional cross-correlation method," *IEEE Trans. Ultrason., Ferroelec., Freq. Contr.*, vol. x, pp. Accepted, 2005.

[22] N. Oddershede and J. A. Jensen, "Synthetic aperture flow angle estimation on in-vivo data from the carotid artery," in *Proc. IEEE Ultrason. Symp.*, 2005, pp. 1331–1334.

[23] M. E. Anderson, "Spatial quadrature: a novel technique for multi-dimensional velocity estimation," in *Proc. IEEE Ultrason. Symp.*, 1997, vol. 45, pp. 1233–1238.

[24] M. E. Anderson, "A heterodyning demodulation technique for spatial quadrature," in *Proc. SPIE - med. imag.*, 2000, pp. 1487–1490.

[25] L. E. Kinsler, A. R. Frey, A. B. Coppens, and J. V. Sanders, *Fundamentals of Acoustics*, John Wiley & Sons, New York, third edition, 1982.

[26] J. W. Goodman, *Introduction to Fourier optics*, McGraw Hill Inc., New York, second edition, 1996.

[27] G. R. Lockwood, P-C. Li, M. O'Donnell, and F. S. Foster, "Optimizing the radiation pattern of sparse periodic linear arrays," *IEEE Trans. Ultrason., Ferroelec., Freq. Contr.*, vol. 43, pp. 7–14, 1996.

[28] A. P. G Hoeks, J. J. W. van de Vorst, A. Dabekaussen, P. J. Brands, and R. S. Reneman, "An efficient algorithm to remove low frequency Doppler signal in digital Doppler systems," *Ultrason. Imaging*, vol. 13, pp. 135–145, 1991a.

[29] S. Bjaerum and H. Torp, "Statistical evaluation of clutter filters in color flow imaging," *Ultrasonics*, vol. 38, pp. 376–380, 2000.

[30] M. Schlaikjer, *Development and characterization of algorithms for estimation of blood velocity with ultrasound*, Ph.D. thesis, Ørsted•DTU, Technical University of Denmark, Kgs. Lyngby, Denmark, 2001.

[31] J. Udesen, F. Gran, and J. A. Jensen, "A frequency splitting method for blood flow estimation," *Working paper.*, 2005.